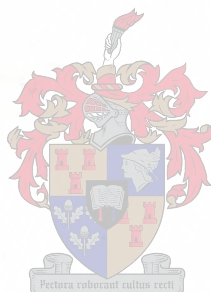


Polymer Networks at Surfaces

By

WENDY LEIGH VANDOOOLAE GHE



This thesis presented in partial fulfilment of the requirements for the degree of
MASTER OF SCIENCE at the University of Stellenbosch.

Supervisor : Dr. Kristian Müller-Nedebock

April 2003

DECLARATION

I, the undersigned, hereby declare that the work contained in this thesis is my own original work and that I have not previously in its entirety or in part submitted it at any university for a degree.

ABSTRACT

In this thesis the formation and properties of a polymer gel on and at a surface are investigated. The gel under investigation is defined as a three-dimensional network of macromolecules that form permanent links with one another and also with confining planar surfaces. The precise location of the crosslinks on the wall or on another macromolecule is not known prior to linking, and will differ from sample to sample. However, once the crosslinks are formed, they are assumed to be permanent. This random linking is the source of the disorder in the system, over which a quenched average has to be taken. An existing model [9] of network formation, with polymer-polymer crosslinks, is extended to incorporate a surface and polymer-surface crosslinks. Within the framework of replica theory, statistical averages and physical properties of the system are calculated by means of a variational approach. Macroscopic information, in terms of the free energy of deformation, is obtained by using two *different* potentials to simulate the crosslinks mathematically.

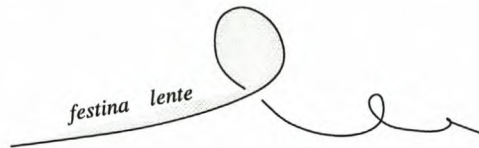
OPSOMMING

In hierdie tesis word die vorming en eienskappe van 'n polimeergel, wat teen 'n oppervlak gevorm word, ondersoek. Die gel word gedefinieer as 'n drie-dimensionele netwerk van makromolekules wat permanente bindings met mekaar, maar ook met twee inperkende, platvlakke, vorm. Die presiese ligging van die bindings op die muur en op ander makromolekules is nie vooraf bekend nie, en sal verskil van een gel-monster tot die volgende. Sodra die konneksies egter gevorm is, word aanvaar dat hulle permanent is. Die lukrake bindingsproses is die oorsprong van wanorde in die sisteem, waaroor 'n wanorde-gemiddelde bereken moet word. 'n Bestaande model [9] van netwerkvorming, met polimeer-polimeer bindings, word uitgebrei om 'n oppervlakte en polimeer-oppervlak bindings in te sluit. Statistiese fisika gemiddeldes en fisiese eienskappe van die sisteem word binne die raamwerk van replika-teorie en 'n variasie benadering bereken. Makroskopiese inligting, in terme van die vrye energie van vervorming, word verkry deur twee *verskillende* potensiale te gebruik om die konneksies wiskundig voor te stel.

ACKNOWLEDGEMENTS

I am indebted to many:

- Dr Kristian Müller-Nedebock, my thesis supervisor, who gave me patient guidance, sage advice and had endless enthusiasm throughout. I could not have asked for a better mentor.



- Past en present colleagues (and visitors) at the Institute of Theoretical Physics, including Lucian, Pavel and Harry.
- Professor Hendrik Geyer, who initiated me in the study of statistical mechanics *aeons* ago.
- My examiners — for all the reading and thoughtful commentary.
- My friends — for proper distraction — in particular: Neilen, Jack, Lude (*Muzik!*), Nicholas (*action at a distance*), Karien, Cheryl and the US Wine club.

Special thanks to Melt – his support and calmness is my repose.

The realization of this thesis would not have been possible without financial assistance from Stellenbosch University, the National Research Foundation (NRF) and the Harry Crossley bursary. The financial assistance of the Department of Labour (DoL) towards this research is hereby acknowledged. Opinions expressed and conclusions derived at, are those of the author and are not necessarily to be attributed to the DoL.

*

I dedicate this thesis to my parents, for all their generosity and love throughout my life and my education. They have always encouraged me to independence, never trying to limit my aspirations.

Table of Contents

Abstract — Opsomming	ii
Acknowledgements	iii
Table of Contents	iv
1 Introduction	1
1.1 What is a polymer?	1
1.1.1 Flexibility	2
1.1.2 Ideality	2
1.1.3 The Entropic Spring	3
1.1.4 Elasticity	3
1.1.5 Polymer Gels	4
1.2 Outline of chapters	5
2 The Single Confined Chain	6
2.1 A free Gaussian chain	6
2.2 A Single Chain in a Box	8
2.3 A polymer <i>stitch</i>	9
2.3.1 Three limiting cases	10
2.4 <i>Stitch</i> Strains	11
2.4.1 Case 1: Deforming the plate system	12
2.4.2 Case 2: Deforming the box system	14
2.5 One bulk-link	15
2.6 Contemplating stitches	18
3 The Stitch Network	19
3.1 A random bulk link	19
3.2 Quenched disorder	21
3.2.1 Green's functions	21
3.2.2 Averaging	22
3.2.3 Replicas to the rescue	23
3.3 The actual calculation	25
3.3.1 The method of steepest descents	25

TABLE OF CONTENTS

v

3.4	Deforming the <i>stitch network</i>	27
4	The Real Confined Network	28
4.1	The Collection of Phantom chains	28
4.2	Confining the Melt	29
4.3	Confined Network Formation	30
4.3.1	The Origin of disorder	31
4.3.2	Linking Formalism	32
4.3.3	Implementing Replicas	33
4.4	Planning the variational calculation	36
4.4.1	Introducing transformation coordinates	36
4.4.2	Introducing a trial localization potential	36
4.4.3	Notation	38
4.4.4	The variational Hamiltonian	39
4.5	The variational calculation (for $\langle \mathbb{A} - \mathbb{A}_0 \rangle = 0$)	41
4.5.1	The Green's functions	41
4.5.2	The Averages	42
4.5.3	The variational Free energy	43
4.6	Results	45
5	The Brush Network	47
5.1	Formation of the Brush Network	48
5.1.1	Confinement formalism	49
5.1.2	Crosslink formalism	49
5.1.3	Replica formalism	51
5.2	The Variational Approach	53
5.2.1	Trial potential for the brush network	53
5.2.2	Averaging	55
5.3	The variational Free energy	57
5.3.1	The Replica limit	58
5.3.2	The minimization problem	59
5.4	Analysis and Results	60
5.4.1	The homogeneous brush limit	60
5.4.2	The single chain limit	61
5.4.3	Localization of the polymer brush network	62
5.4.4	Confinement and the free energy	63
5.4.5	Elasticity	64
6	Concluding Remarks	68
A	Coordinate transformation	71
B	The average $\langle \mathbb{A} - \mathbb{A}_0 \rangle$ in the variational principle	73

TABLE OF CONTENTS

vi

C The First Variational Calculation	75
C.1 The Bulk Cross-links $\langle \mu_c \mathbb{X}_c \rangle$	75
C.2 The Wall Crosslinks $\langle \mu_w \mathbb{X}_w \rangle$	77
C.3 The harmonic trial potential $\langle Q \rangle$	79
D The Second Variational Calculation	80
D.1 The Bulk Cross-links $\langle \mu_c \mathbb{X}_c \rangle$	80
D.2 The Wall Crosslinks $\langle \mu_w \mathbb{X}_w \rangle$	81
D.3 The harmonic trial potential $\langle Q \rangle$	82
Bibliography	83
List of Figures	85

Chapter 1

Introduction

Polymers in restricted geometries exhibit very specific and interesting properties. The widespread interest in polymers in confined media, is proof of the importance of understanding these properties, which play a vital role in many industrial applications, but also in nature¹. Fundamental theoretical physics research provides the basis for investigating and predicting properties of these systems. Problems related to this field are diverse, and include the adsorption behaviour of gels, surface coatings, membranes in nano pores and biopolymers in restricted geometries.

In particular, the formation of polymer *networks* at surfaces, is crucial for a number of applications, where surfaces have to be protected against forms of mechanical or chemical stress, such as abrasion and corrosion [39]. Surface-attached networks also play an important role in several biomedical concepts, for example, to provide biocompatible, but stable coatings on implant surfaces [41]. Most theoretical treatments of these types of systems have been on the level of scaling theory, and analytical treatments have been lacking. Recently, Allegra and Raos [1] investigated a confined polymer network, but modelled the effect of confining walls on a network by an harmonic potential and completely ignored the possibility of wall attachments.

The aim of this thesis is to gain a better understanding, of a polymer network (or gel) that has formed at a confining surface. In particular, we investigate the simplest case where the confining geometry is two parallel planar surfaces. However, before we embark on the statistical physics theory treatment of this problem, some relevant polymer background should be given.

1.1 What is a polymer?

A polymer is a substance² composed of macromolecules, which have long sequences of one or more types of atoms or groups of atoms linked to each other by primary, usually covalent, bonds.

¹Polymers in confined geometries is a multidisciplinary field, attracting research interest from scientists in chemistry, material science, biology and experimental, simulation, and theoretical physics. In 1998 the European Associated Laboratory (of the Institut Charles Sadron, Strasbourg and the Max Planck Institute for Polymer Research, Mainz) was created for the purpose of studying polymers in confined media.

²Although the terms *polymer* and *macromolecule* are used interchangeably, the former strictly refers to any type of polymeric material (rubbers, biopolymers, fibres, glassy and crystalline polymers) of which the macromolecule is the essential, common building block [47].

Macromolecules are formed by the process of polymerization, that is, by linking together many, say N , monomer units through chemical reactions. The long chain nature of macromolecules is responsible for the characteristic properties of polymers and sets them apart from other materials.

1.1.1 Flexibility

Flexible polymers have a large number of internal degrees of freedom. The typical primary structure of macromolecules is a linear chain (the backbone) of atoms connected by chemical bonds and some *pendant* atoms or groups to satisfy the remaining valencies. By rotation about the single bonds in the backbone the molecule changes its shape or conformation. Since there are many of these bonds, a wide spectrum of conformations is available to a macromolecule³. The rotation of chemical bonds may be hindered by bulky pendant groups, so that some of the conformations become unfavourable. Sometimes the interaction between neighbouring groups leads to preferred sequences of bond orientations, which emerge as helical or folded sections in the molecules. Thus, a polymer is termed flexible if thermal motion is strong compared to the energy barriers associated with backbone rotation.

1.1.2 Ideality

The simplest measure of the length of a polymer chain is the contourlength L . This is the length of the stretched-out molecule, that is, for a chain of N bonds of length ℓ the contourlength is $N\ell$. However, this length does not give a realistic measure of the size of the polymer chain, which in a molten state or in a dilute solution is *coiled* up.

The conformational properties of long flexible chains can be described by the universal random walk model first introduced by Kuhn [33]. A chain is considered as a sequence of N randomly orientated bonds, each of length ℓ . If the bonds are completely independent of each other, the conformation of the polymer chain resembles the trajectory of a diffusing particle under the action of a random force, for which the solution is well known [21, 53]. If \mathbf{R} is the end-to-end vector of the linear macromolecule, the mean square displacement is given by

$$\langle R^2 \rangle = \ell^2 N \quad (1.1)$$

Therefore, the characteristic size⁴ R of the polymer is proportional to $N^{\frac{1}{2}}$. The probability

³The degree of polymerization, N is usually more than a hundred. For example, polymerization of $N \sim 10^4$ ethylene ($\text{CH}_2 = \text{CH}_2$) monomers will yield a giant polyethylene ($[-\text{CH}_2-]_N$) macromolecule. Imagine now that this molecule only had three possible bond rotations; then the total number of shapes it may assume will be $\sim 3^N$. Furthermore, the conformation is continuously changing due to thermal motion. A DNA molecule has $N \approx 10^9$ links. Detailed analysis of these configurations is futile! In order to investigate the properties of a system of molecules, it is beneficial to consider a macroscopic system. In the case of macromolecules, even a *single* molecule is a macroscopic system with infinitely many possible conformations. Consequently, we can calculate relevant thermodynamic quantities of even single polymer chains by means of statistical mechanics.

⁴For non-linear, branched or star-polymers the radius of gyration R_g , which is the root mean square distance of the segments from the centre of mass, is the appropriate quantity, and is given by $R_g^2 = \frac{1}{6} \ell^2 N$.

distribution of an ideal chain endpoint to be at a distance R from the initial point is given by the Gaussian probability function $P(R, N) \propto \exp\left(-\frac{3R^2}{2Nl^2}\right)$ [also see Section 2.1].

For ideal chains, the finite volume of the segments and solvency effects are completely ignored. In reality, segments cannot overlap — called volume exclusion — which leads to chain expansion. The statistics of real, non-intersecting chains are described by self-avoiding walks instead of random walks [8].

However, polymers can adopt *ideal* dimensions in solutions in a so-called Θ -solvent. In a good solvent, a chain expands from its unperturbed, ideal dimensions to maximize the number of *segment-solvent* contacts and the coil is said to be swollen. In a poor solvent, the chains will contract to minimize interactions with the solvent. However, competing with this effect is the tendency for chains to expand to reduce unfavourable *segment-segment* interactions (which is the excluded volume effect). If these two interactions are in balance, the polymer molecule will adopt unperturbed dimensions, and the solvent is said to be a Θ -solvent [8]. In short, if the concentration of molecules is high enough to be classified as a dense melt, the molecules will be forced to interpenetrate, so that (ideal) *screened* excluded-volume statistics may be assumed.

1.1.3 The Entropic Spring

The entropy of a macromolecule is described by the formula

$$S = k_B \ln \Omega, \quad (1.2)$$

where k_B is the Boltzmann constant and Ω is the number of possible conformations. When the chain is deformed, the entropy change ΔS is given by, $\Delta S = k_B \ln \Omega_\lambda / \Omega_0$, where the subscripts 0 and λ refer to the initial condition of no strain and the condition of the oriented state under stress, respectively.

Near an impenetrable surface, the geometric restriction leads to a *lower* conformational entropy of the polymer.

1.1.4 Elasticity

Rubberlike elasticity is the consequence of molecular arrangements — in other words — chain flexibility. This is quite different from the elasticity of ordinary solids such as pure metals and crystals, where the elasticity or the resistance to deformation under external force, arises from the distortion of the intermolecular potential fields. For macromolecules under strain, the intermolecular potential energy U remains nearly constant with or without strain [48]. The elastic driving force is therefore entirely from the tendency for macromolecules to randomize in order to attain the maximum entropy, and minimum free energy. For this reason, a macromolecule is often called the *entropic spring*. The entropy spring becomes stiffer at higher temperature T , since the tendency to randomize becomes stronger with more vigorous segmental Brownian motions like those of molecules in a liquid. This is in contrast with the behaviour of most crystalline solids in which the potential energy is weakened and the stiffness is diminished at higher temperatures as a consequence of thermal expansion, which moves atoms further apart.

The above discussion on polymer elasticity can be summarized in terms of a thermodynamic equation of state for the stress f , given by

$$f \propto \left(\frac{dF}{d\varepsilon} \right)_T = \underbrace{\left(\frac{dU}{d\varepsilon} \right)_T}_{\cong 0} - T \left(\frac{dS}{d\varepsilon} \right)_T, \quad (1.3)$$

where F is the Helmholtz free energy and ε is the length of the strained sample. For an ordinary solid, like a diamond, the reverse of (1.3) is true, that is, $T \left(\frac{dS}{d\varepsilon} \right)_T$ is zero.

1.1.5 Polymer Gels

Gels are macroscopic network polymers that have three-dimensional structures in which each chain is connected to all the others by a sequence of junction points, called crosslinks.

The crosslinks, *together* with the condition of chain flexibility, are responsible for rubber elasticity⁵. The classical theory of rubber elasticity [33] predicts that the free energy, \mathcal{F} of deformation is proportional to the sum of squares of the principal extension ratios:

$$\mathcal{F} = \frac{N_c k_B T}{V} \sum_{i=x,y,z} \lambda_i^2, \quad (1.4)$$

where N_c/V is the crosslink density of the network sample. A major discrepancy of this model is that it assumes an *affine* deformation: if a macroscopic rubber sample is deformed by λ , then the end-to-end vector \mathbf{R} of any subchain between two junction points will be equal to $\lambda \cdot \mathbf{R}$, after deformation. The affinity assumption implies that the crosslinks are spatially fixed, and do not fluctuate. In the James and Guth model [31], the crosslinks are essentially unrestricted, and the resultant free energy in (1.4) is altered by a factor of $\frac{1}{2}$. In 1975 a pioneering network model was introduced by Deam and Edwards [9], which models the effect of the network on a given chain by a harmonic localizing potential. In order to calculate the free energy of deformation, they resorted to the replica method from spin glass theory. The resultant Deam and Edwards free energy (4.66), again shows the same strain-dependency than (1.4), but with a different front factor and more terms depending on the crosslink density. In these *phantom* models, excluded volume interactions are ignored, and the polymer chains can pass through each other.

In reality, polymers displaying rubber elastic behaviour, will deviate from phantom models like (1.4) mainly due to the presence of chain entanglements [3]. A detailed review of the role of entanglements and attempts to understand these topological constraints, like the slip-link and tube models, can be found in [18, 32].

Although network models are numerous⁶, the demand for theoretical treatments of *surface-attached, confined* networks, has remained unfulfilled.

⁵This is the simplest view of a material that is expected to contain network inhomogeneities [38] and other defects, like trapped entanglements, which will alter its elastic behaviour.

⁶A recent review, and experimental comparison between different models of unconfined networks is given by [49].

1.2 Outline of chapters

The thesis is structured as follows. In Chapter 1 we present a single, free macromolecule that is subsequently confined in box and plate systems. Within this simple single chain-system we introduce the concept of a *stitch* and deterministic bulk and wall crosslinkages.

Chapter 2 deals with quenched disorder, due to random crosslinking, in the context of confinement and a simple stitch-network model.

In Chapter 3 the basic statistical crosslinking model for a confined, surface-attached model is presented. We extend the Deam and Edwards [9] phantom model, to include two parallel confining walls and the possibility of surface attachments or *wall-links*. This model treats the localizing effect of the crosslinks on the system, by a harmonic potential with a strength that is isotropic and strain-independent. In Chapter 4 we improve upon this assumption, by employing an inhomogeneous localization potential. For simplicity, this is done in the framework of a *brush-network*. In both models, we start by formulating the problem in the language of statistical mechanics and constructing the partition function. Thereafter, the free energy of deformation and the stress-strain equation are calculated.

In this thesis we adopt the philosophy of first finding a tractable theory, under reasonable assumptions, before attempting more realistic situations. The first simplification, used throughout this work, is the assumption of *ideal*, Gaussian chains. The omission of excluded-volume effects (in contrast with the neglect of trapped entanglements) from the theory, is still a laboratory-attainable assumption to make. These flexible, intersecting chains are illustrated throughout the text by kinky, spaghetti-like lines, emphasizing the fact that we are dealing with theoretic, simplified entities. The second assumption, is that of a sufficiently crosslinked network. This underlines the fact that we do not work near the so-called *sol-gel* (second-order) phase transition region [24].

In the last chapter we briefly conclude the work and give an outline of possible improvements and future developments.

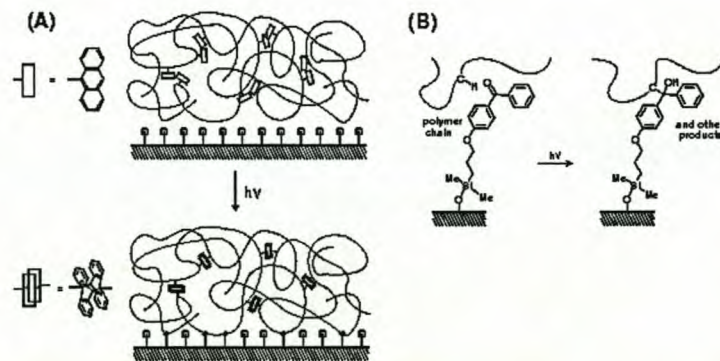


Figure 1.1: (A) A schematic description of the preparation of a surface-attached network by simultaneous photochemical crosslinking and surface attachment. (B) The photochemical reaction used for surface attachment. [Picture taken from [40].]

Chapter 2

The Single Confined Chain

Before we can probe the physics of a polymer network formed at a surface, we have to formulate the problem in terms of a specific mathematical model. In this chapter we present the fundamental concepts that we shall employ to construct such a model. A vital approach throughout is to use suitable Green's functions to investigate the statistical properties of the system. Using the Green's function approach, we firstly introduce a free Gaussian chain¹, and then place it in a confining environment. The behaviour of a macromolecule is determined by the number of different conformations it can take. By placing the polymer in a restricted geometry, only certain specific conformations are selected. After confining the chain, we link its two endpoints onto the confining surface. These surface links define the simplest case of *wall-links*, and restrict the confined polymer to an even greater extent. Lastly, we introduce a single polymer-polymer link, a so-called *bulk-link*, under very specific conditions.

The work in this chapter together with the prefatory treatment of disorder in Chapter 3 will serve as a platform for the full calculations.

2.1 A free Gaussian chain

One way of representing an ideal macromolecule is via the standard Gaussian or *bead-spring* model, Figure 2.1 (b). For the standard Gaussian model, the chain conformation is specified by the set $S = \{\mathbf{R}_0, \mathbf{R}_1, \dots, \mathbf{R}_N\}$ of N *beads*, which can be thought of as N repeating monomer units of the chain. The conformations of an ideal macromolecule coincide with the random walk path of a Brownian particle. Since Brownian motion is a Markovian process, the ideal chain also belongs to the class of Markov chains. Let $\psi(\mathbf{R}_n, \mathbf{R}_{n-1})$ represent the linear memory that describes the bonds between a pair of link neighbours. The memory of the chain direction is lost over a distance comparable to its persistence length² $\approx \ell$. The probability of a given polymer

¹We do not attempt to give a complete introduction to the mathematics of ideal chains, random flight polymers and the random walk analogy, as this will (and already does) expend many polymer theory textbooks [16, 53, 8, 13]. A comprehensive study of the Brownian chain and associated probability law is given in [12].

²The persistence length of a long, flexible, ideal chain is related to the effective Kuhn segment length ℓ of a freely jointed chain of $N = L/\ell$ segments, such that $\langle \mathbf{R}^2 \rangle = N\ell^2$. In the context of the Gaussian chain model, the Kuhn step length is defined by $\langle (\mathbf{R}_n - \mathbf{R}_{n-1})^2 \rangle = \ell^2$, and denoted by the term (RMS) *link length*.

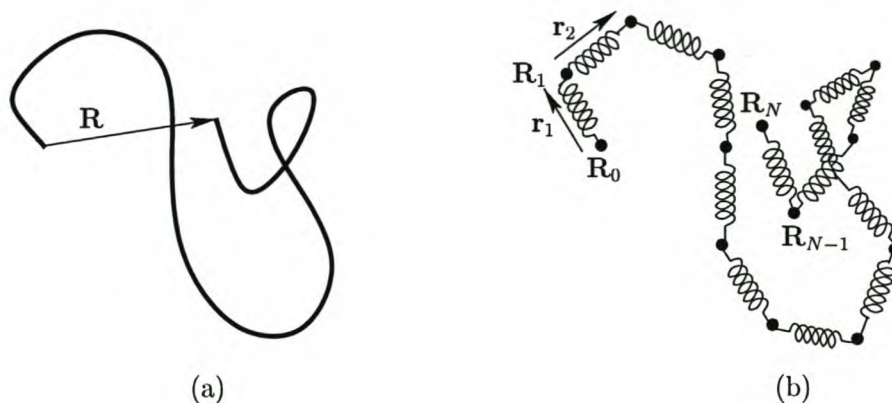


Figure 2.1: (a) An ideal, long flexible phantom chain, and (b) its Gaussian model counterpart. The shape of the polymer can be represented by the set of position vectors of the beads $S = \{\mathbf{R}_0, \mathbf{R}_1, \dots, \mathbf{R}_N\}$, or by the set of bond vectors $\{\mathbf{r}_1, \mathbf{r}_2, \dots, \mathbf{r}_N\}$, where $\mathbf{r}_n = \mathbf{R}_n - \mathbf{R}_{n-1}$. The end-to-end vector $\mathbf{R} = \mathbf{R}_N - \mathbf{R}_0$ characterizes the size of the chain.

shape S is thus given by $\Psi[S] = \prod_{n=1}^N \psi(\mathbf{R}_n, \mathbf{R}_{n-1})$, and represents the connectivity of the ideal macromolecule. For the bead-spring model, the bond lengths have the Gaussian distribution, such that $\psi(\mathbf{R}_n, \mathbf{R}_{n-1})$ is defined as follows:

$$\psi(\mathbf{R}_n, \mathbf{R}_{n-1}) = \left(\frac{3}{2\pi\ell^2} \right)^{\frac{3}{2}} \exp \left\{ -\frac{3}{2\ell^2} (\mathbf{R}_n - \mathbf{R}_{n-1})^2 \right\}. \quad (2.1)$$

The partition function is computed by integrating the distribution $\Psi[S]$ over all possible conformations [8].

When the chain is very long, the monomer index n may be regarded as a continuous variable. In this continuous representation, the discrete bond vector $\mathbf{r}_n = \mathbf{R}_n - \mathbf{R}_{n-1}$ is replaced by the functional derivative $\partial\mathbf{R}_n/\partial n$ [16]. If the endpoints of the macromolecule are fixed, at say positions \mathbf{r} and \mathbf{r}' in space, the partition function is the Wiener path integral

$$G(\mathbf{r}, \mathbf{r}', N) = \mathcal{N} \int_{\mathbf{R}(0)=\mathbf{r}'}^{\mathbf{R}(N)=\mathbf{r}} [\mathcal{D}\mathbf{R}] \exp \left\{ -\frac{3}{2\ell^2} \int_0^N \left(\frac{\partial\mathbf{R}_n}{\partial n} \right)^2 dn \right\}, \quad (2.2)$$

which is a Green's function and a solution of the following diffusion type equation:

$$\left[\frac{\partial}{\partial N} - \frac{\ell^2}{6} \frac{\partial^2}{\partial \mathbf{r}^2} \right] G(\mathbf{r}, \mathbf{r}'; N) = \delta(\mathbf{r} - \mathbf{r}') \delta(N). \quad (2.3)$$

The solution of (2.2) or (2.3) is the Gaussian distribution, given by

$$G(\mathbf{r}, \mathbf{r}'; N) = \left(\frac{3}{2\pi\ell^2 N} \right)^{3/2} \exp \left\{ -\frac{3}{2\ell^2} \frac{(\mathbf{r} - \mathbf{r}')^2}{N} \right\}. \quad (2.4)$$

If all interactions are neglected, a free polymer chain is characterized by an average end-to-end length of $R = \langle \mathbf{R}^2 \rangle = \ell N^{\frac{1}{2}}$. The number of configurations of a free, ideal chain between points \mathbf{r}'

and \mathbf{r} and chain contourlength L between those points thus corresponds to the statistical weight of a random walk starting at position \mathbf{r}' and ending at \mathbf{r} , in $N = L/\ell$ steps, where ℓ is the Kuhn step-length of a polymer chain.

2.2 A Single Chain in a Box

Consider a phantom molecule confined in a box of volume $V = h^2 h_z$, with length h in the x and y directions, and h_z in the z -direction. The statistical weight of the confined polymer chain which starts at \mathbf{r}' and ends at \mathbf{r} in N steps is given by the Green's function $G(\mathbf{r}, \mathbf{r}'; N)$, written as a Wiener path integral [16] :

$$G(\mathbf{r}, \mathbf{r}'; N) = \mathcal{N} \int_{\mathbf{R}(0)=\mathbf{r}'}^{\mathbf{R}(N)=\mathbf{r}} [\mathcal{D}_{\text{box}} \mathbf{R}] \exp \left\{ -\frac{3}{2\ell^2} \int_0^N \left(\frac{\partial \mathbf{R}_n}{\partial n} \right)^2 dn \right\}, \quad (2.5)$$

where the normalization \mathcal{N} refers to the number of configurations, (2.4) of a completely free polymer chain, starting at \mathbf{r}' and ending at \mathbf{r} in N steps, with Kuhn step length ℓ . The notation $\mathcal{D}_{\text{box}} \mathbf{R}$ means evaluating the path integral only in the allowable box-region. In terms of an attractive potential A , the Green's function (2.5) can be written in terms of unconfined integration [22],

$$G(\mathbf{r}, \mathbf{r}'; N) = \mathcal{N} \int_{\mathbf{R}(0)=\mathbf{r}'}^{\mathbf{R}(N)=\mathbf{r}} [\mathcal{D} \mathbf{R}] \exp \left\{ -\frac{3}{2\ell^2} \int_0^N \dot{\mathbf{R}}_n^2 dn + \int_0^N A(\mathbf{R}_n) dn \right\}, \quad (2.6)$$

where

$$A(\mathbf{R}, n) \equiv \ln \Theta(\mathbf{R}_n), \quad \text{with} \quad \Theta(\mathbf{R}) = \begin{cases} 1 & \text{if } \mathbf{R} \text{ in } V \\ 0 & \text{otherwise} \end{cases} \quad (2.7)$$

represents an infinite potential wall. The solution of (2.5) is equivalent to solving the inhomogeneous differential equation

$$\left[\frac{\partial}{\partial N} - \frac{\ell^2}{6} \frac{\partial^2}{\partial \mathbf{r}^2} - A(\mathbf{r}, N) \right] G(\mathbf{r}, \mathbf{r}'; N) = \delta(\mathbf{r} - \mathbf{r}') \delta(N), \quad (2.8)$$

which, with the substitution of the potential A in (2.7), simplifies to a diffusion equation of the form given by equation (2.3), together with the boundary condition that $G(\mathbf{r}, \mathbf{r}'; N) = 0$ at the confining surface. The solution G is constructed from eigenfunctions that vanish on and outside the boundaries of the box³. The coordinates are separable

$$G(\mathbf{r}, \mathbf{r}'; N) = G_x(x, x'; N) G_y(y, y'; N) G_z(z, z'; N), \quad (2.9)$$

³The solution was obtained by using an eigenfunction expansion method [35], but can also be obtained by using the method of images [5].

and since the polymer in a box is a symmetric problem, all the parts, for example G_x , have the same form:

$$G_x(x, x'; N) = \frac{2}{h} \sum_{p_x=1}^{\infty} \sin \frac{p_x \pi x}{h} \sin \frac{p_x \pi x'}{h} \exp \left(-\frac{\ell^2 \pi^2}{6 h^2} p_x^2 N \right). \quad (2.10)$$

Equation (2.9) is the probability that one endpoint ($n = N$) of a box-confined polymer is \mathbf{r} , provided that the other endpoint ($n = 0$) is at \mathbf{r}' . The partition function of all possible conformations, for a polymer with *endpoints free*, is given by

$$\mathcal{Z} = \int d\mathbf{r} \int d\mathbf{r}' G(\mathbf{r}, \mathbf{r}'; N) \quad (2.11)$$

$$= \left(\frac{2}{\pi} \right)^6 \sum_{p_x, p_y, p_z=1,3,\dots}^{\infty} \left(\frac{8 h^2 h_z}{p_x^2 p_y^2 p_z^2} \right) \exp \left\{ -\frac{\ell^2 \pi^2 N}{6} \left[\frac{(p_x^2 + p_y^2)}{h^2} + \frac{p_z^2}{h_z^2} \right] \right\}. \quad (2.12)$$

The endpoints of the confined molecule in (2.12) are not *fixed* at positions somewhere in the box or at the boundaries, as will be the case in the next section.

2.3 A polymer *stitch*

Next we add two wall-links to the system by linking the ends of the polymer to the top and bottom planes of the box, creating a polymer *stitch*, as illustrated in Figure 2.2. We are interested

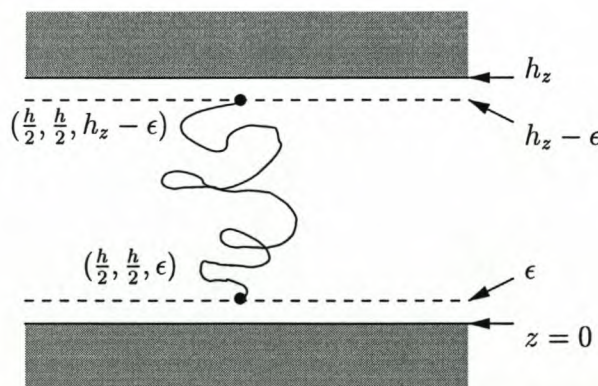


Figure 2.2: A single polymer chain "stitch" with end-points held at two fixed points

in the partition function of a single polymer chain *stitch* in a box with volume $V = h^2 h_z$. To this end, we fix the end points of the chain a small distance ϵ from the floor and lid of the box⁴, permanently, at

$$\mathbf{r}' = \left(\frac{h}{2}, \frac{h}{2}, \epsilon \right) \quad \text{and} \quad \mathbf{r} = \left(\frac{h}{2}, \frac{h}{2}, h_z - \epsilon \right), \quad (2.13)$$

⁴Instead of a polymer that is cross-linked *exactly* on the wall, we have localized the wall cross-link a distance ϵ , of the order of the link length ℓ , away from the walls, otherwise the partition function for the polymer vanishes as should be expected.

By substituting these coordinates in equation (2.9) and (2.10), we obtain the partition function for a *stitch* confined in a box:

$$\mathcal{Z}(\mathbf{r}, \mathbf{r}'; N) = Z_{x,y}(N, h) Z_z(N, h_z), \quad (2.14)$$

with its three Cartesian parts written as follows:

$$Z_{x,y}(N, h) = \left(\frac{2}{h}\right)^2 \sum_{p_x, p_y=1,3,\dots}^{\infty} \exp\left\{-\frac{\ell^2 \pi^2}{6 h^2} (p_x^2 + p_y^2) N\right\}, \quad (2.15)$$

$$Z_z(N, h_z) = \frac{2}{h_z} \sum_{p_z=1}^{\infty} \sin\left(\frac{\pi p_z \epsilon}{h_z}\right) \sin\left(\frac{\pi p_z [h_z - \epsilon]}{h_z}\right) e^{-\frac{\ell^2 \pi^2}{6 h_z^2} p_z^2 N}. \quad (2.16)$$

It is at this point necessary to look at the relationships that exist between the box dimensions, h_z and h and the length scale of the polymer $\sqrt{N}\ell$.

2.3.1 Three limiting cases

The relationship between the confining box dimension, h and h_z , and the size of the chain $\sqrt{N}\ell$ determines the type of physical situation we are facing. It will also dictate in which of these limits future calculations will be done. There exist three distinct limits:

$$(i) \quad \sqrt{N}\ell \ll h_z \ll h \quad (2.17)$$

$$(ii) \quad h_z \ll \sqrt{N}\ell \ll h \quad (2.18)$$

$$(iii) \quad h_z \ll \sqrt{N}\ell \quad \text{and} \quad h \ll \sqrt{N}\ell, \quad (2.19)$$

depicted graphically in Figure 2.3. In the first case (i) (2.17), we have a small polymer in a large

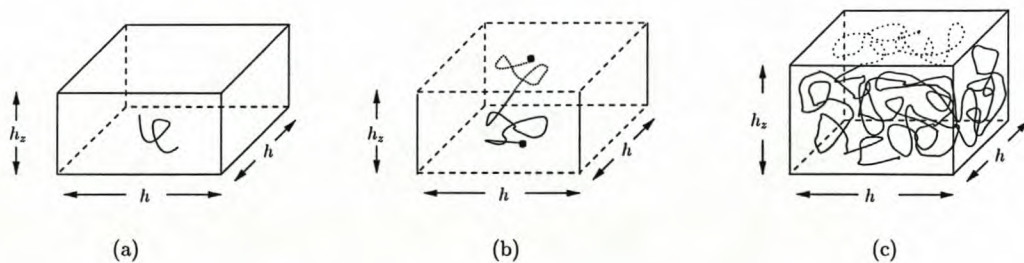


Figure 2.3: Relationship between the size of the polymer and confinement dimensions: (a) A small polymer in a big box, (2.17); (b) Polymer big enough to be a stitch, (2.18); (c) A large polymer, densely occupying the box, (2.19).

confining environment, which intuitively means that it will be very difficult to fix the endpoints a distance h_z from each other. This difficulty is portrayed by the sum argument in (2.16), which in this case oscillates rapidly around zero. Physically, (i) is analogous to a *short* random walk in a *large* cavity [26]. Since the polymer is too small to fix at the top and bottom faces of the confining box, we investigate the original partition function (2.11), for a polymer with *free* ends. Since the characteristic chain size R is small relative to the box dimensions, the sums in the

partition function (2.12) will be dominated by $\frac{1}{p^2}$ terms [16]. In this limit⁵, the free energy F is like that of a perfect gas, with corresponding pressure P , given by:

$$F \approx -k_B T \ln V, \quad \text{and} \quad P = \frac{\partial F}{\partial V} \Rightarrow PV = k_B T. \quad (2.20)$$

In the second relation (ii) (2.18) the stretched out chain is small compared with h , but long enough to reach the endpoint cross-link locations in the \hat{z} direction. The sum in $Z(N, h_z)$ in (2.16) is then entirely dominated by the $p_z = 1$ term, so that the h_z -dependent part is given by:

$$Z_z(N, h_z, \lambda) \cong \frac{2}{h_z} \sin \left[\frac{\pi \epsilon}{h_z} \right] \sin \left[\frac{\pi(h_z - \epsilon)}{h_z} \right] e^{-\frac{\ell^2 \pi^2}{6 h_z^2} N}. \quad (2.21)$$

On the other hand, a continuous Gaussian approximation compares well with the sum over p_x and p_y in (2.15), that is:

$$Z_{x,y}(N, h) \cong \left(\frac{1}{2} \right)^2 \left(\frac{2}{h} \right)^2 \int_0^\infty \int_0^\infty e^{-\frac{N \ell^2 \pi^2 (\rho_x^2 + \rho_y^2)}{6 h^2}} d\rho_x d\rho_y \quad (2.22)$$

$$= \frac{3}{2\pi \ell^2 N}, \quad (2.23)$$

which is the same as not restricting the \hat{x} and \hat{y} dimensions *at all*, and describing each of these components of the chain by a free chain Green's function (2.4). In this limit of sufficiently large h , and infinitesimal ϵ , the problem is equivalent to a chain restricted between two parallel plane surfaces with an h -independent partition function,

$$\mathcal{Z}(h_z) \simeq \frac{\pi \epsilon^2}{3N \ell^2 h_z^3} \exp \left(-\frac{N \ell^2 \pi^2}{6 h_z^2} \right) \iff \text{limit (ii)} \quad [h_z \ll \sqrt{N} \ell \ll h]. \quad (2.24)$$

In the third relation (iii) (2.19) the polymer contourlength is large compared with both h and h_z . Consequently, the dominating contribution to the sums in (2.15) and (2.16), is given by the $p_x = p_y = p_z = 1$ term, leading to a partition function (in the limit of small ϵ),

$$\mathcal{Z}(h, h_z) \simeq \frac{8\pi^2 \epsilon^2}{h^2 h_z^3} \exp \left\{ -\frac{N \ell^2 \pi^2}{6} \left(\frac{2}{h^2} + \frac{1}{h_z^2} \right) \right\} \iff \text{limit (iii)} \quad [h_z \ll h \ll \sqrt{N} \ell], \quad (2.25)$$

which is dependent on all the parameters of the confinement. In this instance the single polymer chain will tend to *fill* up all the available space.

2.4 *Stitch* Strains

The mechanical properties of a polymer *stitch* may be investigated by looking at what happens during strain. It is possible to characterize the stress acting at a point on a substance in terms of

⁵If $\sqrt{N} \ell \ll h_i$, the partition function $\mathcal{Z} \simeq h^2 h_z \equiv V$, since $\exp\{-\frac{1}{6} \pi^2 p_i^2 (\frac{\sqrt{N} \ell}{h_i})^2\} \simeq 1$, $i = \{x, y, z\}$. The remaining sum is then of the form $\sum_{p=1,3,\dots}^\infty 1/p^2$, which converges to $\frac{\pi^2}{8}$.

three *principal* stresses or extension ratios, acting along mutually perpendicular principal axes [48, 54]. The extension ratio λ_i is defined as the deformed length in direction \hat{i} divided by the original length of the sample [47].

In principle there are many possible deformations that can be employed to verify the predictive ability of theoretical elastomer models describing stress-strain behaviour. However, in practice it is uniaxial deformation that is most often studied, due to its experimental simplicity⁶.

An important characteristic of macromolecules in the gel state is that any type of applied stress will most readily influence the gel's shape, without appreciably changing its volume [46, 48]. This observation has led to the terminology *incompressible* or *indilatable* to describe the mechanical behaviour of gels. In most cases we shall thus be concerned with an *isovolumetric*, uniaxial deformation (2.26), where an elongation (compression) by a factor λ along the \hat{z} axis results in compression (dilation) by a factor $1/\sqrt{\lambda}$ along the other axes. The tensor Λ expresses the isovolumetric, uniaxial (macroscopic) deformation of a point $\mathbf{r} \rightarrow \mathbf{r}' = \Lambda \cdot \mathbf{r}$,

$$\Lambda = \begin{pmatrix} \lambda^{-\frac{1}{2}} & 0 & 0 \\ 0 & \lambda^{-\frac{1}{2}} & 0 \\ 0 & 0 & \lambda \end{pmatrix}, \quad \lambda > 0. \quad (2.26)$$

The fundamental property of polymer gels, namely the constancy of volume during deformation, makes it possible to define the complete state of strain in terms of a single parameter λ .

2.4.1 Case 1: Deforming the plate system

Firstly, we investigate the effect of strain, defined by Λ , on a macromolecule linked at fixed positions to two parallel plates (Figure 2.4). This situation corresponds to limit (ii) with $h \rightarrow \infty$. In this case it is appropriate to use the partition function \mathcal{Z} , already derived in (2.24), to calculate

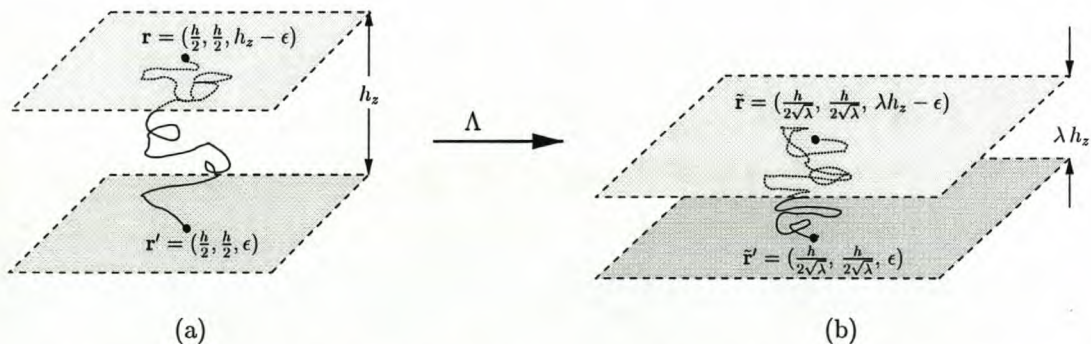


Figure 2.4: Polymer stitch in the (a) the unstrained state; (b) strained (unidirectional compression) state, confined between two long parallel plates, corresponding to limit (ii).

⁶However, only general *bi*-axial strains cover all accessible pure homogeneous deformations for an incompressible material, and is the preferred method of testing real network theories that account for topological features like trapped entanglements [49].

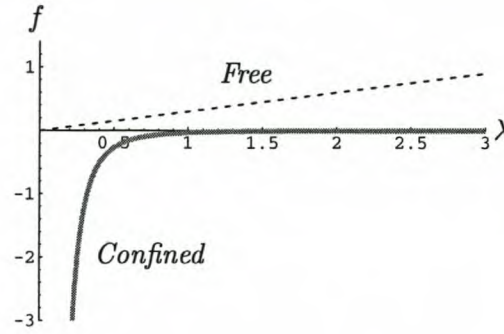


Figure 2.5: Plot of the stress f (2.31) versus the deformation ratio λ for a plate system, in limit (ii). The solid line is for a stitch confined between the plates; the dashed line corresponds to a free chain (with fixed endpoints). Since the free energy was evaluated in the limit (ii), only small elongations, $\lambda h_z \ll \sqrt{N}\ell$ are allowed.

the free energy of the plate-system as follows:

$$F = -k_B T \ln \mathcal{Z}(h_z) \quad (2.27)$$

$$= -k_B T \ln \left[\frac{\pi \epsilon^2}{3N\ell^2 h_z^3} \right] + \frac{k_B T N \pi^2 \ell^2}{6h_z^2}. \quad (2.28)$$

If we perform a simple elongation ($\lambda > 1$) or compression ($\lambda < 1$), the change in free energy is given by:

$$\Delta F = k_B T \ln \lambda + \frac{k_B T N \pi^2 \ell^2}{6h_z^2} \left(\frac{1}{\lambda^2} - 1 \right), \quad (2.29)$$

which has similar characteristics to that of De Gennes' scaling theory calculation [8] for the energy required to squeeze an ideal chain (of unperturbed size R_0) trapped in a tube or cavity of diameter h_z :

$$\Delta F_{\text{deGennes}} \cong k_B T \frac{R_0^2}{h_z^2}, \quad R_0 = N^{\frac{1}{2}} \ell. \quad (2.30)$$

The free energy of the form in (2.30) holds generally for any type of ideal chain confinement [26]. It originates from the decrease in the number of available conformations — or lowering of the entropy — when the polymer is restricted. The only force acting on the system during strain is the tensile force in the direction of extension (or compression) λ . The magnitude of the force per unit cross-sectional area measured in the unstrained state, depicted in Figure 2.5, is given by

$$f = \frac{1}{V} \frac{\partial(\Delta F)}{\partial \lambda} = \frac{k_B T}{V} \left(\frac{1}{\lambda} - \frac{N\pi^2 \ell^2}{3h_z^2} \frac{1}{\lambda^3} \right). \quad (2.31)$$

An alternative way to model a *stitch* is to simulate the effect of the wall confinement by a simple harmonic potential [1]. If the potential is $U = \frac{q^2 \ell^2}{6} \int_0^N \mathbf{R}^2 dn$, the wall-confinement is enforced by choosing the localization parameter to be of the form $q \simeq h_z^{-\frac{1}{2}}$. The partition function in

this case is analogous to the propagator⁷ of a particle in an harmonic potential, with initial and terminal points of its trajectory fixed on one of the plates [19]. The elastic free energy calculated from the harmonic approximation is consistent with (2.29), and confirms the form of the stress-strain graph, Figure 2.5.

When an *unconfined* ideal chain (2.4) is deformed from an end-to-end length h_z to λh_z , its end links will undergo an external stretching force of magnitude $f = k_B T \frac{3\lambda h_z^2}{N\ell^2}$ [8, 26]. The important difference between a confined and unconfined polymer *stitch*, is illustrated by the stress-strain relationship in Figure 2.5.

2.4.2 Case 2: Deforming the box system

Secondly, we investigate the effect of strain, defined by Λ , on a macromolecule in the limit (iii), $\sqrt{N}\ell \gg h$, as shown in Figure 2.6. In this limit it is appropriate to perform calculations using the partition function already derived in (2.25).

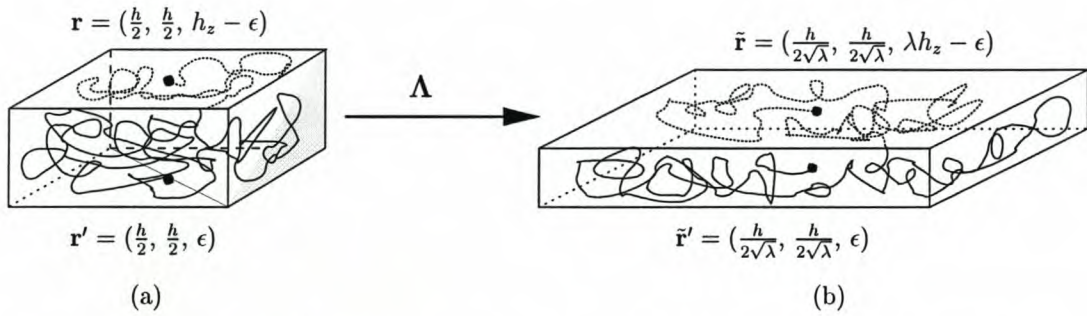


Figure 2.6: Polymer stitch in the (a) the unstrained state; (b) strained (unidirectional compression) state, in the limit (iii).

It is found that the work done to strain the system,

$$\Delta F = \frac{1}{6} k_B T N \ell^2 \pi^2 \left(\frac{2\lambda - 1}{h^2} + \left(\frac{1}{\lambda^2} - 1 \right) \frac{1}{h_z^2} \right), \quad (2.32)$$

is both h and h_z dependent. The only force acting on the system during strain is the tensile force in the direction of extension (or compression) λ . The stress-strain relationship is given by

$$f = \frac{1}{V} \frac{\partial(\Delta F)}{\partial \lambda} = \frac{k_B T N \ell^2 \pi^2}{3V} \left(\frac{1}{h^2} - \frac{1}{\lambda^3 h_z^2} \right) \quad (2.33)$$

and is only valid for small elongations $\lambda h_i \ll \sqrt{N}\ell$. Both elongation ($\lambda > 1$) and compression ($\lambda < 1$) is represented by a single curve on the next page (Figure 2.7), illustrating the theoretical relationship between force (stress) and λ when relation (iii) holds.

⁷Similar calculations that employ a Green's function solution for a harmonic localization of the crosslinks, is given in more detail in Chapter 4.

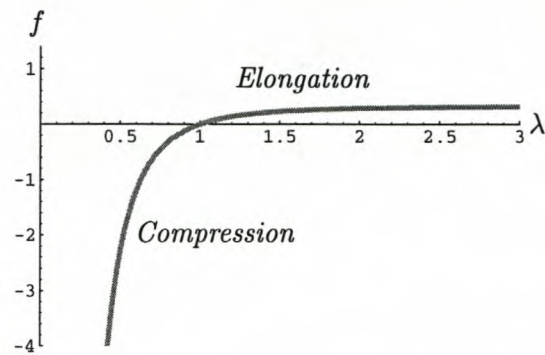


Figure 2.7: Plot of the stress (f) (2.33) versus the deformation ratio (λ), in limit (iii) when $h \ll \sqrt{N}\ell$, for a long polymer confined in a box.

2.5 One bulk-link

Consider two, identical macromolecule *stitches*, each of length $L = N\ell$, confined between two parallel plates, in Figure 2.8(a). Next, the chains are joined together permanently at position \mathbf{R} ,

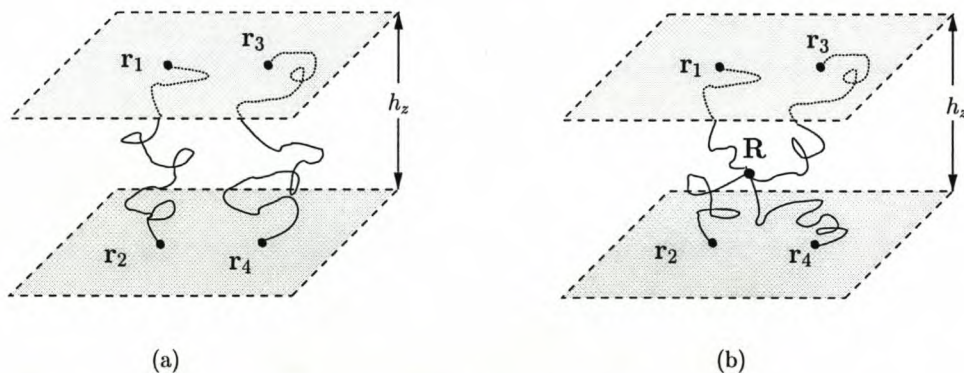


Figure 2.8: Two polymer stitches, (a) without a junction point; (b) with a junction point at $\mathbf{R} = (X, Y, Z)$. The wall links are situated at permanent points, $\mathbf{r}_1 = (x_1, y_1, h_z - \epsilon)$, $\mathbf{r}_2 = (x_2, y_2, \epsilon)$, $\mathbf{r}_3 = (x_3, y_3, h_z - \epsilon)$ and $\mathbf{r}_4 = (x_4, y_4, \epsilon)$.

such that both chains meet at half of their respective contourlengths, $\frac{1}{2}N$. We obtain a system consisting of four wall-links and one bulk-link, as shown in Figure 2.8 (b). The partition function for the system is thus the statistical weight of one large star polymer⁸ of total length $2L$. The statistical weight is determined by averaging over all possible positions of the junction point \mathbf{R} for the four half-chains [16], that is:

$$\mathcal{Z} = \int d\mathbf{R} G(\mathbf{r}_1, \mathbf{R}; \frac{N}{2}) G(\mathbf{R}, \mathbf{r}_2; \frac{N}{2}) G(\mathbf{r}_3, \mathbf{R}; \frac{N}{2}) G(\mathbf{R}, \mathbf{r}_4; \frac{N}{2}), \quad (2.34)$$

⁸A regular n -star polymer is a macromolecule containing a single branch point from which n linear chains (identical with respect to constitution and degree of polymerization) emanate [26]. The size of such a macromolecule is described by the mean square of the radius of gyration: $R_{g4 \text{ arms}}^2 = \frac{5}{4} N\ell^2/6$.

with the points \mathbf{r}_1 , \mathbf{r}_2 , \mathbf{r}_3 and \mathbf{r}_4 at fixed positions on the plates, shown in Figure 2.8 (b). The Green's function $G(\mathbf{r}_1, \mathbf{R}; \frac{N}{2})$ represents the statistical weight of a chain portion which starts at \mathbf{r}_1 and ends at \mathbf{R} in $\frac{N}{2}$ steps. Since the chains are only confined in the \hat{z} dimension, each Green's function G is the product of two free chain contributions, (2.4) and one confined statistical weight contribution (2.10), for example:

$$G(\mathbf{r}_1, \mathbf{R}; \frac{N}{2}) = G_x(x_1, X; \frac{N}{2}) G_y(y_1, Y; \frac{N}{2}) G_z(z_1, Z; \frac{N}{2}) \quad (2.35)$$

$$= \frac{3}{\pi \ell^2 N} \exp \left\{ -\frac{3}{N \ell^2} \left((X - x_1)^2 + (Y - y_1)^2 \right) \right\} \\ \times \frac{2}{h_z} \sum_{p=1}^{\infty} \sin \frac{\pi p Z}{h_z} \sin \frac{\pi p (h_z - \epsilon)}{h_z} e^{-\frac{\ell^2 \pi^2 p^2}{12 h_z^2} N}. \quad (2.36)$$

If this one-link system is strained by simple elongation Λ , as defined in (2.26), the change in free energy is given by

$$\Delta F = -k_B T \ln \frac{Z_\lambda}{Z_1}, \quad (2.37)$$

where Z_λ denotes the strained and Z_1 the unstrained states of the system, defined in (2.34). In the limit (ii), $\sqrt{N} \ell > h_z \gg \epsilon$, equation (2.37) reduces to:

$$\Delta F \simeq k_B T \left\{ 7 \ln \lambda + \frac{\ell \pi^2 N}{3 h_z^2} \left(\frac{1}{\lambda^2} - 1 \right) \right. \\ \left. + \frac{3}{N \ell^2} \underbrace{\left[\left(\sum_{i=1}^4 (x_i^2 + y_i^2) \right) - \frac{1}{4} \left(\sum x_i \right)^2 - \frac{1}{4} \left(\sum y_i \right)^2 \right]}_{\equiv d^2} \left(\frac{1}{\lambda} - 1 \right) \right\}, \quad (2.38)$$

with d^2 depending on the chosen, albeit fixed, relationship of the wall linkages. The constant d^2 is translation invariant and ought not play a dominant role, since the problem is symmetric in the \hat{x} and \hat{y} coordinates⁹. However, for the above expression to be valid in the limit (2.18), one must limit the distance between wall links for this two-stitch system. This can most easily be seen, when the number of coordinate constants x_i and y_i is reduced, such that $x_1 = x_2 \equiv x_a$ and $x_3 = x_4 \equiv x_b$. In this case $d^2 = (x_a - x_b)^2 + (y_a - y_b)^2$, and gives a measure of the distance between two wall-linkages on each plate. The entropy of the system will thus increase as the distance between points \mathbf{r}_a and \mathbf{r}_b decreases (Figure 2.9). Conversely, when d , or the distance between wall-links in the x - y plane, increases, the chain portions are more stretched out and fewer configurations are available to the polymer.

When the stress f is calculated in the manner of (2.31), we obtain a stress-strain relationship

⁹The deformation factor $(1/\lambda - 1)$ after the constant d^2 is zero if the plates are simply stretched in the \hat{z} coordinate by a factor λ . In Equation (2.38) d^2 is present since an (optional) *isovolumetric* deformation was enforced.

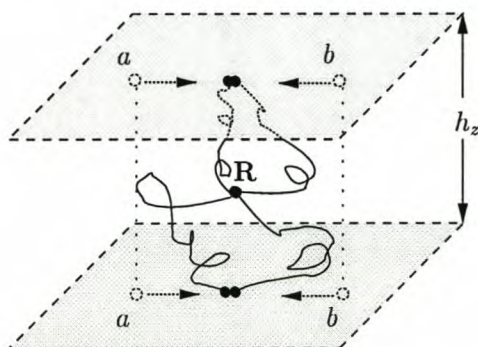


Figure 2.9: Two polymer stitches with a junction point at $\mathbf{R} = (X, Y, Z)$. The top and bottom wall links are situated at permanent positions with equal x and y coordinates, such that the left links have coordinates (x_a, y_a, ϵ) and $(x_a, y_a, h_z - \epsilon)$, and the right has coordinates (x_b, y_b, ϵ) and $(x_b, y_b, h_z - \epsilon)$, for top and bottom plates, respectively. The arrows show movement of the fixed links to a common position that correspond to maximum entropy.

similar to (2.31):

$$f_{\text{link}} = \frac{k_B T}{V} \left(\frac{7}{\lambda} - \frac{2N\pi^2\ell^2}{3h_z^2} \frac{1}{\lambda^3} - \frac{3d}{N\ell^2} \frac{1}{\lambda^2} \right). \quad (2.39)$$

The coefficient of the confinement term in (2.39), $\frac{2N\pi^2\ell^2}{3h_z^2}$ has increased by a factor two compared to (2.31), which portrays the relative difficulty in deforming a system consisting of two chains with an added bulk linkage. Also, if we let $d^2 \equiv 0$, we recover the case of only two wall-links. Since $d^2 \ll \sqrt{N}\ell$, the second term in (2.39) will dominate, such that the stress f_{link} will not differ much from f for the simple stitch system (Figure 2.5). This is illustrated by a similar stress-strain plot of (2.39), shown in comparison with the classic stress-strain curve for an unconfined “network” of only one bulk-link (and no wall-links) [48].

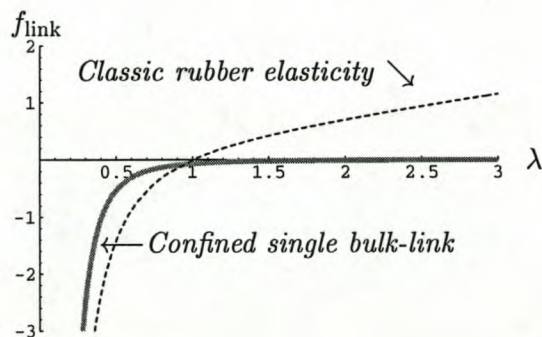


Figure 2.10: Plot of the stress (f_{link}) (2.39) versus the deformation ratio (λ) for the confined, single bulk-link plate system (solid line), in limit (ii). The dashed line is the stress-strain curve corresponding to the classic rubber elasticity model, with $f \propto \lambda - 1/\lambda^2$, for only one bulk link.

2.6 Contemplating stitches

In this chapter we briefly introduced the basic concepts which play a part in the formation of a network at a surface: the Gaussian chain, confinement, homogeneous strain, wall-links and lastly a *non-random*, single bulk link.

Confinement reduces the number of possible chain shapes, and decreases the entropy. In a confined chain, the role of the characteristic chain dimension R_0 is reversed, relative to its free chain counterpart. This leads to a chain which does not obey the Hooke “law” for stretching, so typical of an ideal chain.

Since the Green’s function of confinement included intractable sums, we were forced to work in certain limits, most notably, $h_z \ll \sqrt{N}l$. Consequently the stitches were not allowed to stretch too much. This restraining condition also applies to an unconfined phantom chain. Its force-extension relation is subject to the same limitations as the Gaussian distribution function from which it is derived. For end-to-end extensions approaching the total contourlength of the chain, the Gaussian approximation becomes progressively inaccurate, and will fail if $\lambda_{\max} \sim \sqrt{N}$.

It might be a reasonable, first approximation to simulate the real network (discussed in the Introduction) by a *network* of stitches: two parallel planar surfaces stitched together, with the possibility of link-formation in the bulk region between the plates. If we envisage such a network, restricted between two walls, we should work in the limit (2.18) since the *stitch*-system has only confinement in one coordinate (as opposed to a box-confinement). Each chain must also be large enough so that it can be fixed to opposite walls with ease. These links are formed an infinitesimal distance ϵ from the walls. It was shown, for example in Section 2.4, that ϵ does not influence the macroscopic properties of the system.

During network formation, crosslinkages are formed at random. However, in this chapter we placed them at completely deterministic positions. This discrepancy will be attended to in the next chapter.

Chapter 3

The Stitch Network

How does one model a system with permanent, but random, constraints?

In this thesis we are investigating the properties of a polymer gel, formed at a surface. The gel consists of long macromolecules that form cross links with the surface, in addition to the polymer-polymer links. We specifically consider a gel confined between two parallel plane surfaces. This symmetric problem is related to two plates, which are *stitched* together by very long chain threads as shown in Figure 3.1. In the previous chapter we isolated one long thread, and fixed its terminal ends to the top and bottom confining plates. This was called a *stitch*. We included a *mock* bulk link that had its exact location on the chains, chosen beforehand. In a real network, the precise location of the linkages is *not* known beforehand, and will tend to vary from one sample to the next. Any realistic network model should thus take account of this randomness.

In the present chapter we shall apply the replica method to the stitch network model to show how one can describe and handle random cross-linking mathematically.

3.1 A random bulk link

The first crucial step is to rectify the assumption of a *given* bulk link (Section 2.5) by making it random. Let s measure the arc length, $s \in [0, L]$, along a Gaussian chain of contour length¹ L . We simplify the toy model of stitches by having specific, but arbitrarily placed wall links.

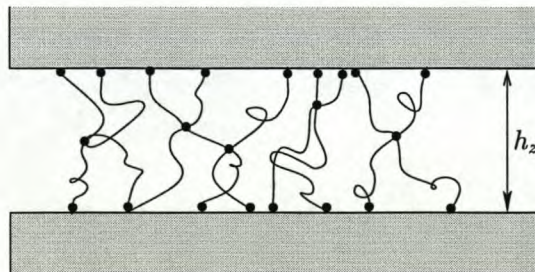


Figure 3.1: A polymer network of stitches, confined between two plates of spacing h_z .

¹In terms of the notation previously used, $s = n\ell$, such that $L = N\ell$, where ℓ is the average link length introduced in Section 2.2.

They are always chosen to be at the terminal points, corresponding to $s = 0$ and $s = L$, of the polymer chain. We choose to divide the stitch network into a macroscopic number of, say M , subsystems, each having one random bulk link. The total free energy of the stitch network system would then consist of the sum of the free energies of the M subsystems, plus a contribution that comes from the interactions of the subsystems. For a system of phantom chains, we shall ignore any interactions.

We continue by isolating a subsystem, a portion of the stitch network, as follows. Consider two stitches, each of length $L = N\ell$, confined between two walls of spacing h_z , illustrated in Figure 3.2.

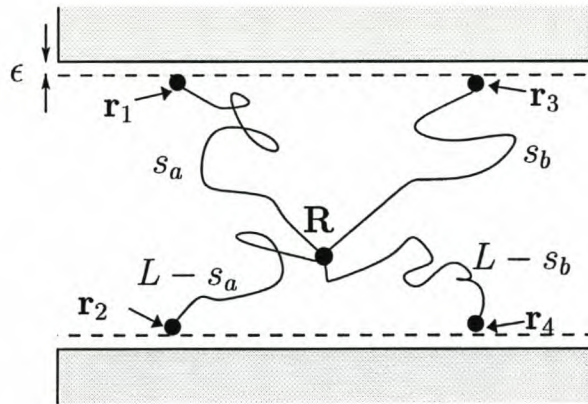


Figure 3.2: A portion of the stitch network, as seen in isolation, consisting of two stitches linked at spatial position \mathbf{R} .

The wall links are formed an infinitesimal distance ϵ from the walls², at spatial positions \mathbf{r}_1 , \mathbf{r}_2 , \mathbf{r}_3 and \mathbf{r}_4 , which do *not* vary from sample to sample. The bulk link is formed at a *random* arc length location s_a and s_b on the two chains. This random linking is the source of the disorder in the system. Intuitively, any relevant observable of the stitch-system should depend on some general averaged characteristics of the random crosslinking.

The main goal of this chapter is to *introduce* general methods for dealing systematically with the statistical mechanics of a random system. For the simple case of one bulk link, it might not seem worthwhile to employ strategies like the replica method (Section 3.2.3). This is especially the case when the crosslinkages are distributed uniformly.

In the sections that follow we adapt the basic Green's function approach, developed in Chapter 2, to a system with disorder.

²The parameter ϵ does not influence the physical properties of the system. For example, the stress-strain relationship is entirely independent of ϵ , as investigated in section 2.4.

3.2 Quenched disorder

In Chapter 2 we used standard statistical averaging to compute the free energy of the system at a *given* cross linking position. For a real network, the linkage positions $\{S\}$ on the chains are unknown, but we will assume that they are variables which vary randomly from sample to sample – called quenched variables – distributed according to a probability distribution $P(S)$. Statistical physics averages that are generally employed, should be altered for quenched variables.

3.2.1 Green's functions

The partition function, or statistical weight, of the system with its degrees of freedom frozen at a particular set $S = \{s_a, s_b\}$, and with its junction point at a specific spatial position \mathbf{R} , is given by

$$\mathcal{Z}(\mathbf{R}, S) = G(\mathbf{r}_1, \mathbf{R}; s_a) G(\mathbf{R}, \mathbf{r}_2; L - s_a) G(\mathbf{r}_3, \mathbf{R}; s_b) G(\mathbf{R}, \mathbf{r}_4; L - s_b). \quad (3.1)$$

In Equation (3.1) we employed the composition property of the Green's function to divide the total contour length ($= 2L$) into four smaller chain intervals. This is done analogous to Section 2.5, but with one crucial difference, namely that the interval lengths are not pinned down at $L/2$. The Green's function (2.36) of one chain section, with unknown radius length s_a , is thus given by

$$G(\mathbf{r}_1, \mathbf{R}; s_a) = G_x(x_1, X; s_a) G_y(y_1, Y; s_a) G_z(z_1, Z; s_a) \quad (3.2)$$

$$= \frac{3}{2\pi\ell s_a} \exp\left\{-\frac{3}{2s_a\ell} [(X - x_1)^2 + (Y - y_1)^2]\right\} \\ \times \frac{2}{h_z} \sum_{p=1}^{\infty} \sin \frac{\pi p Z}{h_z} \sin \frac{\pi p (h_z - \epsilon)}{h_z} e^{-\frac{\ell\pi^2 p^2}{6h_z^2} s_a}. \quad (3.3)$$

In order to obtain the partition function of all possible conformations of the system with a *particular* set of quenched variables, we have to average over all possible spatial positions of the junction point \mathbf{R} :

$$\mathcal{Z}(S) = \int d\mathbf{R} G(\mathbf{r}_1, \mathbf{R}; s_a) G(\mathbf{R}, \mathbf{r}_2; L - s_a) G(\mathbf{r}_3, \mathbf{R}; s_b) G(\mathbf{R}, \mathbf{r}_4; L - s_b), \quad (3.4)$$

It might be possible to compute the chain configuration, for a specific choice of the quenched variables s_a and s_b , that minimizes the free energy of a specific sample. However, in a general disordered system such a calculation would be deemed intractable, since the number of quenched variables per sample is usually much larger than two³. Luckily, methods of statistical mechanics often prove fruitful in the limit of large systems.

³For example, in the Edwards-Anderson model [15] for a spin glass the interaction J_{ij} between every spin pair σ_i and σ_j is random. For N spins there will be $\frac{1}{2}N(N-1)$ quenched variables per sample. Even numerical averaging over different realizations is too time-consuming [34].

3.2.2 Averaging

In the statistical mechanics of a random system, there is a need to perform two distinct averages [20]. Firstly, there is the *thermal* average that is carried out for every possible conformation, in a specific realization of $\{\mathcal{S}\}$. This kind of average was performed in (3.4), by means of a Green's function approach. Secondly, there is the disorder or *configuration* average, which is an average over all possible distributions of the quenched variables.

In order to make the scenario of the random linking more general, the *thermal* average may be rewritten as follows. Let $\mathcal{H}_{\mathcal{S}}$ denote the generalized Edwards Hamiltonian of a network subsystem composed of two randomly linked stitches,

$$\mathcal{H}_{\mathcal{S}}[\{\mathbf{R}_i\}]/k_{\text{B}}T \equiv \sum_{i=1}^4 \frac{3}{2\ell} \int_0^L \dot{\mathbf{R}}_i^2(s_i) ds_i - \int_0^L A[\mathbf{R}_i(s_i)] ds, \quad (3.5)$$

where $\mathbf{R}_i(s)$ is the position vector of the i th chain segment at the arc length s . The Hamiltonian describes the connectivity and \hat{z} -confinement of the chain system [22]. Although the four chain pieces seem to emanate from a common junction point at \mathbf{R} (Figure 3.2), the respective arc lengths are not independent of one another, since they were formed from just two *stitches*. This adds a constraint to (3.5): $s_1 = s_a \iff s_2 = L - s_a$ and $s_3 = s_b \iff s_4 = L - s_b$. For a specific sample, the partition function is expressed as the product of separable path integrals,

$$\mathcal{Z}_{\mathcal{S}} = \int d\mathbf{R} \int_{\mathbf{R}_1(s_a)=\mathbf{R}}^{\mathbf{R}_1(0)=\mathbf{r}_1} \int_{\mathbf{R}_2(0)=\mathbf{r}_2}^{\mathbf{R}_2(L-s_a)=\mathbf{R}} \int_{\mathbf{R}_3(s_b)=\mathbf{R}}^{\mathbf{R}_3(0)=\mathbf{r}_2} \int_{\mathbf{R}_4(0)=\mathbf{r}_4}^{\mathbf{R}_4(L-s_b)=\mathbf{R}} \left[\prod_{i=1}^4 \mathcal{D}\mathbf{R}_i(s_i) \right] e^{-\frac{\mathcal{H}_{\mathcal{S}}[\mathbf{R}_i]}{k_{\text{B}}T}}, \quad (3.6)$$

which is equivalent to the previous Green's function expression (3.4). The free energy of a system in some particular crosslinkage state $\mathcal{S} = \{s_a, s_b\}$ is the logarithm of (3.6):

$$F(\mathcal{S}) = -k_{\text{B}}T \ln \mathcal{Z}(\mathcal{S}). \quad (3.7)$$

Let the probability of finding this particular state be $P_{\mathcal{S}}$. Then for a canonical ensemble the effective free energy is given by

$$\mathcal{F} = \sum_{\{\mathcal{S}\}} P_{\mathcal{S}} F(\mathcal{S}), \quad \text{where} \quad \sum_{\{\mathcal{S}\}} P_{\mathcal{S}} = 1. \quad (3.8)$$

The effective free energy is the observable or experimental free energy. A correct theoretical calculation of the average value of \mathcal{F} over the entire ensemble is expected to correspond to its experimental value. The sample free energy $F(\mathcal{S})$ is an extensive quantity and known to be *self-averaging* [20, 34]. We can thus expect that variations in $F(\mathcal{S})$ from one sample to the next and deviations from the average value \mathcal{F} , will go to zero in the thermodynamic limit $V \rightarrow \infty$. In order to obtain an experimentally relevant quantity, only variables with the self-averaging property should be disorder-averaged.

Taking a sample average of the partition function (3.6) instead of the free energy, is known

as the so-called *annealed* case:

$$\mathcal{F}_{\text{annealed}} = -k_B T \ln \left[\sum_{\{\mathcal{S}\}} P_{\mathcal{S}} \mathcal{Z}_{\mathcal{S}} \right], \quad (3.9)$$

and would give the wrong physics, since the crosslinkage in (3.9) is allowed to change in response to the chain conformations. In reality, $\{\mathcal{S}\}$ is fixed for each sample. Even if the substance between the planar surface is deformed, the crosslinkage for a particular sample will stay fixed in response to the deformation. Beyond what has been said, the partition function $\mathcal{Z}_{\mathcal{S}}$ is also not suitable for averaging since it is not self-averaging and not physically observable.

The correct strategy is thus to average the self-averaging free energy $F(\mathcal{S})$ over the distribution of the permanent, but randomly chosen arc lengths:

$$\mathcal{F} \equiv [F(\mathcal{S})]_{\mathcal{S}} \equiv \sum_{\{\mathcal{S}\}} P_{\mathcal{S}} F(\mathcal{S}) \quad (3.10)$$

$$= -k_B T \int_0^L ds_a \int_0^L ds_b P_{\mathcal{S}} \ln \mathcal{Z}(\mathcal{S}). \quad (3.11)$$

The configuration average is denoted by $[\dots]_{\mathcal{S}}$. Since the free energy for a specific \mathcal{S} agrees with its configuration average $[F(\mathcal{S})]_{\mathcal{S}}$ in the thermodynamic limit, it seems that either quantities may be used in further calculations. However, the average $[F(\mathcal{S})]_{\mathcal{S}}$ is more suitable to work with, since it is a physically *measurable* quantity⁴.

3.2.3 Replicas to the rescue

Performing the average (3.11) is *usually*⁵ not feasible, because the dependence of $\ln \mathcal{Z}$ on \mathcal{S} is often very complicated. In order to address the averaging the following identity,

$$\lim_{n \rightarrow 0} \frac{\mathcal{Z}^n - 1}{n} = \ln \mathcal{Z} \quad \text{or} \quad \frac{\partial}{\partial n} \mathcal{Z}^n \Big|_{n=0} = \ln \mathcal{Z} \quad (3.12)$$

was first employed by [15, 44] in theoretical models to predict the spin glass phase in disordered magnetic systems. This technical trick (3.12), called the replica method, is useful because it is often easier to evaluate $[\mathcal{Z}^n]$ than $[\ln \mathcal{Z}]$. Consider the partition function (3.6) taken to the *integer* power n :

$$\mathcal{Z}^n(\mathcal{S}) = \left[\prod_{\alpha=1}^n \int d\mathbf{R}^{(\alpha)} \left(\prod_i \int_i \mathcal{D}\mathbf{R}_i^{(\alpha)} \right) \right] \exp \left\{ - \sum_{\alpha=1}^n \mathcal{H}_{\mathcal{S}}[\mathbf{R}_i^{(\alpha)}] / k_B T \right\}. \quad (3.13)$$

The above quantity is the partition function of n independent identical copies or replicas of the original system. In (3.13) the subscript α labels the replicas, and not the quenched variables \mathcal{S} .

⁴The free energy is not the only self-averaging quantity. For example, the neutron scattering form factor is also a useful measurable quantity to average [52].

⁵An example of a model where the disorder average has been solved analytically, without implementing replicas, is the random-energy model [10, 11]. In this model the independent energy levels $\{E_i\}$ are the quenched variables, and the sample average of the free energy is calculated by a microcanonical argument. The infinite range Ising model with p -spin quenched random interactions is also exactly solvable, and the results confirm the replica method [27].

The chain conformation may fluctuate from replica to replica, but the cross link constraints are fixed for each sample replica. The scheme of the replica method can be described as follows. Firstly, the quenched average of the replicated partition function (3.13) for integer n must be calculated. Next, the analytic continuation of the the resulting function, $[\mathcal{Z}^n(S)]_S$, should be made for an arbitrary non-integer n . Lastly, the limit $n \rightarrow 0$ should be taken. In the end, the effective free energy is uncovered:

$$\mathcal{F} \equiv -k_B T \lim_{n \rightarrow 0} \frac{1}{n} \left([\mathcal{Z}^n]_S - 1 \right). \quad (3.14)$$

The replica method might initially seem mathematically dubious since one evaluates $[\mathcal{Z}^n(S)]_S$ for integer n and then extrapolates the result to $n \rightarrow 0$. In the pioneering decade of spin glass theory, the replica method was thought to be the cause of some controversial and inconsistent results. In particular, the free energy of the Sherrington and Kirkpatrick (SK) model [44] was shown to be unstable and exhibit a negative entropy in the low temperature ($< T_c$) region. However, these unphysical results were a consequence of the replica symmetry ansatz and possibly the incorrect reversal of limits [50], and not due to the replica procedure itself. Alternative mathematical efforts, including replica symmetry breaking schemes and the mean-field TAP (Thouless, Anderson and Palmer) approach⁶, agree with the SK solution at and above the critical temperature T_c . In all cases where the calculations can be performed by a different method, the replica approach is confirmed and gives sensible results [10, 27].

In polymer network theories the use of the replica method is simpler and undisputed [2, 3, 37, 36], because there are no competing interactions (“frustration”) or need for replica symmetry breaking as in the case of spin glasses⁷.

⁶Comprehensive literature and reviews exist on the subject of the theory of spin glasses [20, 34, 4]. Recently it has been shown that the TAP and replica methods are equivalent in the SK model [6].

⁷An example of where various methods are used to probe the disorder in a polymer system, is the problem of a Gaussian chain trapped in a medium with randomly frozen obstacles [17]. Variational calculations are performed with and without the breaking of replica symmetry, and shown to be consistent. It is also shown that the annealed and quenched cases are two distinctly different situations.

Furthermore, many network theory problems have been approached without the use of replicas [45], and corroborate the replica results. An example is that of determining the neutron scattering function of polymer networks [43, 42, 52].

3.3 The actual calculation

In this section we apply all the available *tools* — the Green's functions of Section 3.2.1 and the replica method — to a subsystem of the stitch network (Figure 3.2). The replicated partition function of the single bulk-link system can be abstractly expressed as:

$$\mathcal{Z}^n = \left(\int d\mathbf{R}^{(1)} \mathcal{G}^{(1)} \right) \left(\int d\mathbf{R}^{(2)} \mathcal{G}^{(2)} \right) \dots \left(\int d\mathbf{R}^{(n)} \mathcal{G}^{(n)} \right) \quad (3.15)$$

where the Green's functions in (3.2) are also replicated

$$\mathcal{G}^{(\alpha)} \equiv G^{(\alpha)}(\mathbf{r}_1, \mathbf{R}^{(\alpha)}; s_a) G^{(\alpha)}(\mathbf{R}^{(\alpha)}, \mathbf{r}_2; L - s_a) G^{(\alpha)}(\mathbf{r}_3, \mathbf{R}^{(\alpha)}; s_b) G^{(\alpha)}(\mathbf{R}^{(\alpha)}, \mathbf{r}_4; L - s_b). \quad (3.16)$$

The first step of the replica procedure involves the configurational average of \mathcal{Z}_S^n (3.13), which in terms of Green's functions, is given by

$$[\mathcal{Z}^n]_S = \int_0^L ds_a \int_0^L ds_b \prod_{\alpha=1}^n \left[\int d\mathbf{R}^{(\alpha)} \mathcal{G}^{(\alpha)} \right] P(s_a, s_b). \quad (3.17)$$

For the sake of illustrating the replica method in the simplest manner, we choose $P(S)$ to be the uniform distribution, that is, $P(S) = 1/L^2$. Although the bulk links are uniformly distributed, we do not allow them to form exactly at the ends, $s = 0$ and $s = L$, where the wall links are situated. Since the location of the wall links of a stitch network is by definition chosen to be non-random, the x and y coordinates of the stitch ends may be taken to coincide at the top and bottom plates respectively⁸. In the limit $\sqrt{N}\ell \gg h_z$, the first term in the eigenfunction expansion (3.2), corresponding to $p_1^{(\alpha)} = p_2^{(\alpha)} = p_3^{(\alpha)} = p_4^{(\alpha)} = 1$ in (3.16), dominates the partition function. In the case of the uniform distribution of the quenched variables, the configurational average of the n th power of the partition function is

$$[\mathcal{Z}^n]_S = \frac{1}{L^2} (\text{const})^n \int_{\epsilon}^{L-\epsilon} ds_a \int_{\epsilon}^{L-\epsilon} ds_b [s_a(L - s_a) + s_b(L - s_b)]^{-n} \exp \left\{ -\frac{3nL}{2\ell} \left[\frac{(x_1 - x_2)^2 + (y_1 - y_2)^2}{s_a(L - s_a) + s_b(L - s_b)} \right] \right\} \quad (3.18)$$

where "const" refers to a constant factor, dependent on the wall spacing h_z , but not on the disorder. The ϵ -factor in the integration, mathematically prohibits the bulk-links from being formed at the walls, which would result in *double* crosslinking.

3.3.1 The method of steepest descents

It is convenient to transform to a new set of integration variables, $\sigma_1 = |s_a - \frac{L}{2}|$ and $\sigma_2 = |s_b - \frac{L}{2}|$, where $\sigma_i \in (-\frac{L}{2}, \frac{L}{2})$. Let the measure of the distance between points on the top and bottom plates be denoted by d^2 , analogous to Section 2.5: $d^2 = (x_1 - x_2)^2 + (y_1 - y_2)^2$. After the

⁸This was also discussed in Section 2.5 and illustrated in Figure 2.9.

transformation, the exponential in (3.18) only has terms quadratic in σ_i :

$$[\mathcal{Z}^n]_S = \frac{1}{L^2} (\text{const})^n \int_{\epsilon - \frac{L}{2}}^{\frac{L}{2} - \epsilon} d\sigma_1 \int_{\epsilon - \frac{L}{2}}^{\frac{L}{2} - \epsilon} d\sigma_2 e^{-g(\sigma_1, \sigma_2)}, \quad (3.19)$$

with the exponent g defined as follows

$$g(\sigma_1, \sigma_2) \equiv n \ln \left[\frac{L^2}{2} - \sigma_1^2 - \sigma_2^2 \right] + \frac{3nLd^2}{2\ell} \left(\frac{L^2}{2} - \sigma_1^2 - \sigma_2^2 \right)^{-1}. \quad (3.20)$$

If the dominating factor $\frac{3nLd^2}{2\ell}$ in g is large, it is possible to evaluate the integral by the method of steepest descents or saddle point approximation [28]. The point (σ_1^*, σ_2^*) where g is minimized is found by making g stationary with respect to σ_1 and σ_2 ; $\frac{\partial g(\sigma_1^*, \sigma_2^*)}{\partial \sigma_1} = 0$ and $\frac{\partial g(\sigma_1^*, \sigma_2^*)}{\partial \sigma_2} = 0$. A global minimum is found at $(\sigma_1^*, \sigma_2^*) = (0, 0)$, only if $L < 3d^2/\ell$. In terms of the original arc length coordinates, the system will thus favour a bulk link to be formed at $s_a = L/2$ and $s_b = L/2$.

Next, the function $g(\sigma_1, \sigma_2)$ may be expanded in a Taylor series around (σ_1^*, σ_2^*) :

$$g(\sigma_1, \sigma_2) = g(\sigma_1^*, \sigma_2^*) + \frac{1}{2} \left\{ (\sigma_1 - \sigma_1^*)^2 \frac{\partial^2 g(\sigma_1^*, \sigma_2^*)}{\partial \sigma_1^2} + 2(\sigma_1 - \sigma_1^*)(\sigma_2 - \sigma_2^*) \frac{\partial^2 g(\sigma_1^*, \sigma_2^*)}{\partial \sigma_1 \partial \sigma_2} + (\sigma_2 - \sigma_2^*)^2 \frac{\partial^2 g(\sigma_1^*, \sigma_2^*)}{\partial \sigma_2^2} \right\} + \dots \quad (3.21)$$

$$\simeq \frac{3nd^2}{\ell L} + n \ln \frac{1}{2} L^2 + \frac{2n}{L^3} \left(\frac{3d^2}{\ell} - L \right) (\sigma_1^2 + \sigma_2^2). \quad (3.22)$$

We choose to work with very long macromolecules, such that the contour length L is very large (but finite) throughout the above Taylor expansion. In this limit, the higher order terms in (3.21) are insignificant, so that (3.19) becomes

$$[\mathcal{Z}^n]_S = \frac{1}{L^2} (\text{const} \frac{2}{L^2})^n e^{-\frac{3nd^2}{\ell L}} \int d\sigma_1 \int d\sigma_2 e^{-\frac{2n}{L^3} (3d^2/\ell - L) (\sigma_1^2 + \sigma_2^2)} \quad (3.23)$$

$$= \frac{1}{L^2} (\text{const} \frac{2}{L^2})^n e^{-\frac{3nd^2}{\ell L}} \int d\sigma_1 \int d\sigma_2 \sum_{k=0}^{\infty} \frac{(-1)^k}{k!} \left[\frac{2n}{L^3} \left(\frac{3d^2}{\ell} - L \right) (\sigma_1^2 + \sigma_2^2) \right]^k \quad (3.24)$$

However, since the integration limits are finite, we are forced to revert to a series representation of the exponential in the integrand (3.23). The average of the replicated partition function (3.24), is then given by

$$[\mathcal{Z}^n]_S \approx 1 - n \left\{ \frac{\ell \pi^2 L}{3h_z^2} + \frac{4d^2}{\ell L} - \ln \left[\frac{6\epsilon^4}{h_z^7} \left(\frac{3}{2\ell} \right)^4 \frac{2}{L^2} \right] - \frac{1}{3} \right\} + \mathcal{O}(\geq n^2) \text{ terms} \quad (3.25)$$

Lastly, by taking the replica limit $n \rightarrow 0$ as in (3.14), the effective free energy \mathcal{F} is obtained

$$\mathcal{F}/k_B T \simeq \frac{\ell \pi^2 L}{3h_z^2} + \frac{4d^2}{\ell L} - \ln \left[\frac{6\epsilon^4}{h_z^7} \left(\frac{3}{2\ell} \right)^4 \frac{2}{L^2} \right] - \frac{1}{3}, \quad (3.26)$$

which is only valid for large, but finite chain length L , such that $\sqrt{\ell L} \gg h_z$, and when the relation $L < 3d^2/\ell$ holds.

3.4 Deforming the *stitch network*

In Section 3.1 we defined the free energy of the phantom stitch network as a whole, to be the sum of M subsystems. Each single-bulk link system has an effective free energy \mathcal{F} (3.26). If a stitch network is fabricated from long, but finite length chains, and the relation $h_z \ll L < 3d^2/\ell$ holds, the replica procedure results in the following elastic free energy:

$$\mathcal{F}_{\text{network}} \simeq k_B T M \left\{ \frac{\ell \pi^2 L}{3h_z^2} + \frac{4d^2}{\ell L} - \ln \left[\frac{6\epsilon^4}{h_z^7} \left(\frac{3}{2\ell} \right)^4 \frac{2}{L^2} \right] \right\}. \quad (3.27)$$

The first contribution to the free energy, $\frac{\ell \pi^2 L}{3h_z^2}$ is ascribed to the \hat{z} -confinement, and is typical for an ideal chain trapped in a one dimensional cavity of diameter h_z [26]. The second term, $\frac{4d^2}{\ell L}$, corresponds to the free energy of four *unconfined*, ideal chains (in two dimensions) with an end-to-end distance d . The last term in (3.27) comes from the normalization factor. In the case of a uniform distribution, $P(\mathcal{S}) = 1/L^2$, it is possible to find a similar free energy, without the replica method, by minimizing $F(\mathcal{S})$ (3.7) with respect to s_a and s_b .

Using the above free energy (3.27), it is possible to investigate what happens during strain. Let the stitch network between plates, be strained by an isovolumetric, uniaxial deformation Λ (2.26), $\mathbf{R}_i \rightarrow \Lambda \cdot \mathbf{R}_i$. The stress as a function of the deformation ratio λ , can be calculated as in Section 2.4,

$$f_{\text{network}} = \frac{k_B T M}{V} \left(\frac{7}{\lambda} - \frac{2\pi^2 \ell L}{3h_z^2} \frac{1}{\lambda^3} - \frac{4d^2}{\ell L} \frac{1}{\lambda^2} \right), \quad (3.28)$$

and is found to resemble the stress-strain relationship for a network of stitches that has an average number of M *non-random bulk-links*, chosen beforehand to be at $(s_a, s_b) = (\frac{L}{2}, \frac{L}{2})$.

The stitch network model served as an exercise in the application of the replica method, and as motivation for the search of a better network model.

Chapter 4

The Real Confined Network

In this chapter we shall extend Deam and Edwards' pioneering model of network formation [9], to include a confining surface and random polymer-polymer and polymer-wall links.

A polymer network formed at a surface is a system governed by a variety of constraints. The surface at which the gel forms, plays the role of a confining geometry that restricts the network chain conformations and positions. During network formation, the macromolecules form permanent links with one another as well as with the confining surface. Since the links are unbreakable, the junction points will be localized to a certain extent dependent on the crosslink-density. In a *real* network the exact location of the links is unknown prior to fabrication and varies from one specimen to the next. However, any two samples having different cross-link realizations are expected to exhibit similar macroscopic properties.

In previous chapters we investigated single-chain systems subject to similar conditions of confinement and random linking. This was done to provide the basic groundwork for understanding and approaching the actual network (many-chain) problem. In the present chapter we traverse through the "making" of an ideal polymer network formed at a surface, starting from a group of chains to the finished gel-product¹.

4.1 The Collection of Phantom chains

Prior to linking, we have a system of M independent chains. They are assumed to be long, linear and have no charge. The calculations in this chapter are performed on phantom (pure Gaussian) chains, thus neglecting any effects due to inter- and intra-molecular forces. The term "phantom" emphasizes the fact that the assumption of no steric effect is clearly unphysical. In reality each monomer segment of a chain will possess some volume which is excluded from other segments [2, 16], and consequently the polymer will swell. However, in a *dense* polymer solution the excluded volume interactions are screened, and each chain is essentially ideal and Gaussian [8]. The collection of phantom chains may thus be visualized as a rather dense, overlapping

¹Note: this is done through the eyes of a theoretical physicist, not a chemist. In referring to an "ideal network", we mean a 3-dimensional network of phantom chains, joined together and fixed to the walls by random, unbreakable chemical bonds or crosslinks. All forces between the chains, except at the points of crosslinkage, are ignored and each chain is assumed to be free to take on any conformation in the confined region.

polymer solution, called a melt.

For a system of M phantom chains, the partition function is written as a product of M Wiener path integrals (Section 2.1):

$$\mathcal{Z} (\{\mathbf{R}_i, \mathbf{R}'_i; L_i\}) = \mathcal{N} \left\{ \prod_{i=1}^M \int_{\mathbf{R}_i(0)=\mathbf{R}'_i}^{\mathbf{R}_i(L_i)=\mathbf{R}_i} [D\mathbf{R}_i(s)] \right\} \exp \left\{ -\frac{3}{2\ell} \sum_{i=1}^M \int_0^{L_i} \left(\frac{\partial \mathbf{R}_i(s)}{\partial s} \right)^2 ds \right\}. \quad (4.1)$$

For the sake of generality, each polymer i , defined by its path $\mathbf{R}_i(s)$ in (4.1), has its associated contourlength L_i . For present purposes, this extra notation is unnecessary. Henceforth, all chains are chosen to be identical with respect to constitution and degree of polymerization, and will have equal length L . The notation \mathcal{L} will refer to the total contourlength of all the chains, that is, $\mathcal{L} = \sum_i^M L_i$.

4.2 Confining the Melt

The macromolecules are confined between two parallel planar surfaces or *walls*, as in Figure 4.1, since symmetric problems are usually simpler to treat, and widen the scope of the problem. If one wall is situated at $z = 0$ and the other at $z = h_z$, then the problem of a network at a single surface is retrieved by taking the limit $h_z \rightarrow \infty$.

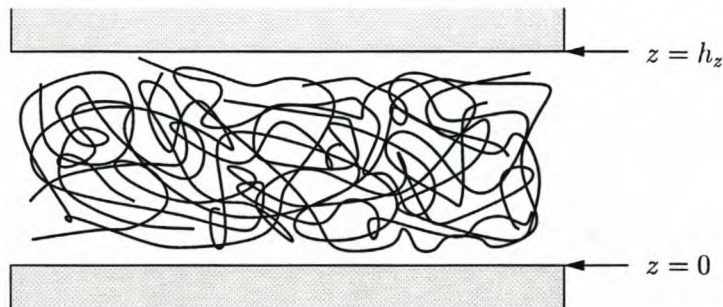


Figure 4.1: Simple illustration of a very dense melt of phantom chains, confined between two walls. There is no tendency towards adsorption.

The formalism chosen to represent the confinement, must ensure that all $\mathbf{R}(s)$ vanish beyond the boundaries. The partition function in (4.1) is modified, by noting that the path integral has to be carried out only in the allowable region [22]. In Section 2.2 a single chain was confined. Since the chains are independent, the partition function is the product of M single-chain

contributions (2.6):

$$\begin{aligned} \mathcal{Z} (\{\mathbf{R}_i, \mathbf{R}'_i; L_i\}) &= \mathcal{N} \left\{ \prod_{i=1}^M \int_{\mathbf{R}_i(0)=\mathbf{R}'_i}^{\mathbf{R}_i(L)=\mathbf{R}_i} [\mathcal{D}\mathbf{R}_i(s)]_{\text{walls}} \right\} e^{-\frac{3}{2\ell} \sum_{i=1}^M \int_0^L \left(\frac{\partial \mathbf{R}_i(s)}{\partial s} \right)^2 ds} \quad (4.2) \\ &= \mathcal{N} \int \prod_{i=1}^M [\mathcal{D}\mathbf{R}_i(s)] e^{-\frac{3}{2\ell} \sum_{i=1}^M \int_0^L \dot{\mathbf{R}}_i^2(s) ds} \\ &\quad \times \prod_s \left[\Theta(\mathbf{R}_i(s) \cdot \hat{z}) \Theta(h_z - \mathbf{R}_i(s) \cdot \hat{z}) \right]. \quad (4.3) \end{aligned}$$

The normalization \mathcal{N} refers to the number of configurations of a collection of M completely free polymer chains, each starting at \mathbf{R}'_i and ending at \mathbf{R}_i in N steps, with Kuhn step-length ℓ . The confining walls, which act as a constraint in the partition function, can be rewritten to resemble an attractive potential in terms of continuous arclength variables (Section 2.2):

$$A[\mathbf{R}_i(s)] \equiv \ln[\Theta(\mathbf{R}_i(s) \cdot \hat{z})] + \ln[\Theta(h_z - \mathbf{R}_i(s) \cdot \hat{z})], \quad \text{and} \quad \Theta(R) = \begin{cases} 1 & \text{if } R > 0 \\ 0 & \text{otherwise} \end{cases} \quad (4.4)$$

Since the chains are only confined in the \hat{z} -coordinate, the complete partition function for the confined melt will look as follows:

$$\begin{aligned} \mathcal{Z}_{\text{melt}} &= \mathcal{N} \prod_{i=1}^M \int_{R_{xi}(0)=R'_x}^{R_{xi}(L)=R_x} [\mathcal{D}R_{xi}(s)] \exp \left\{ -\frac{3}{2\ell} \int_0^L \dot{R}_{xi}^2(s) ds \right\} \\ &\quad \times \int_{R_{yi}(0)=R'_y}^{R_{yi}(L)=R_y} [\mathcal{D}R_{yi}(s)] \exp \left\{ -\frac{3}{2\ell} \int_0^L \dot{R}_{yi}^2(s) ds \right\} \\ &\quad \times \int_{R_{zi}(0)=R'_z}^{R_{zi}(L)=R_z} [\mathcal{D}R_{zi}(s)] \exp \left\{ -\frac{3}{2\ell} \int_0^L \dot{R}_{zi}^2(s) ds \right\} \\ &\quad + \sum_{i=1}^M \int_0^L A[R_{zi}(s)] ds \}. \quad (4.5) \end{aligned}$$

It might be possible to approximate the infinitely deep well represented by $\ln \Theta(\mathbf{R}(s) \cdot \hat{z})$ by a function that is more suitable to mathematical manipulations.

4.3 Confined Network Formation

Given the collection of phantom chains, they should be crosslinked to each other (*polymer-polymer* links) and to the confining surface (*polymer-wall* links) in order to constitute a polymer network linked to the walls, Figure 4.2.

In practice, polymer-polymer² cross links are usually formed by joining two segments from different chains by means of sulphur vulcanisation, peroxide or radiation cross-linking [54]. In this problem, polymer adsorption to a surface does not play a role whatsoever. Wall-links are

²Henceforth, polymer-polymer links will mostly be denoted by the term *bulk-links*, and polymer-wall links by *wall-links*.

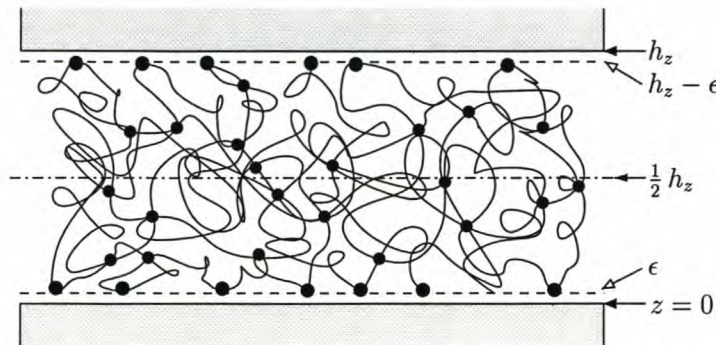


Figure 4.2: A simplified illustration of a gel network formed between two parallel planar surfaces of width h_z . The wall-links are situated an infinitesimal distance ϵ from the wall surface. The dash-dot line is the line of symmetry at $z = \frac{1}{2}h_z$.

therefore synthesized in the same manner (for example irradiation) as bulk-links, but with a lower functionality. In a real cross-linking process, the links build up in time. One link will affect the neighbouring chain density, therefore influencing the position of the next link, and clusters of links may appear. As the crosslink density is increased there is an abrupt change of the melt from a viscous liquid to a solid, elastic gel that shows no tendency to flow. At this stage — the so-called *gel-point* — a giant cluster or network spans the whole sample. Theoretical explanations for how the transition actually takes place, still remain difficult [23, 24]. We shall only be concerned with the case of sufficiently high crosslink density; not a system close to the gel point.

Here we assume that we are dealing with a homogeneous material where *local* clustering of crosslinks are negligible. This is a reasonable assumption to make if the network is formed from a dense melt system, or the crosslinker density is high enough. Furthermore, it has been shown that macroscopic quantities, for example the free energy, are insensitive to microscopic details such as inhomogeneities in crosslink-density [51].

4.3.1 The Origin of disorder

Both types of linkages are permanent, and impose certain topological constraints between the polymers, given that the crosslink density is high enough. The randomness of the link formation is the origin of the quenched disorder in the system (Section 3.2). *What is the probability of this disorder?* We can imagine that the chains — constituting a given, random link — were just touching prior to the permanent linking. The probability of the disorder is then given by the same weight as that of thermal equilibrium of the melt prior to network formation. This idea of an instantaneous linking mechanism, was first proposed by Deam and Edwards [9].

4.3.2 Linking Formalism

If a crosslink joins arclength point s_i^* on chain i with point s_j^* on chain j , then we have the constraint, illustrated in Figure 4.3(b),

$$\mathbf{R}_i(s_i^*) = \mathbf{R}_j(s_j^*) \quad (4.6)$$

which is unbreakable and stays fixed at the same place on the chain. Mathematically, we use a Dirac-delta formalism to pick out the set of linkages, with the arc-locations of the crosslinks specifying the crosslink topology of the network. The crosslinks are constraints in the partition function of the system, which have to be approximated by a more tractable potential.

We proceed, by considering a melt with chains touching at their future crosslink positions whilst incorporating the confinement formalism of Section 4.2. A simplified way to think about the manner of introducing crosslinkages, is by first adding N_c sliding links [2] in the bulk and N_w touching links at both walls, at random. This is of course completely hypothetical, but will facilitate statistical calculations of fast crosslinking and accommodate the chosen probability of disorder in Section 4.3.1.

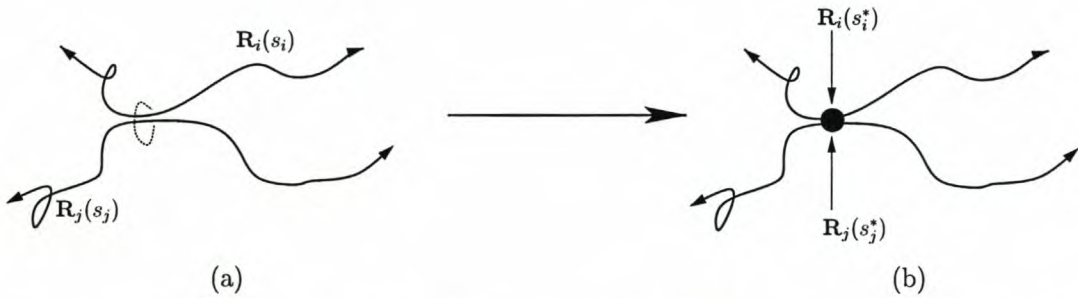


Figure 4.3: Two polymer chains, $\mathbf{R}_i(s_i)$ and $\mathbf{R}_j(s_j)$, in close proximity (a) modelled by a slip-link, and (b) a permanent crosslinkage constraint (4.6), after a fast crosslinking procedure.

After the *touching* and *sliding* links reach equilibrium with the system, they have a free energy F' given by

$$\begin{aligned} e^{-F'/k_B T} = \mathcal{Z}(\{\mathbf{R}_i, \mathbf{R}'_i, L\}) &= \mathcal{N} \int \left[\prod_{i=1}^M \mathcal{D}\mathbf{R}_i(s) \right]_{\text{walls}} e^{-\frac{3}{2l} \sum_{i=1}^M \int_0^L \left(\frac{\partial \mathbf{R}_i}{\partial s} \right)^2 ds} \\ &\times \left[\sum_{i,j=1}^M \int_0^L ds \int_0^L ds' \delta(\mathbf{R}_i(s) - \mathbf{R}_j(s')) \right]^{N_c} \\ &\times \left[\sum_{i=1}^M \int_0^L ds \int dx dy \delta(\mathbf{R}_i(s) - \eta(x, y, 0)) \right]^{N_w} \\ &\times \left[\sum_{i=1}^M \int_0^L ds \int dx dy \delta(\mathbf{R}_i(s) - \eta(x, y, h_z)) \right]^{N_w}, \quad (4.7) \end{aligned}$$

with η a certain vector determining the positions of the crosslinks at the walls. The notation

$[\mathcal{DR}_i(s)]_w$ indicates that the path integration for the confined z -coordinates should only be carried out in the allowable region. Due to the \hat{z} confinement the partition function (4.7) is not symmetric in space. Nevertheless, in each partition function, the crosslink arc-locations in the Dirac-delta functions are the same, since they are quenched variables. The crosslinks therefore act as a common combining factor between the confined and unconfined contributions to the partition function.

4.3.3 Implementing Replicas

The formation of the network on the walls is done by “freezing” the *sliding* and *touching* links (Figure 4.3) of Section 4.3.2, such that the system reaches its final free energy F_S , given by the logarithm of:

$$e^{-F_S(\{X_i\})/k_B T} = \sum_{\{\mathbf{R}_i\}} \exp(-\mathcal{H}_s[\{\mathbf{R}_i\}]/k_B T). \quad (4.8)$$

In the above equation, the free energy F_S is that of a specific *sample* associated with a specific set of quenched variables $\mathcal{S} = \{X_i\}$. The notation $\sum_{\{\mathbf{R}_i\}}$ denotes the integration over all possible conformations of the confined system with degrees of freedom frozen at \mathcal{S} . In Section 3.2.2 it was shown that for a system with permanent constraints, the free energy of the system with a specific crosslink-state \mathcal{S} should be evaluated first, followed by a disorder-average over all possible constraints. This procedure would give the correct experimental free energy \mathcal{F} of the system:

$$\mathcal{F} = \int \mathcal{P}_S(\{X_i\}) F_S[\{X_i\}] dX_i = \int \mathcal{P}_S(\{X_i\}) \ln \mathcal{Z}[\{X_i\}] dX_i, \quad (4.9)$$

where $\mathcal{P}_S(\{X_i\})$ is the probability of arclength coordinates being frozen at a specific set $\{X_i\}$. Each sample’s fabrication probability \mathcal{P}_S — the initial probability of the chains when touching — can be expressed as a formation Hamiltonian³.

In Section 3.2.2 we averaged over the randomness of formation of a *single* bulk link by means of the replica method, replicating the system n times. This was done because the quenched average of a logarithm as in (4.9) is generally difficult to evaluate. We shall now extend this idea to a macroscopic number of permanent crosslinks. The probability $\mathcal{P}_S(\{X_i\})$ is now given by the ideas of Section 4.3.1. In the Deam and Edwards formulation the *fabrication* probability is manifested in the *zeroth* replica, coupled to the other n replicas [9]. The free energy of the network system is then identified as the coefficient of n in the generalised partition function $\mathcal{Z}(n)$ of $n + 1$ replicas. Here, the generalised partition functions for the x and y coordinates coincide with the existing Deam and Edwards model for an unconfined phantom chain network [9]. In the z dimension, the walls act as a secondary localization of the chain coordinates. The

³The formation Hamiltonian is given by the $\alpha = 0$ part of the replica Hamiltonian \mathcal{H} in (4.14).

generalised partition function for the $n + 1$ replicas of a *confined* gel is given by

$$\begin{aligned}
 e^{-\mathcal{F}(n)/k_B T} = \mathcal{Z}(n) &= \mathcal{N} \int \left[\prod_{i=1}^M \mathcal{D}\mathbf{R}_i^{(0)}(s) \right]_{\text{w}} \int \left[\prod_{\alpha=1}^n \prod_i^M \mathcal{D}\mathbf{R}_i^{(\alpha)}(s) \right]_{\text{w}} e^{-\frac{3}{2l} \sum_{i,\alpha} \int_0^L (\dot{\mathbf{R}}_i^{(\alpha)})^2 ds} \\
 &\times \left[\sum_{i,j=1}^M \int_0^L ds \int_0^L ds' \prod_{\alpha=0}^n \delta(\mathbf{R}_i^{(\alpha)}(s) - \mathbf{R}_j^{(\alpha)}(s')) \right]^{N_c} \\
 &\times \left[\sum_{i=1}^M \int_0^L ds \int dx dy \prod_{\alpha=0}^n \delta(\mathbf{R}_i^{(\alpha)}(s) - \eta^{(\alpha)}(x, y, 0)) \right]^{N_w} \\
 &\times \left[\sum_{i=1}^M \int_0^L ds \int dx dy \prod_{\alpha=0}^n \delta(\mathbf{R}_i^{(\alpha)}(s) - \eta^{(\alpha)}(x, y, h_z)) \right]^{N_w}, \quad (4.10)
 \end{aligned}$$

where $\eta^{(\alpha)}$ determines the positions of the crosslinks at the walls. Each three-dimensional $\eta^{(\alpha)}$ is an element in a $(n + 1)$ -dimensional vector, given by

$$\boldsymbol{\eta} = \left(\eta^{(0)} \dots \eta^{(\alpha)} \dots \eta^{(n)} \right)^{\text{T}}. \quad (4.11)$$

For the sake of easing the notation, we proceed by modeling the network by one large polymer of length \mathcal{L} .

In any network synthesized from many chains, there will be network “defects” [21, 48]. The

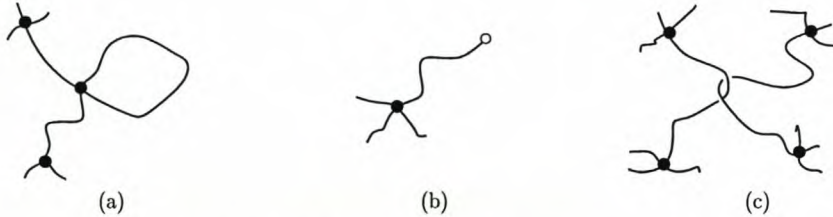


Figure 4.4: Illustrating three types of network imperfections: (a) A closed loop resulting from intramolecular crosslinking; (b) A dangling end (represented by the open circle) and (c) A trapped entanglement.

first defect, in Figure 4.4(a), occurs due to the linkage of two points on the same chain, forming a closed loop that is not linked with any other chain. The second imperfection [Figure 4.4(b)] is when only one end of a chain is attached to the network, creating a so-called *dangling* end. Dangling ends and closed loops do not contribute to the elasticity or strength of a substance, and should be excluded when probing the elastic properties of the gel. In contrast to the previous defects, entanglements, Figure 4.4(c), should *not* be omitted from calculations, since they can (in sufficient number) play the same role as crosslinkages [3, 18]. However, we shall assume the net contribution of above mentioned three defects to be negligible.

By rewriting the Dirac-delta constraints in (4.10) as pole integrations⁴, we arrive at the most compact formulation:

$$e^{-\mathcal{F}^{(n)}/k_B T} = \mathcal{N} \oint \frac{N_c! d\mu_c}{2\pi i} \oint \frac{N_w! d\mu_w}{2\pi i} \int \tilde{\int} \dots \tilde{\int} \left[\prod_{\alpha=0}^n \mathcal{D}\mathbf{R}^{(\alpha)}(s) \right] \times \exp \left\{ -\mathcal{H}/k_B T - (N_c + 1) \log \mu_c - 2(N_w + 1) \log \mu_w \right\}, \quad (4.13)$$

with \mathcal{H} giving the *pseudo*-Hamiltonian for network connectivity and confinement

$$\begin{aligned} \mathcal{H}/k_B T \equiv & -\frac{3}{2\ell} \sum_{\alpha=0}^n \int_0^{\mathcal{L}} ds \left[\left(\frac{\partial \mathbf{R}^{(\alpha)}(s)}{\partial s} \right)^2 + A[\mathbf{R}^{(0)}(s)] + \sum_{\alpha=1}^n \tilde{A}[\mathbf{R}^{(\alpha)}(s)] \right] \\ & + \mu_c \int_0^{\mathcal{L}} ds \int_0^{\mathcal{L}} ds' \prod_{\alpha=0}^n \delta(\mathbf{R}^{(\alpha)}(s) - \mathbf{R}^{(\alpha)}(s')) \\ & + \mu_w \int_0^{\mathcal{L}} ds \int dx dy \prod_{\alpha=0}^n \delta(\mathbf{R}^{(\alpha)}(s) - \eta^{(\alpha)}(x, y, 0)) \\ & + \mu_w \int_0^{\mathcal{L}} ds \int dx dy \prod_{\alpha=0}^n \delta(\mathbf{R}^{(\alpha)}(s) - \eta^{(\alpha)}(x, y, h_z)) \end{aligned} \quad (4.14)$$

where μ_c and μ_w are the chemical potentials of the bulk- and wall-links respectively. We have thus, in a convenient manner, represented the linking constraints as in a grand canonical ensemble. The crosslinks naturally confine the chain(s) to a well-defined region which must adhere to the defined region between the plates.

The replicas 1 to n can describe strained versions of the 0'th replica, and can therefore have different volumes and temperature. The integrations $\tilde{\int}$ in (4.13) imply integration over the n deformed systems, each with volume $\tilde{V} = \mathbf{\Lambda} V$, with V the volume of the undeformed replica system and $\mathbf{\Lambda}$ the deformation tensor. After extension or compression of the system by $\mathbf{\Lambda}$, the system will conserve its crosslinking topology that it had at fabrication, and therefore each replica must have the same set of crosslink arclength coordinates. The infinite deep square well potential representing the wall confinement (4.4), is given by A in the unstrained system and by \tilde{A} for the strained replicas:

$$\tilde{A}[\mathbf{R}(s)] \equiv \ln[\Theta(\mathbf{R}(s) \cdot \hat{z})] + \ln[\Theta(\lambda_z h_z - \mathbf{R}(s) \cdot \hat{z})], \quad \text{with} \quad \Theta(R) = \begin{cases} 1 & \text{if } R > 0 \\ 0 & \text{otherwise} \end{cases}. \quad (4.15)$$

⁴The constraint terms are exponentiated by implementing the following complex integral:

$$\mathbb{B}^N = \frac{N!}{2\pi i} \oint_{\mathbb{C}} e^{\mu \mathbb{B} - (N+1) \ln \mu} d\mu, \quad (4.12)$$

where contour \mathbb{C} encloses the origin.

4.4 Planning the variational calculation

Only a handful of statistical mechanics models have been solved exactly. For the rest it is necessary to resort to some approximation method. The current replica model falls in the latter class due to the intractable path integrals in (4.13). In this section we shall employ the Feynman variational principle, which follows from the inequality,

$$\langle e^X \rangle \geq e^{\langle X \rangle} \quad (4.16)$$

which is valid for any real stochastic variable X , due to the concave nature of the e^X graph [19].

4.4.1 Introducing transformation coordinates

It is expected that the crosslinks will physically pin down the giant network chain in space, so that for any s , the coordinates of the different replicas, $\mathbf{R}^{(0)}(s)$, $\mathbf{R}^{(1)}(s)$, \dots , $\mathbf{R}^{(n)}(s)$, will be correlated in some way. The coordinates of the undeformed (zeroth) replica, are free to be anywhere between the constraining walls. Before we show how to mimic a crosslink constraint, we introduce a new set of coordinates $\{\mathbf{X}^{(0)}, \mathbf{X}^{(1)}, \mathbf{Y}^{(m)}\}_{\{m=1\dots(n-1)\}}$, with $\mathbf{X}^{(1)}$ a relative coordinate, and $\mathbf{X}^{(0)}$ being the centre-of-mass coordinate of all the replicas. The $n-1$ remaining coordinates are simply rotations in replica space and give the deviation of the chains from the affine position. We define the new set of coordinates in the standard way [14]:

$$X_j^{(0)} = \frac{R_j^{(0)} + \sum_{\alpha=1}^n \lambda_j R_j^{(\alpha)}}{(1 + n\lambda_j^2)^{\frac{1}{2}}} \quad (4.17)$$

$$X_j^{(1)} = \frac{\sqrt{n}\lambda_j R_j^{(0)} - \frac{1}{\sqrt{n}} \sum_{\alpha=1}^n R_j^{(\alpha)}}{(1 + n\lambda_j^2)^{\frac{1}{2}}} \quad (4.18)$$

$$Y_j^{(m)} = \frac{1}{\sqrt{n}} \sum_{\alpha=1}^n e^{(2\pi i m \alpha)/n} R_j^{(\alpha)}, \quad m = 1, 2, \dots, (n-1) \quad (4.19)$$

where the j 's are Cartesian indices. These coordinates define an orthonormal transformation \mathbf{T} with Jacobian equal to one. The λ_j 's are the elements on the diagonal of the deformation tensor $\mathbf{\Lambda}$. As a rule, a gel substance is only weakly susceptible to volume change during strain, as already mentioned in Section 2.4. Consequently, the λ 's are suitably defined by the isovolumetric deformation tensor $\mathbf{\Lambda}$ given by (2.26). The matrix form and other details of the transformation \mathbf{T} are relegated to Appendix A.

4.4.2 Introducing a trial localization potential

To make the problem more solvable in terms of the variational procedure, we introduce a trial potential to simulate the Dirac-delta crosslink constraints. Under strain the mean positions of the crosslinks may deform affinely, but it would be wrong to enforce the condition that all the crosslinks *themselves* should deform affinely. We therefore allow them freedom to oscillate around these affine positions. It seems reasonable to simulate the crosslink constraints by a trial

harmonic potential of the form⁵, first proposed in [14]:

$$Q = \frac{1}{6\ell} \int_0^{\mathcal{L}} ds \sum_{i=x,y,z} q_i^2 \sum_{\beta=1}^n X_i^{(\beta)2} \quad (4.20)$$

with q_i being the localization parameter and a measure of the limits within which each crosslink is allowed to fluctuate. If q_i is small, the crosslinking is weak. The dimension of q_i^{-1} is length². The inverse of q_i defines the mean distance in which the crosslinks are localised in the \hat{i} -direction. In other words, $(q_x q_y q_z)^{-\frac{1}{2}}$ defines the allowable volume which a crosslink may explore. In this chapter, we assume that the type of localization at the walls does not differ considerably from the bulk localization. Due to the symmetry of the problem in the x and y coordinates, we set $q_x = q_y$, and henceforth work with two scalar parameters q_x and q_z .

⁵Note that the replica indices in the transformed coordinates, $\{\mathbf{X}^{(0)}, \mathbf{X}^{(1)}, \mathbf{Y}^{(m)}\}_{\{m=1\dots(n-1)\}}$, are now denoted by β , to avoid any misconceptions. Before the transformation \mathbb{T} , the formation (unstrained) replica was $\alpha = 0$, and the remaining ($\alpha > 0$) replicas were strained versions. Now, the replica $\beta = 0$ represents the centre-of-gravity of all the replicas, with the remaining ($\beta > 0$) replicas being relative to it. Henceforth, any references to α indices should be understood as pertaining to the physical $\mathbf{R}^{\alpha \geq 0}$ coordinate model.

4.4.3 Notation

In this section we list all the constituents⁶ of the model that we shall refer to frequently during the actual variational calculation.

- The connectivity of the chains (approximated by one long polymer of length \mathcal{L}) is denoted by the Wiener term \mathbb{W} .

$$\mathbb{W} \equiv -\frac{3}{2\ell} \int_0^{\mathcal{L}} \left[\dot{\mathbf{X}}^{(0)2}(s) + \dot{\mathbf{X}}^{(1)2}(s) + \sum_{m=1}^{n-1} |\dot{\mathbf{Y}}^{(m)}(s)|^2 \right] ds \quad (4.21)$$

- The bulk crosslinks are denoted by $\mu_c \mathbb{X}_c$

$$\begin{aligned} \mu_c \mathbb{X}_c &\equiv \mu_c \int_0^{\mathcal{L}} ds \int_0^{\mathcal{L}} ds' \delta(\mathbf{X}^{(0)}(s) - \mathbf{X}^{(0)}(s')) \delta(\mathbf{X}^{(1)}(s) - \mathbf{X}^{(1)}(s')) \\ &\quad \times \prod_{m=1}^{n-1} \delta(\mathbf{Y}^{(m)}(s) - \mathbf{Y}^{(m)}(s')) \end{aligned} \quad (4.22)$$

- The wall crosslinks are denoted by $\mu_w \mathbb{X}_w$. [We assume the same chemical potential μ_w for both walls.]

$$\begin{aligned} \mu_w \mathbb{X}_w &\equiv \mu_w \int_0^{\mathcal{L}} ds \int_{-\infty}^{+\infty} dx dy \left[\delta(\mathbf{X}^{(0)}(s) - \nu^{(0)}(x, y, \epsilon)) \delta(\mathbf{X}^{(1)}(s)) \prod_{m=1}^{n-1} \delta(\mathbf{Y}^{(m)}(s)) \right. \\ &\quad \left. + \delta(\mathbf{X}^{(0)}(s) - \nu^{(0)}(x, y, h_z - \epsilon)) \delta(\mathbf{X}^{(1)}(s)) \prod_{m=1}^{n-1} \delta(\mathbf{Y}^{(m)}(s)) \right] \end{aligned} \quad (4.23)$$

- The trial potential is \mathbb{Q} .

$$\mathbb{Q} \equiv \sum_{i=x,y,z} \frac{q_i^2 \ell}{6} \int_0^{\mathcal{L}} ds \left[X_i^{(1)2} + \sum_{m=1}^{n-1} |Y_i^{(m)}|^2 \right] \quad (4.24)$$

- The wall-constraints are denoted by \mathbb{A} .

$$\begin{aligned} \mathbb{A} &\equiv \int_0^{\mathcal{L}} ds \left\{ A(T_z^{00} X_z^{(0)} + T_z^{10} X_z^{(1)}) \right. \\ &\quad \left. + \sum_{\beta=1}^n \bar{A}(T_z^{0\beta} X_z^{(0)} + T_z^{1\beta} X_z^{(1)} + \sum_{m=1}^{n-1} T_z^{(m+1)\beta} Y_z^{(m)}) \right\} \end{aligned} \quad (4.25)$$

- The constant chemical potential terms associated with the contour integrals, we group together as \mathfrak{c} , that is,

$$\mathfrak{c} \equiv -(N_c + 1) \log \mu_c - 2(N_w + 1) \log \mu_w. \quad (4.26)$$

⁶The vector $\nu^{(0)}$ in (4.23), defined in Appendix A, describes the wall-link locations, which were defined by the vector η prior to the transformation \mathbb{T} .

In terms of the new variables $\{\mathbf{X}^{(0)}, \mathbf{X}^{(1)}, \mathbf{Y}^{(m)}\}$ and above notation⁷, the generalised partition function of (4.13) can be summarized as follows:

$$e^{-F(\mu_w, \mu_c, n)/k_B T} = \int [\text{int}] e^{-W + \mu_c \mathbb{X}_c + \mu_w \mathbb{X}_w + \mathbb{A} + c} \equiv \int [\text{int}] e^{-\mathcal{H}/k_B T}. \quad (4.27)$$

4.4.4 The variational Hamiltonian

The motivation behind the variational (mean-field type) approximation is the relative ease with which one can obtain some understanding of the constrained system.

The crosslinks play the role of a localization potential that restrains each chain to some mean path in the gel. If the confined gel is strained by Λ (2.26) the *average* trajectory of a Gaussian chain will also transform affinely. However, in the strained state (corresponding to replica indices $\alpha > 0$) the chains will probably tend to deviate from their mean paths [3], depending on the degree of crosslinking. The fluctuations should not be ignored, but rather simulated by a suitable trial potential. In Section 4.4.2 an harmonic trial potential (4.20) was elected, because it is simple enough so that the relevant path integrals in (4.13) can be calculated.

We model the constrained system variationally by means of two variational parameters, namely the localization parameters q_x and q_z . Using the trial potential \mathbb{Q} , the parameters can be found by minimizing the variational free energy \mathcal{F}_{var} . Using the Feynman variational principle the expression (4.27) changes to

$$\begin{aligned} e^{-F(\mu_w, \mu_c, n)/k_B T} &\geq \int [\text{int}] e^{\langle \mathbb{Q} + \mu_c \mathbb{X}_c + \mu_w \mathbb{X}_w \rangle - W - \mathbb{Q} + \mathbb{A}} \\ &= \int [\text{int}] e^{\langle \mathbb{Q} + \mu_c \mathbb{X}_c + \mu_w \mathbb{X}_w \rangle} \left(\int \mathcal{G}' \right) \\ &\equiv e^{-F'_{\text{var}}(q_x, q_z)/k_B T} \end{aligned} \quad (4.28)$$

where $\langle \dots \rangle$ means averaging with respect to the Green's function given by

$$\int \mathcal{G}' = \int [\mathcal{D}\mathbf{X}^{(0)}][\mathcal{D}\mathbf{X}^{(1)}][\prod_{m=1}^{n-1} \mathcal{D}\mathbf{Y}^{(m)}] \underbrace{e^{-W - \mathbb{Q} + \mathbb{A}}}_{e^{-\mathcal{H}'_{\text{var}}/k_B T}}. \quad (4.29)$$

Calculating the Green's function in (4.29) seems intractable at this stage, especially due to the \mathbb{A} term for the $\mathbf{X}^{(1)}$ and $\mathbf{Y}^{(m)}$ variables. For now, we circumvent this problem by implementing another trial potential that only contains the centre-of-mass coordinate $\mathbf{X}^{(0)}$, and which is defined as follows:

$$\mathbb{A}_0 \equiv \int_0^{\mathcal{L}} ds \ln \left[\Theta(T^{00} X_z^{(0)}(s)) \Theta(h_z - T^{00} X_z^{(0)}(s)) \right] \quad (4.30)$$

⁷The shortcut notation $[\text{int}]$ refers to $\oint \frac{N_c! d\mu_c}{2\pi i} \oint \frac{N_w! d\mu_w}{2\pi i} \int [\mathcal{D}\mathbf{X}^{(0)}][\mathcal{D}\mathbf{X}^{(1)}][\prod_{m=1}^{n-1} \mathcal{D}\mathbf{Y}^{(m)}]$

such that we now choose to have to work with an exactly solvable Green's function given by

$$\mathcal{G} = \int [\mathcal{D}\mathbf{X}^{(0)}][\mathcal{D}\mathbf{X}^{(1)}][\prod_{m=1}^{n-1} \mathcal{D}\mathbf{Y}^{(m)}] \underbrace{e^{-\mathbb{W}-\mathbb{Q}+\mathbb{A}_0}}_{\equiv e^{-\mathcal{H}_{\text{var}}/k_{\text{B}}T}}. \quad (4.31)$$

In terms of the partition function, it is required to calculate

$$\mathcal{Z}(n, \mu_w, \mu_c) = \langle e^{(\mu_c \mathbb{X}_c + \mu_w \mathbb{X}_w + \mathbb{Q} + \mathbb{A} - \mathbb{A}_0)} \rangle_{\mathcal{G}} \left(\int \mathcal{G} \right) \quad (4.32)$$

$$\geq e^{\langle \mu_c \mathbb{X}_c + \mu_w \mathbb{X}_w + \mathbb{Q} + \mathbb{A} - \mathbb{A}_0 \rangle_{\mathcal{G}}} \left(\int \mathcal{G} \right) \quad (4.33)$$

$$\equiv e^{-F_{\text{var}}(q_x, q_z)/k_{\text{B}}T} \quad (4.34)$$

The free energy of the network can now be performed by using the simple trial form (4.31) for the distribution of the chains. The resultant variational free energy is then minimised with respect to the trial function, to give the best possible approximation to the real free energy \mathcal{F} (for the specific choice of \mathcal{H}_{var}):

$$\mathcal{F} \approx \min_{\mathcal{H}_{\text{var}}} \{ F_{\text{var}} \}. \quad (4.35)$$

The average in the exponent in (4.33) contains a *reduced* wall-constraint, $\mathbb{A} - \mathbb{A}_0$, which we show in Appendix B to be negligible,

$$\langle \mathbb{A} - \mathbb{A}_0 \rangle \simeq 0, \quad (4.36)$$

under the conditions of our variational calculation and a *softened* wall potential \mathbb{A} .

4.5 The variational calculation (for $\langle \mathbb{A} - \mathbb{A}_0 \rangle = 0$)

The actual calculation of the variational free energy $\mathcal{F}_{\text{var}}(q_x, q_z)$ involves two steps. The first is calculating the Green's functions needed in order to average the exponent in (4.33). The second is evaluating the weighted averages.

4.5.1 The Green's functions

The task of computing the Green's function \mathcal{G} in (4.31) is equivalent to evaluating three different analytically solvable propagators⁸.

For the \hat{x} and \hat{y} coordinates, the Green's function corresponding to the "centre-of-gravity" replica ($\beta = 0$), $\mathcal{G} = \int [\text{int}] e^{-\mathbb{W}}$, satisfies the partial differential equation

$$\left(\frac{\partial}{\partial s} - \frac{\ell}{6} \nabla_{X_i^{(0)}}^2 \right) \mathcal{G}_0 = \delta(X_i^{(0)}(s) - X_i^{(0)}(s')) \delta(s - s'), \quad (4.37)$$

for a system in the transformed volume, namely a $(n + 1)$ -tuple *cuboid*, given by

$$\tilde{V} = V \prod_{i=x,y,z} (1 + n\lambda_i^2)^{\frac{1}{2}}. \quad (4.38)$$

The path integral for the remaining replicas ($\beta > 0$) includes the trial potential \mathbb{Q} which mimics the fluctuations of the strained ($\alpha > 0$) from the unstrained ($\alpha = 0$) replicas. In this case, (4.31) simplifies to evaluating $\mathcal{G} = \int [\text{int}] e^{-\mathbb{W} - \mathbb{Q}}$. The solution satisfies the differential equation

$$\left(\frac{\partial}{\partial s} - \frac{\ell}{6} \nabla_{X_i^{(\beta)}}^2 + \frac{\ell q_i^2}{6} X_i^{(\beta)2}(s) \right) \mathcal{G}_0(X_{i_s}^{(\beta)}, X_{i_{s'}}^{(\beta)}; |s - s'|) = \delta(X_{i_s}^{(\beta)} - X_{i_{s'}}^{(\beta)}) \delta(s - s'), \quad (4.39)$$

and is related to the propagator of a quantum particle⁹ in an harmonic potential [19].

For the confined \hat{z} coordinate, there is an added wall-constraint, which exclusively influences¹⁰ the centre-of-mass coordinate $X_z^{(0)}$. The Green's function, $\mathcal{G} = \int [\text{int}] e^{-\mathbb{W} + \mathbb{A}_0}$, for the "centre-of-gravity" ($\beta = 0$) replica satisfies a partial differential equation

$$\left(\frac{\partial}{\partial s} - \frac{\ell}{6} \nabla_{X_z^{(0)}}^2 - A[X_z^{(0)}(s)] \right) \mathcal{G}_0(X_{z_s}^{(0)}, X_{z_{s'}}^{(0)}; |s - s'|) = \delta(X_{z_s}^{(0)} - X_{z_{s'}}^{(0)}) \delta(s - s'), \quad (4.40)$$

analogous to (2.8).

The different solutions to the various path integrals are well-known [53, 19], and are summarised as follows:

⁸Henceforth, the bottom indices shall refer to the integration variable. For example: \mathcal{G}_m indicates to a path integration with respect to $Y_i^{(m)}$, where $m \in 1, 2, \dots, n - 1$. The index i refers to the three Cartesian coordinates, except when otherwise stated. The original sample volume is V , and V_i the box length in the i coordinate.

⁹The kernel of a quantum particle of mass m in an harmonic oscillator of frequency ω can easily be retrieved from the polymer result (4.43) by the following substitution: $s \rightarrow it$, $\frac{3}{2\ell} \rightarrow \frac{m}{2\hbar}$ and $q \rightarrow \frac{3\omega}{\ell}$.

¹⁰This follows from our choice of a Green's function in (4.31).

$$\begin{aligned}
\bullet \quad \mathcal{G}_0(X_i^{(0)}(s), X_i^{(0)}(s'), |s-s'|) &= \mathcal{N} \int_{-\infty}^{\infty} [\delta X_i^0] e^{-\frac{3}{2\ell} \int_0^{\mathcal{L}} \dot{X}_i^{(0)2} ds} \\
&= \frac{1}{V_i (1+n\lambda^2)^{\frac{1}{2}}} + \left(\frac{3}{2\pi\ell|s-s'|} \right)^{1/2} e^{-\frac{3}{2\ell} \frac{(X_i^{(0)}(s)-X_i^{(0)}(s'))^2}{|s-s'|}} \quad \text{for } i = \{x, y\}. \quad (4.41)
\end{aligned}$$

$$\begin{aligned}
\bullet \quad \mathcal{G}_0(X_z^{(0)}(s), X_z^{(0)}(s'), |s-s'|) &= \mathcal{N} \int [\mathcal{D}X_z^0] \exp \left\{ -\frac{3}{2\ell} \int_0^{\mathcal{L}} \dot{X}_z^{(0)2} ds \right\} \\
&\quad \times \exp \left\{ \int_0^{\mathcal{L}} \ln [\Theta(T^{00} X_z^{(0)}) \Theta(h_z - T^{00} X_z^{(0)})] ds \right\} \\
&= \frac{2}{\sqrt{1+n\lambda^2} h_z} \sum_{p=1}^{\infty} e^{-\frac{\ell\pi^2 p^2}{6h_z^2} |s-s'|} \sin \left[\frac{\pi p X_z^{(0)}(s)}{\sqrt{1+n\lambda^2} h_z} \right] \sin \left[\frac{\pi p X_z^{(0)}(s')}{\sqrt{1+n\lambda^2} h_z} \right] \quad (4.42)
\end{aligned}$$

$$\begin{aligned}
\bullet \quad \mathcal{G}_1(X_i^{(1)}(s), X_i^{(1)}(s'), |s-s'|) &= \mathcal{N} \int [\mathcal{D}X_i^{(1)}] e^{-\frac{3}{2\ell} \int_0^{\mathcal{L}} \dot{X}_i^{(1)2} ds - \frac{q_i^2}{6} \int_0^{\mathcal{L}} X_i^{(1)2} ds} \\
&= \left[\frac{q_i}{2\pi \sinh \frac{1}{3} \ell q_i |s-s'|} \right]^{\frac{1}{2}} e^{-\frac{q_i}{2} \frac{[X_i^{(1)2}(s)+X_i^{(1)2}(s')] \cosh \frac{1}{3} \ell q_i |s-s'| - 2X_i^{(1)}(s)X_i^{(1)}(s')}{\sinh \frac{1}{3} \ell q_i |s-s'|}} \quad (4.43)
\end{aligned}$$

$$\begin{aligned}
\bullet \quad \mathcal{G}_m(Y_i^{(m)}(s), Y_i^{(m)}(s'), |s-s'|) &= \mathcal{N} \int [\mathcal{D}Y_i^{(m)}] e^{-\frac{3}{2\ell} \int_0^{\mathcal{L}} |\dot{Y}_i^{(m)}|^2 ds - \frac{q_i^2}{6} \int_0^{\mathcal{L}} |Y_i^{(m)}|^2 ds} \\
&= \left[\frac{q_i}{2\pi \sinh \frac{1}{3} \ell q_i |s-s'|} \right]^{\frac{1}{2}} e^{-\frac{q_i}{2} \frac{[Y_i^{(m)2}(s)+Y_i^{(m)2}(s')] \cosh \frac{1}{3} \ell q_i |s-s'| - 2Y_i^{(m)}(s)Y_i^{(m)}(s')}{\sinh \frac{1}{3} \ell q_i |s-s'|}} \quad (4.44)
\end{aligned}$$

4.5.2 The Averages

The average $\langle \mathbb{Q} + \mu_c \mathbb{X}_c + \mu_w \mathbb{X}_w \rangle$ in (4.32) in terms of the trial Hamiltonian \mathcal{H}_{var} , is evaluated by means of the Green's functions in Section 4.5.1. The full calculation is presented in Appendix C, and here we shall simply list the results.

The Bulk Crosslinks $\langle \mu_c \mathbb{X}_c \rangle$

The weighted average of the polymer-polymer link contribution, defined in (4.22) and calculated in Appendix C.1, is given by

$$\begin{aligned}
\langle \mu_c \mathbb{X}_c \rangle &= \mu_c \langle \mathbb{X}_{cx} \mathbb{X}_{cy} \mathbb{X}_{cz} \rangle \\
&= \left\langle \mu_c \int_0^{\mathcal{L}} ds \int_0^{\mathcal{L}} ds' \prod_{i=x,y,z} \delta(X_i^{(0)}(s) - X_i^{(0)}(s')) \delta(X_i^{(1)}(s) - X_i^{(1)}(s')) \right. \\
&\quad \left. \times \prod_{m=1}^{n-1} \delta(Y_i^{(m)}(s) - Y_i^{(m)}(s')) \right\rangle \quad (4.45)
\end{aligned}$$

$$= \frac{3\mu_c}{2\sqrt{1+n\lambda^2} h_z} \left(\frac{q_z q_i^2}{8\pi^3} \right)^{n/2} \left[\frac{\mathcal{L}^2}{A(1+n/\lambda)} + \frac{3\mathcal{L}}{2\pi\ell} \ln \left(\frac{\mathcal{L}}{\ell_c} \right) \right], \quad (4.46)$$

where A is the cross-sectional area of the undeformed volume containing the sample. The chain *cutoff*-length ℓ_c , over which the chain is not flexible but stiff, is of the order of magnitude of the

Kuhn length ℓ . In order to compute the average $\langle \mathbb{X}_{cz} \rangle_{\mathcal{G}_0}$ of the *zeroth* replica, we limited the calculations to the limit of total chain length larger than the spacing between the plates, that is $h_z \ll \sqrt{\mathcal{L}\ell}$ of (2.18).

The Wall Crosslinks $\langle \mu_w \mathbb{X}_w \rangle$

The wall crosslinks are completely specified by the vectors $\nu^{(0)}(x, y, \epsilon)$ and $\nu^{(0)}(x, y, h_z - \epsilon)$, for crosslinks situated an infinitesimal distance ϵ from the wall “surface”:

$$\nu^{(0)}(x, y, \epsilon) \equiv \left(x \sqrt{1 + n/\lambda}, y \sqrt{1 + n/\lambda}, \epsilon \sqrt{1 + n\lambda^2} \right) \quad (4.47)$$

$$\nu^{(0)}(x, y, h_z - \epsilon) \equiv \left(x \sqrt{1 + n/\lambda}, y \sqrt{1 + n/\lambda}, (h_z - \epsilon) \sqrt{1 + n\lambda^2} \right). \quad (4.48)$$

The weighted average of the polymer-wall link contribution calculated in Appendix C.2 is

$$\begin{aligned} \langle \mu_w \mathbb{X}_w \rangle &= \mu_w \langle \mathbb{X}_{wx} \mathbb{X}_{wy} \mathbb{X}_{wz} \rangle \\ &= \left\langle 2\mu_w \int_0^{\mathcal{L}} ds \int_{-\infty}^{+\infty} dx dy \delta(X_x^{(0)}(s) - \nu_x^{(0)}) \delta(X_y^{(0)}(s) - \nu_y^{(0)}) \delta(X_z^{(0)}(s) - \nu_z^{(0)}) \right. \\ &\quad \left. \times \delta(X_x^{(1)}) \delta(X_y^{(1)}) \delta(X_z^{(1)}) \prod_{m=1}^{n-1} \delta(Y_x^{(m)}) \delta(Y_y^{(m)}) \delta(Y_z^{(m)}) \right\rangle \end{aligned} \quad (4.49)$$

$$\simeq \frac{16\mu_w \pi^2 \epsilon^2 \mathcal{L}}{h_z^3 (1 + n\lambda^2)^{1/2}} \left(\frac{q_z}{\pi} \right)^{n/2} \left(\frac{q}{\pi} \right)^n, \quad (4.50)$$

which is valid only if $h_z \ll \mathcal{L}$ and $\frac{\ell q_i}{3} \geq 1$.

The harmonic trial potential $\langle \mathbb{Q} \rangle$

The average over the harmonic trial potential consists of n identical terms (Appendix C.3) that differ only in terms of the variational parameters q_x and q_z .

$$\langle \mathbb{Q} \rangle = \left\langle \sum_{i=x,y,z} \frac{q_i^2 \ell}{6} \int_0^{\mathcal{L}} ds \left[X_i^{(1)2} + \sum_{m=1}^{n-1} |Y_i^{(m)}|^2 \right] \right\rangle \quad (4.51)$$

$$= \frac{n}{4} \left(3 + \frac{\ell}{3} q_z \mathcal{L} \coth \frac{\ell}{3} q_z \mathcal{L} + \frac{2\ell}{3} q_x \mathcal{L} \coth \frac{\ell}{3} q_x \mathcal{L} \right) \quad (4.52)$$

$$= \frac{n}{4} \left(3 + \frac{\ell \mathcal{L}}{3} (q_z + 2q_x) \right) \quad \text{for } \frac{q_i \ell \mathcal{L}}{3} \geq 1. \quad (4.53)$$

4.5.3 The variational Free energy

The variational free energy (4.34) of $n + 1$ replica systems is given by

$$\mathcal{Z}_{\text{var}}(n, q_x, q_z) = e^{-\mathcal{F}_{\text{var}}(n, q_x, q_z)/k_B T} \quad (4.54)$$

$$= e^{\langle \mu_c \mathbb{X}_c + \mu_w \mathbb{X}_w + \mathbb{Q} + \mathbb{A} - \mathbb{A}_0 \rangle_{\mathcal{G}}} \left(\int \mathcal{G} \right) \quad (4.55)$$

$$\begin{aligned} &= \oint \frac{N_c! d\mu_c}{2\pi i \mu_c^{N_c+1}} e^{\mu_c \langle \mathbb{X}_c \rangle} \oint \frac{N_w! d\mu_w}{2\pi i \mu_w^{N_w+1}} e^{\mu_w \langle \mathbb{X}_w \rangle} e^{\frac{n}{4} \left(3 + \frac{\ell \mathcal{L}}{3} (q_z + 2q_x) \right)} \\ &\quad \times \left(\frac{2\pi}{q_z} \right)^{\frac{n}{2}} \left(\frac{2\pi}{q_x} \right)^n e^{-\frac{\ell \pi^2 \mathcal{L}}{6(1+n\lambda^2)h_z^2}} \frac{8V \prod \sqrt{1 + n\lambda^2}}{\pi^2} e^{-\frac{n\ell}{2} (2q_x + q_z)} \end{aligned} \quad (4.56)$$

In the above expression the integrals over the chemical potentials μ_c and μ_w can be evaluated using (4.26) and the identity (4.12) [9], such that the variational generalised partition function can be written as follows:

$$\begin{aligned} \mathcal{Z}_{\text{var}} &= \langle \mathbb{X}_c \rangle^{N_c} \langle \mathbb{X}_w \rangle^{N_w} e^{\frac{n}{4}[3 - \frac{\ell c}{3}(q_z + 2q_x)]} \left(\frac{2\pi}{q_z}\right)^{\frac{n}{2}} \left(\frac{2\pi}{q_x}\right)^n e^{-\frac{\ell \pi^2 \mathcal{L}}{6(1+n\lambda_z^2)h_z^2}} \frac{8V \prod \sqrt{1+n\lambda^2}}{\pi^2} \quad (4.57) \\ &= \left\{ \frac{3\mu_c}{2} \left[\frac{\mathcal{L}^2}{V \prod_i \sqrt{1+n\lambda_i^2}} + \frac{3\mathcal{L}}{2\pi \ell h_z \sqrt{1+n\lambda_z^2}} \ln\left(\frac{\mathcal{L}}{\ell_c}\right) \right] \right\}^{N_c} \left(\frac{q_z q_x^2}{8\pi^3}\right)^{\frac{n(N_c-1)}{2}} \\ &\quad \left\{ \frac{16\mu_w \pi^2 \epsilon^2 \mathcal{L}}{h_z^3 (1+n\lambda^2)^{1/2}} \left(\frac{q_z q_x^2}{\pi^3}\right)^{n/2} \right\}^{N_w} e^{\frac{n}{4}[3 - \frac{\ell c}{3}(q_z + 2q_x)]} e^{-\frac{\ell \pi^2 \mathcal{L}}{6(1+n\lambda_z^2)h_z^2}} \frac{8V \prod \sqrt{1+n\lambda^2}}{\pi^2} \quad (4.58) \end{aligned}$$

In Deam and Edwards [9] the replica limit $n \rightarrow 0$ is taken prior to minimizing the free energy with respect to q . The variational free energy $\mathcal{F}_{\text{var}}(q_x, q_z)$ of the original gel system can be identified as the coefficient of n as follows:

$$\begin{aligned} -\mathcal{F}_{\text{var}}/k_B T &= \frac{\partial \mathcal{Z}_{\text{var}}/\partial n|_{n=0}}{\mathcal{Z}_{\text{var}}(n=0)} \quad (4.59) \\ &= \frac{1}{2} \frac{N_c}{(1+c/\rho)} \left[\sum_{i=x,y,z} \lambda_i^2 + \frac{c\lambda_z^2}{\rho} \right] + \frac{(N_w-1)\lambda_z^2}{2} - \frac{\ell \pi^2 \lambda_z^2 \mathcal{L}}{6h_z^2} \\ &\quad + \frac{\ell \mathcal{L}}{12} (q_z + 2q_x) - \frac{(N_c + N_w - 1)}{2} \sum_i \ln\left(\frac{q_i}{2\pi}\right) \quad (4.60) \end{aligned}$$

where

$$c = \frac{3}{2\pi \ell h_z} \ln \frac{\mathcal{L}}{\ell_c} \quad \text{and} \quad \rho = \mathcal{L}/V. \quad (4.61)$$

Next the free energy should be minimized with respect to q_x and q_z to find the best approximation (for the given trial Hamiltonian function in (4.31)) to the real free energy of the system. The resultant stationary points are isotropic, and deformation-independent:

$$q_x = \frac{6(N_w + N_c)}{\ell \mathcal{L}} = q_z. \quad (4.62)$$

Substituting the q -values in (4.60) we find that the free energy on deformation, \mathcal{F} , has the following upper bound:

$$\begin{aligned} \mathcal{F} &\leq k_B T \left[\frac{1}{2} \frac{N_c}{(1+c/\rho)} \left\{ \sum_{i=x,y,z} \lambda_i^2 + \frac{c\lambda_z^2}{\rho} \right\} + \frac{(N_w-1)\lambda_z^2}{2} - \frac{\ell \pi^2 \lambda_z^2 \mathcal{L}}{6h_z^2} \right. \\ &\quad \left. + \frac{3N_w}{2} - \frac{(N_c + N_w - 1)}{2} \sum_i \ln\left(\frac{3(N_w + N_c)}{\pi \ell \mathcal{L}}\right) \right]. \quad (4.63) \end{aligned}$$

4.6 Results

In this chapter we extended the Deam-Edwards theory [9] to a polymer network that has formed at and between two confining, parallel plane surfaces.

The free energy on deformation, including only the λ_i -dependent terms in (4.63), is

$$\mathcal{F} \leq k_B T \left[\frac{1}{2} \frac{N_c}{(1+c/\rho)} \left\{ \sum_{i=x,y,z} \lambda_i^2 + \frac{c \lambda_z^2}{\rho} \right\} + \frac{N_w \lambda_z^2}{2} - \frac{\ell \pi^2 \lambda_z^2 \mathcal{L}}{6 h_z^2} \right] \quad (4.64)$$

where N_c and N_w are the total number of bulk-links and wall-links respectively. The above result is only valid when the crosslink density is sufficiently high, such that we are definitely dealing with a *solid* gel. Secondly, the chain-density of the melt, and the effective contour length \mathcal{L} of the polymer network contributing to the elasticity should be greater than the spacing between the wall h_z .

In this model the fluctuations of the crosslinks were simulated with an harmonic potential and variational parameters q_x and q_z . The physical significance of these parameters is that they play the role of localizing the fluctuations a distance proportional to $q_x^{-\frac{1}{2}}$ in the x and y dimensions, and $q_z^{-\frac{1}{2}}$ in the z dimension. The fluctuation volume that each crosslink may explore can thus be estimated as

$$q^{-3/2} = \left[\frac{\ell \mathcal{L}}{6(N_c + N_w)} \right]^{\frac{3}{2}}, \quad (4.65)$$

since the localisation parameters (4.62) are isotropic and λ -independent.

The above result is similar to the Deam and Edwards result [9] for an unconfined phantom network, with no wall-links. In the case of a free, phantom network the localization parameter is given by the above result (4.62) with no wall-links ($N_w \equiv 0$), that is $q_i = \frac{6 N_c}{\ell \mathcal{L}}$. The Deam and Edwards result for the free energy on deformation

$$\tilde{\mathcal{F}}_{DE} \leq k_B T \left[\frac{1}{2} \frac{N_c}{(1+c/\rho)} \sum_{i=x,y,z} \lambda_i^2 \right] \quad (4.66)$$

$$\text{with } c \equiv \left(\frac{3}{2\pi\ell} \right)^{\frac{3}{2}} \frac{1}{2\sqrt{\ell_c}} \quad \text{and} \quad \rho \equiv \mathcal{L}/V, \quad (4.67)$$

is consistent with the confined-network result (4.64) in the limit of a gel only confined by a single wall ($h_z \rightarrow \infty$), and having no wall-links ($N_w = 0$).

From (4.64) the stress¹¹ f , in the specific case of a uniaxial, isovolumetric deformation (2.26), is given by

$$f = \frac{1}{V} \frac{\partial \mathcal{F}}{\partial \lambda} = \frac{k_B T}{V} \left[\frac{N_c}{(1+c/\rho)} \left\{ \lambda - \frac{1}{\lambda^2} + \frac{c}{\rho} \lambda \right\} + \left(N_w - \frac{\ell \pi^2 \mathcal{L}}{3 h_z^2} \right) \lambda \right]. \quad (4.68)$$

¹¹The stress is the elastic force per unit area of the undeformed cross-section of the sample. The stress was also computed for simpler systems (Sections 2.4 and 2.5).

The underlined part in (4.68) coincides with the well-known result of the classical theory of high elasticity of polymer networks [31], apart from the different front factor, which may be attributed to wasted loops [9].

The wall-confinement introduces new terms in the free energy of the network, dependent on the spacing h_z between the walls. For example, the typical confinement term $\frac{\ell\pi^2\mathcal{L}}{6h_z^2}$, is consistent with earlier results for a stitch network (Section 3.4) and a single chain (Section 2.4.1) with an effective contourlength \mathcal{L} .

To summarize: So far, we have applied the Deam and Edwards idea of homogeneous crosslinking and consequently obtained a similar deformation free energy (apart from confinement terms). It was found that the harmonic potential \mathbb{Q} , controlling the fluctuations away from the mean (affine), depends on the inverse distance between $(N_c + N_w)$ crosslinks and *not* on the strain λ . This means that the affine macroscopic deformation of the gel-plate system, results in a microscopic deformation of the chains, which consists of an affine contribution and a *non-affine* fluctuation contribution.

Unfortunately the model employed in this chapter is too crude to differentiate between the types of crosslinking. This resulted in the wall-links and bulk-links being treated in the same manner. Intuitively the degree of localization, manifested in the values q_x and q_z , is expected to depend on the spatial coordinate.

In the next chapter a network, formed from polymer brushes, is investigated. Within this framework, it is possible to distinguish, in a simple albeit concise manner, between the localization that each type of crosslink imposes.

Chapter 5

The Brush Network

In this chapter we consider a network formed from two grafted polymer brushes. The term *polymer brush* was invented by de Gennes [7] to describe an architecture in which polymer chains are terminally tethered to a surface at a high density. This is the case when the separation κ between anchors, is much smaller than the coil dimension, as shown in Figure 5.1.

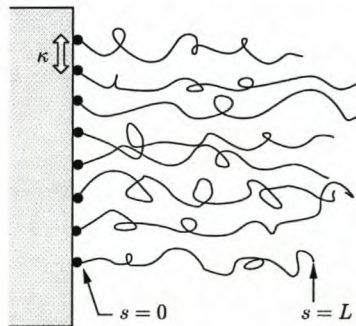


Figure 5.1: Simplified illustration of a brush, consisting of polymer chains attached to a flat, solid surface permanently, with average anchor distance κ between chains.

The anticipated behaviour (within the replica scheme) of a surface-attached, crosslinked polymer includes some kind of localization of the polymer. In Chapter 4 we employed the idea of Deam and Edwards [9], which treats this localization to be homogeneous and translation invariant, that is $q_x = q_z = \text{constant}$ in the trial potential \mathbb{Q} of Section 4.4.2. The *average* polymer network between planar surfaces is symmetric about $z = \frac{1}{2}h_z$ (Figure 4.2), but certainly not translationally invariant in the z -direction. Moreover, we expect the polymer to be localized differently near the surface than in the bulk region away from the surfaces¹. This implies that the variational parameters q_i should depend on the spatial height $z(s)$, of a polymer segment s , between the plates. The only coordinate in the transformed replica system (Section 4.4.1), which represents physical position of the chain segments, is the “centre-of-mass” coordinate $\mathbf{X}^{(0)}$. The remaining coordinates $\{\mathbf{X}^{(1)}, \mathbf{Y}^{(m)}\} |_{\{m=1\dots(n-1)\}}$ are simply relative coordinates. Mathematically, it is thus possible to distinguish between different localizations, by using a trial

¹This is especially so if the distance between the plates becomes sufficiently large. There exists also the freedom of choosing the bulk and surface crosslink densities independently.

potential of the form

$$\mathbb{Q} \sim \int ds q^2(z(s)) \sum_{\beta=1}^n \mathbf{X}^{(\beta)2}, \quad \alpha > 0, \quad (5.1)$$

with the localization parameter q a function of $z(s) \equiv \hat{z} \cdot \mathbf{X}^{(0)}(s)$. Unfortunately, the path integration of an harmonic potential, which is dependent on the arclength coordinate s and a mixture of configurational coordinates of *different* replicas, seems intractable.

However, in a brush network each stretched-out chain is only attached by one *endpoint* ($s = 0$) to the grafting surface. Consequently, we choose the average localization to be solely dependent on the arc distance s , and not the spatial position of the chain. It is with this simplification in mind, that we set out to investigate *inhomogeneous* localization, in terms of a brush architecture.

5.1 Formation of the Brush Network

In order to obtain a surface-attached polymer network, the chains of two polymer brushes should be sufficiently crosslinked. Each *chain* has the same molecular weight N (they are monodisperse) and contourlength L , such that $L = N\ell$. Each *brush* consists of $\frac{1}{2}N_w$ phantom chains that are permanently attached via endpoints to a solid surface at very high density, that is $\kappa \ll \sqrt{\ell L}$, Figure 5.1. Attachment occurs in the *absence* of adsorption: the chains are not attracted to the wall, as in Figure 5.3(a). In practice, real chains will tend to stretch perpendicular to the surface due to overcrowding, until the loss in entropy balances the enthalpic gain of segment dilution. We again choose to work with phantom (Gaussian) chains, which are not subject to excluded volume effects and therefore overcrowding should not affect them.

The best way to realize a brush network, is to grow chains directly at the surface of the wall. This approach is called *grafting* and is shown in Figure 5.2.

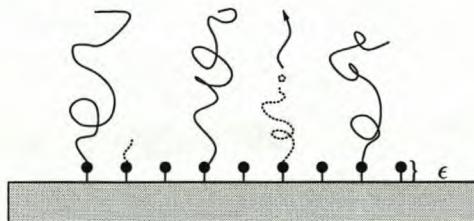


Figure 5.2: Schematic (cross-section) illustration of polymers grafting from a solid surface. The black circles represent the initiator molecules.

Firstly the surface is covered with a monolayer of *initiator* molecules, from which long molecules grow like a lawn². Secondly, the network is formed, by crosslinking the chains. There are a multitude of chemical fabrication techniques that can be used to effect crosslinking [54]. For

²We assume, as in previous chapters, that the polymer chains are linked an infinitesimal distance ϵ away from the wall surface. In this case, the ϵ can be interpreted as the *size* of the initiator molecules, from which the chains are grafted.

example, if the molecules have photoreceptive groups, the chains are crosslinked by irradiation with UV light [40, 30]. The formation of a brush network thus differs from the one considered in Chapter 4, because surface attachment and crosslinking are not performed simultaneously, but in subsequent steps.

5.1.1 Confinement formalism

Prior to network formation, we have two brushes, that is, a dense system of N_w independent chains, already attached to the wall surfaces. The planar surfaces are brought within a distance h_z of each other, so as to confine the grafted polymers in the \hat{z} direction perpendicular to the surface. Mathematically, the confinement is represented by an infinite square well potential A , defined in (4.4) and depicted in Figure 5.3(b).

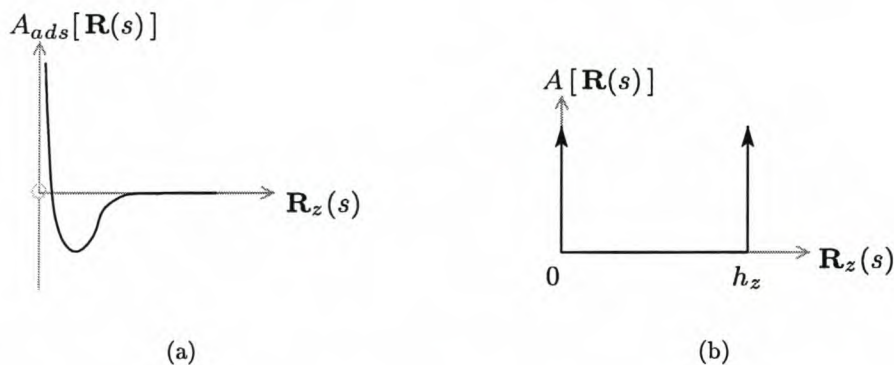


Figure 5.3: Characteristic plots of the spatial profiles of two different situations: (a) A potential well corresponding to a hard, adsorbing wall; (b) An infinite square well potential, for confinement in the \hat{z} direction between two confining plates of width h_z .

The partition function for a collection of N_w confined, grafted chains is given by:

$$\mathcal{Z}(\{\mathbf{R}_i, \mathbf{R}'_i; L\}) = \mathcal{N} \left\{ \prod_{i=1}^{N_w} \int_{\mathbf{R}_i(0)=\mathbf{R}'_i}^{\mathbf{R}_i(L)=\mathbf{R}_i} [\mathcal{D}_{walls} \mathbf{R}_i(s)] \right\} e^{-\frac{3}{2\ell} \sum_{i=1}^{N_w} \int_0^L \left(\frac{\partial \mathbf{R}_i(s)}{\partial s} \right)^2 ds} \quad (5.2)$$

$$= \mathcal{N} \prod_{i=1}^{N_w} \int [\mathcal{D} \mathbf{R}_i(s)] e^{-\int_0^L \left[\frac{3}{2\ell} \dot{\mathbf{R}}_i^2(s) - A(\mathbf{R}_i(s)) \right] ds}, \quad (5.3)$$

where \mathcal{N}^{-1} refers to the statistical weight of N_w free polymer chains, each starting at \mathbf{R}'_i (on the wall) and ending at \mathbf{R}_i in L/ℓ steps.

5.1.2 Crosslink formalism

After confining the polymer brushes, the chains should be crosslinked to each other, in order to constitute a surface-attached network, Figure 5.4. Let the set of crosslink locations on the chains be denoted by $\{S\}$. These links are formed randomly, such that the crosslink positions $\{S_a\}$ of gel sample a will differ from $\{S_b\}$ of sample b . However, once the links are formed, they are assumed to be permanent within a specific sample.

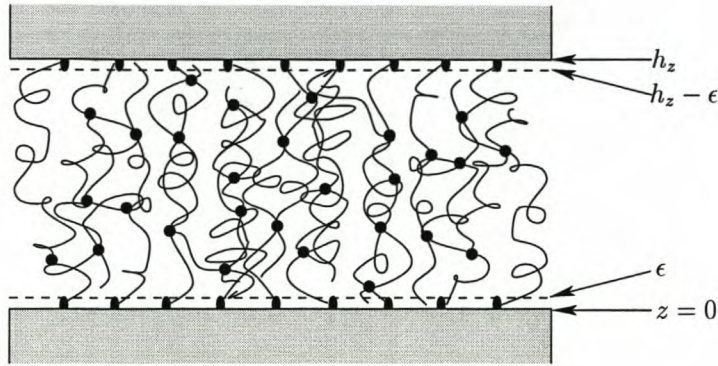


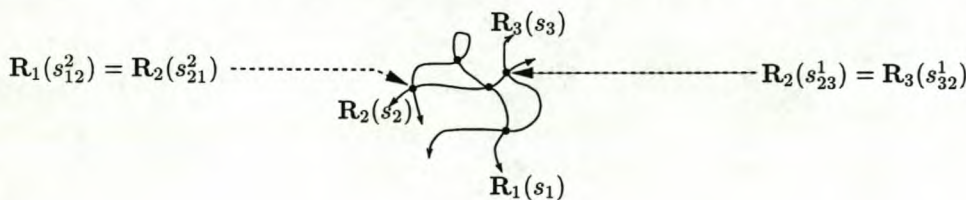
Figure 5.4: An illustrated, simplified view of a brush network. The walls are a distance, h_z , apart and the long polymer chains are fixed at ϵ from the surface.

A cross linkage that joins points s_i^* and s_j^* on chains labeled i and j respectively, is described mathematically by a Dirac delta constraint, $\delta[\mathbf{R}_i(s_i^*) - \mathbf{R}_j(s_j^*)]$. A product of N_c δ -constraints stipulates the topology of a network having N_c crosslinks³. Since the set $\{\mathcal{S}\}$ of crosslinkages is *unknown* prior to network formation, we assume that the linkage positions are distributed according to a probability distribution $\mathcal{P}(\mathcal{S})$. Let the distribution of the crosslinkages in the resultant network, be given by the probability of the crosslinkages an *instant* before linking, that is,

$$\begin{aligned} \mathcal{P}(\{\mathcal{S}\}) \propto & \int \left[\prod_{i=1}^{N_w} \mathcal{D}\mathbf{R}_i(s) \right] e^{-\sum_{i=1}^{N_w} \int_0^L \left[\frac{3}{2l} \dot{\mathbf{R}}_i^2(s) - A(\mathbf{R}_i) \right] ds} \\ & \times \underbrace{\prod_{\{\mathcal{S}\}} \delta[\mathbf{R}_i(s_i^*) - \mathbf{R}_j(s_j^*)]}_{\text{Bulk}} \\ & \times \prod_{i=1}^{N_w/2} \underbrace{\delta[\mathbf{R}_i(s=0) - \eta(x_i, y_i, \epsilon)]}_{\text{Wall at } z=\epsilon} \underbrace{\delta[\mathbf{R}_i(s=0) - \eta(x'_i, y'_i, h_z - \epsilon)]}_{\text{Wall at } z=h_z-\epsilon}, \end{aligned} \quad (5.4)$$

where the η 's are wall-link position vectors [see Section 4.3.2]. This simplified *history-dependent* situation, first proposed by Edwards [14], is equivalent to a system where the future crosslinks

³A more suitable notation for s_i^* mentioned above, would be s_{ij}^k , where i and j are the chains involved in the linkage, and k the degeneracy of the pair. For example: A small network, consisting of three chains, could have the following incidence set $\{\mathcal{S}\} = \{(s_{11}^1, s_{11}^2), (s_{12}^1, s_{21}^1), (s_{12}^2, s_{21}^2), (s_{23}^1, s_{32}^1), (s_{13}^1, s_{31}^1)\}$.



are just touching prior to an instantaneous linking⁴.

5.1.3 Replica formalism

Since the set $\{\mathcal{S}\}$ is fixed for a specific sample, the set and its linking history will remain unaltered if the specimen is deformed in some way. Let $F(\{\mathcal{S}\})$ be the free energy of a particular sample that has been subject to strain Λ (Section 2.4), after network formation. The effective free energy of elasticity, $\mathcal{F}(\Lambda)$, is obtained by taking the quenched average of the sample free energy over all possible realizations of the arclength locations $\{\mathcal{S}\}$,

$$\mathcal{F}(\Lambda) = \int \mathcal{P}(\{\mathcal{S}\}) F(\{\mathcal{S}\}) d\mathcal{S}_i = \int \mathcal{P}(\{\mathcal{S}\}) \ln \mathcal{Z}(\{\mathcal{S}\}) d\mathcal{S}_i. \quad (5.5)$$

The averaging of the logarithm in (5.5) is facilitated by using the mathematical identity (3.12), $Z^n = 1 + n \ln Z + \dots$, and replicating the system n times. At this point, it is possible to incorporate the probability distribution $P(\{\mathcal{S}\})$ of $\{\mathcal{S}\}$, when the chains are touching *before* strain, as a *zeroth* replica. The effective free energy can then be identified as the coefficient of n in the following generalized partition function [9]:

$$e^{-F(n)/k_B T} = \int \mathcal{Z}^{(0)}(\{\mathcal{S}\}) [\mathcal{Z}(\{\mathcal{S}\})]^n \exp(F_0/k_B T) \equiv \mathcal{Z}(n). \quad (5.6)$$

The factor⁵, $e^{F_0/k_B T}$ in (5.6), is the normalization factor of the probability $P(\mathcal{S})$, and the statistical weight of a system where the arclength variables are not constrained to be a fixed set $\{\mathcal{S}\}$. Note that the crosslink points $\{\mathcal{S}\}$ are common to *all* the replicas, and so we can easily average over them. Since we are interested in a resulting network with a sufficiently high crosslink density, we assume that each long macromolecule is involved in numerous crosslinkages. The constraint — averaged over all possible positions of the links — that picks out the N_c crosslinks, is given by

$$\text{Crosslink constraint} \equiv \left[\sum_{i=1}^{N_w} \sum_{j=1}^{N_w} \int_0^L ds \int_0^L ds' \prod_{\alpha=0}^n \delta [\mathbf{R}_i^{(\alpha)}(s) - \mathbf{R}_j^{(\alpha)}(s')] \right]^{N_c}. \quad (5.7)$$

The wall-links are “replicated” in a similar manner [see (5.8)].

We now proceed as in Chapter 4, by calculating the generalized Gibbs formula of $n + 1$

⁴In Chapter 4 the *choice* of probability distribution was done more comprehensively, but also amounts to an instantaneous “freezing” of links.

⁵The free energy F_0 coincides with F' of a slipping link system in (4.7), apart from different naming of constants and wall-link integrations.

replicas,

$$\begin{aligned}
\mathcal{Z}(n) &= \mathcal{N} \int \left[\prod_{i=1}^{N_w} \mathcal{D}\mathbf{R}_i^{(0)}(s) \right] \tilde{\int} \left[\prod_{i=1}^{N_w} \prod_{\alpha=1}^n \mathcal{D}\mathbf{R}_i^{(\alpha)}(s) \right] e^{-\sum_{\alpha} \sum_{i=1}^{N_w} \int_0^L \left[\frac{3}{2l} \dot{\mathbf{R}}_i^2(s) - A(\mathbf{R}_i) \right] ds} \\
&\times \left[\sum_{i=1}^{N_w} \sum_{j=1}^{N_w} \int_0^L ds \int_0^L ds' \prod_{\alpha=0}^n \delta[\mathbf{R}_i^{(\alpha)}(s) - \mathbf{R}_j^{(\alpha)}(s')] \right]^{N_c} \\
&\times \left[\sum_{i=1}^{N_w} \int dx dy \prod_{\alpha=0}^n \delta[\mathbf{R}_i^{(\alpha)}(0) - \eta^{(\alpha)}(x, y, 0)] \right]^{\frac{1}{2}N_w} \\
&\times \left[\sum_{i=1}^{N_w} \int dx dy \prod_{\alpha=0}^n \delta[\mathbf{R}_i^{(\alpha)}(0) - \eta^{(\alpha)}(x, y, h_z)] \right]^{\frac{1}{2}N_w}, \tag{5.8}
\end{aligned}$$

where the notation \int refers to integration in an unstrained *zeroth* replica system, and $\tilde{\int}$ to integration in the remaining n deformed replicas. The bulk crosslink points have the freedom to form anywhere along the length of the chains. However, the *wall* linking always takes place at $s = 0$ for each chain, but the precise location on the xy -plane surfaces is unknown. Therefore, the wall-link constraint in (5.8) is written *without* an s -integration, in contrast with the situation previously formulated in (4.7).

The crosslink constraints are exponentiated by introducing chemical potentials (4.12) μ_c and μ_w for the bulk and wall linkages respectively. This leads to the most compact notation for the generalized partition function,

$$\begin{aligned}
\mathcal{Z}(n) &\equiv \mathcal{N} \oint \frac{N_c! d\mu_c}{2\pi i} \oint \frac{N_w! d\mu_w}{2\pi i} \int \tilde{\int} \dots \tilde{\int} \left[\prod_{\alpha=0}^n \mathcal{D}\mathbf{R}^{(\alpha)}(s) \right] \\
&\times \exp \left\{ -\mathcal{H}(n)/k_B T - N_c \log \mu_c - N_w \log \mu_w \right\}, \tag{5.9}
\end{aligned}$$

where \mathcal{H} is a *pseudo*-Hamiltonian for network connectivity and confinement similar to the previous Hamiltonian encountered in (4.14). The next task at hand is to evaluate the path integrals in (5.9). Thereafter, the free energy of deformation $\mathcal{F}(\Lambda)$ is recovered by taking the the replica limit (3.12).

5.2 The Variational Approach

Evaluation of the difficult path integrals in (5.9) will be tackled by the usual Feynman variational procedure [19], together with the replica coordinate transformation (A.1) of Chapter 4.

5.2.1 Trial potential for the brush network

The reason for investigating a *brush* network in the first place, is the prospect of an inhomogeneous, but integrable (trial) potential, that can simulate the Dirac-delta constraints. With the *brush* network we capitalize on the fact that it is the endpoints, at arc location $s = 0$, that are permanently fixed to the walls. We do this by introducing *two* constant localization parameters. The first, q_0 , describes the localization within a certain region near the wall attachment, and q_1 the bulk region, as illustrated by Figure 5.5:

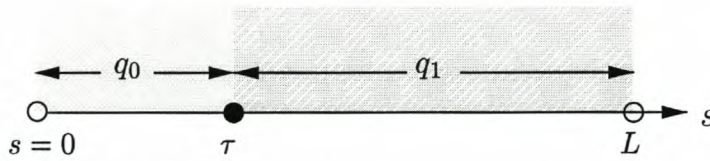


Figure 5.5: The s -line depicts the domains of the variational parameters, q_0 , q_1 , and τ in (5.10).

It is now possible to simulate the cross-link constraints by the following trial harmonic potential [compare with (4.20)],

$$Q = \frac{1}{6\ell} \sum_{\beta=1}^n \left(\int_0^{\tau} ds q_0^2 \mathbf{X}^{(\beta)2} + \int_{\tau}^L ds q_1^2 \mathbf{X}^{(\beta)2} \right), \quad \beta \in [1, 2, \dots, n] \quad (5.10)$$

and thus model the system variationally by means of *three* variational parameters, q_0 , q_1 and τ . In (5.10) the chain conformations were written in terms of more convenient, transformed coordinates $\{\mathbf{X}^{(0)}, \mathbf{X}^{(1)}, \mathbf{Y}^{(m)}\}_{\{m=1 \dots (n-1)\}}$, as previously defined by the transformation matrix \mathbf{T} in (A.1).

In terms of the new set of coordinates, the generalized partition function can be summarized⁶ as follows:

$$e^{-F(\mu_w, \mu_c, n)/k_B T} = \prod_{i=1}^{N_w} \int [\text{int}] e^{-\mathbb{W}_i + \mu_c \mathbb{X}_{ci} + \mu_w \mathbb{X}_{wi} + \mathbb{A}_i + c} \quad (5.11)$$

$$\equiv \prod_{i=1}^{N_w} \int [\text{int}] e^{-\mathcal{H}_i/k_B T} \quad (5.12)$$

In the above and future succinct expressions, we employ the following notation:

- The connectivity of the chains, each of length L , is denoted by the Wiener term \mathbb{W} .

$$\mathbb{W}_i \equiv -\frac{3}{2\ell} \int_0^{\mathcal{L}} \left[\dot{\mathbf{X}}_i^{(0)2}(s) + \dot{\mathbf{X}}_i^{(1)2}(s) + \sum_{m=1}^{n-1} |\dot{\mathbf{Y}}_i^{(m)}(s)|^2 \right] ds \quad (5.13)$$

- The bulk crosslinks are denoted by $\mu_c \mathbb{X}_c$

$$\begin{aligned} \mu_c \mathbb{X}_{ci} &\equiv \mu_c \sum_{j=1}^{N_w} \int_0^{\mathcal{L}} ds \int_0^{\mathcal{L}} ds' \delta(\mathbf{X}_i^{(0)}(s) - \mathbf{X}_j^{(0)}(s')) \delta(\mathbf{X}_i^{(1)}(s) - \mathbf{X}_j^{(1)}(s')) \\ &\quad \times \prod_{m=1}^{n-1} \delta(\mathbf{Y}_i^{(m)}(s) - \mathbf{Y}_j^{(m)}(s')) \end{aligned} \quad (5.14)$$

- The wall cross-links are denoted by $\mu_w \mathbb{X}_w$. The variables ν stand for the transformed vectors describing the wall-linking [see also Appendix A].

$$\begin{aligned} \mu_w \mathbb{X}_{wi} &\equiv \mu_w \int_{-\infty}^{+\infty} dx dy \left[\delta(\mathbf{X}_i^{(0)}(0) - \nu^{(0)}(x, y, \epsilon)) \delta(\mathbf{X}_i^{(1)}(0)) \prod_{m=1}^{n-1} \delta(\mathbf{Y}_i^{(m)}(0)) \right. \\ &\quad \left. + \delta(\mathbf{X}_i^{(0)}(0) - \nu^{(0)}(x, y, h_z - \epsilon)) \delta(\mathbf{X}_i^{(1)}(0)) \prod_{m=1}^{n-1} \delta(\mathbf{Y}_i^{(m)}(0)) \right] \end{aligned} \quad (5.15)$$

- The trial potential is \mathbb{Q} .

$$\mathbb{Q}_i \equiv \frac{\ell}{6} \left(q_0^2 \int_0^{\tau} ds \left[\mathbf{X}_i^{(1)2} + \sum_{m=1}^{n-1} |\mathbf{Y}_i^{(m)}|^2 \right] + q_1^2 \int_{\tau}^{\mathcal{L}} \left[\mathbf{X}_i^{(1)2} + \sum_{m=1}^{n-1} |\mathbf{Y}_i^{(m)}|^2 \right] \right) \quad (5.16)$$

- The wall-constraints are denoted by \mathbb{A} .

$$\begin{aligned} \mathbb{A}_i &\equiv \int_0^{\mathcal{L}} ds \left\{ A(T_z^{00} X_{iz}^{(0)} + T_z^{10} X_{iz}^{(1)}) \right. \\ &\quad \left. + \sum_{\alpha=1}^n \tilde{A}(T_z^{0\alpha} X_{iz}^{(0)} + T_z^{1\alpha} X_{iz}^{(1)} + \sum_{m=1}^{n-1} T_z^{(m+1)\alpha} Y_{iz}^{(m)}) \right\} \end{aligned} \quad (5.17)$$

⁶The shortcut notation $[\text{int}]$ refers to $\oint \frac{N_c! d\mu_c}{2\pi i} \oint \frac{N_w! d\mu_w}{2\pi i} \int [\delta \mathbf{X}^{(0)}] [\delta \mathbf{X}^{(1)}] [\prod_{m=1}^{n-1} \delta \mathbf{Y}^{(m)}]$. The notation c represents the constant chemical potential terms associated with the contour integrals, that is, $c \equiv -(N_c + 1) \log \mu_c - (N_w + 1) \log \mu_w$.

If a second *trial* potential \mathbb{A}_0 (4.30) is introduced⁷, analogous to Section 4.5, we obtain the following generalized partition function:

$$\mathcal{Z}(n, q_0, q_1, \tau) = \prod_{i=1}^{N_w} \langle e^{\mu_c \mathbb{X}_c + \mu_w \mathbb{X}_w + \mathbb{Q} + \mathbb{A} - \mathbb{A}_0} \rangle_{\mathcal{G}} \left(\int \mathcal{G} \right) \quad (5.18)$$

$$\geq \prod_{i=1}^{N_w} e^{\langle \mu_c \mathbb{X}_c + \mu_w \mathbb{X}_w + \mathbb{Q} + \mathbb{A} - \mathbb{A}_0 \rangle_{\mathcal{G}}} \left(\int \mathcal{G} \right) \quad (5.19)$$

$$\equiv e^{-F_{\text{var}}(n, q_0, q_1, \tau) / k_B T} \quad (5.20)$$

where the notation $\langle \dots \rangle_{\mathcal{G}}$ indicates averaging with respect to the Green's function \mathcal{G} . We will again make the Ansatz (4.36), $\langle \mathbb{A} - \mathbb{A}_0 \rangle \simeq 0$. The variational parameters q_0 , q_1 and τ are recovered by minimizing the variational free energy, F_{var} .

5.2.2 Averaging

In order to obtain the variational free energy F_{var} in (5.20), the average $\langle \mathbb{Q} + \mu_c \mathbb{X}_c + \mu_w \mathbb{X}_w \rangle$ is evaluated in terms of the Green function,

$$\mathcal{G} = \int [\delta \mathbf{X}^{(0)}][\delta \mathbf{X}^{(1)}][\prod_{m=1}^{n-1} \delta \mathbf{Y}^{(m)}] \underbrace{e^{-\mathbb{W} - \mathbb{Q} + \mathbb{A}_0}}_{\equiv e^{-\mathcal{H}_{\text{var}} / k_B T}}, \quad (5.21)$$

which can be factored, depending on the replica index and Cartesian coordinate, into well-known Green's functions listed in Section 4.5. Since we are working with a model having two parameters dependent on s , the averages should be performed carefully for each region, for example:

$$\langle f(s) \rangle = \begin{cases} \frac{\int dX_s dX_\tau dX_L \mathcal{G}(X_s, X_0; s, q_0) f(s) \mathcal{G}(X_\tau, X_s; \tau - s, q_0) \mathcal{G}(X_L, X_\tau; L - \tau, q_1)}{\int dX_\tau dX_L \mathcal{G}(X_\tau, X_0; \tau, q_0) \mathcal{G}(X_L, X_\tau; L - \tau, q_1)} & \text{if } 0 < s < \tau \\ \frac{\int dX_\tau dX_s dX_L \mathcal{G}(X_\tau, X_0; \tau, q_0) \mathcal{G}(X_s, X_\tau; s - \tau, q_0) f(s) \mathcal{G}(X_L, X_s; L - s, q_1)}{\int dX_\tau dX_L \mathcal{G}(X_\tau, X_0; \tau, q_0) \mathcal{G}(X_L, X_\tau; L - \tau, q_1)} & \text{if } \tau < s < L. \end{cases} \quad (5.22)$$

This section contains the final results of the averages, but the full calculation is relegated to Appendix D.

⁷Note that \mathbb{A}_0 is not *really* a trial potential, since it has no variational parameters like \mathbb{Q} has. However, since it only depends on the “centre-of-mass” coordinate $\mathbf{X}^{(0)}$, it is integrable.

The Bulk Cross-links $\langle \mu_c \mathbb{X}_c \rangle$

The weighted average of the crosslink contribution, defined in (5.14) and calculated in Appendix D.1, is given by the following lengthy expression:

$$\begin{aligned}
\therefore \langle \mu_c \mathbb{X}_c \rangle &= \mu_c \langle \mathbb{X}_{cx} \mathbb{X}_{cy} \mathbb{X}_{cz} \rangle \\
&= \frac{3\mu_c}{2} \left[\left(\frac{q_0}{2\pi} \right)^{\frac{3n}{2}} \left\{ \frac{2N_w \tau^2}{V \prod \sqrt{1+n\lambda_i^2}} + \frac{3 \left(\ell_c - \sqrt{\ell_c^2 + \tau^2} + \frac{\tau}{2} \ln \left[\frac{\sqrt{\ell_c^2 + \tau^2} + \tau}{\sqrt{\ell_c^2 + \tau^2} - \tau} \right] \right)}{\pi \ell h_z \sqrt{1+n\lambda_z^2}} \right\} \right. \\
&\quad + \left(\frac{q_1}{2\pi} \right)^{\frac{3n}{2}} \left\{ \frac{2N_w (L-\tau)^2}{V \prod \sqrt{1+n\lambda_i^2}} + \frac{3}{\pi \ell h_z \sqrt{1+n\lambda_z^2}} \left(\ell_c - \sqrt{\ell_c^2 + (L-\tau)^2} \right. \right. \\
&\quad \left. \left. + \frac{L}{2} \ln \left[\frac{\sqrt{\ell_c^2 + (L-\tau)^2} + L - \tau}{\sqrt{\ell_c^2 + (L-\tau)^2} - L + \tau} \right] + \frac{\tau}{2} \ln \left[\frac{\sqrt{\ell_c^2 + (L-\tau)^2} - L + \tau}{\sqrt{\ell_c^2 + (L-\tau)^2} + L - \tau} \right] \right) \right\} \quad (5.23) \\
&\quad + \left(\frac{q_0 q_1}{\pi(q_0 + q_1)} \right)^{\frac{3n}{2}} \left\{ \frac{4N_w \tau (L-\tau)}{V \prod \sqrt{1+n\lambda_i^2}} - \frac{3}{\pi \ell h_z \sqrt{1+n\lambda_z^2}} \left(\ell_c + \sqrt{\ell_c^2 + L^2} - \sqrt{\ell_c^2 + \tau^2} \right. \right. \\
&\quad \left. \left. - \sqrt{\ell_c^2 + (L-\tau)^2} - L \ln \left[\frac{\sqrt{\ell_c^2 + (L-\tau)^2} - L + \tau}{\sqrt{\ell_c^2 + L^2} - L} \right] - \tau \ln \left[\frac{\sqrt{\ell_c^2 + \tau^2} - \tau}{\sqrt{\ell_c^2 + (L-\tau)^2} - L + \tau} \right] \right) \right\} \Bigg],
\end{aligned}$$

where the constant ℓ_c is the chain *cut-off* length⁸. Equation (5.23) is valid when the polymer brush chains are long, and when the relation, $\sqrt{N\ell} \gg h_z$ holds.

The Wall Cross-links $\langle \mu_w \mathbb{X}_w \rangle$

The brush chains are attached an infinitesimal distance ϵ from the planar surface. It is shown in Appendix A that any wall-link, after the transformation \mathbb{T} (A.1), is specified by the following two vectors,

$$\nu^{(0)}(x, y, \epsilon) \equiv \left(x \sqrt{1+n/\lambda}, y \sqrt{1+n/\lambda}, \epsilon \sqrt{1+n\lambda^2} \right) \quad (5.24)$$

$$\nu^{(0)}(x, y, h_z - \epsilon) \equiv \left(x \sqrt{1+n/\lambda}, y \sqrt{1+n/\lambda}, (h_z - \epsilon) \sqrt{1+n\lambda^2} \right), \quad (5.25)$$

for the original bottom and top surfaces respectively. The weighted average of the wall-links, calculated in Appendix D.2, is

$$\begin{aligned}
\langle \mu_w \mathbb{X}_w \rangle &\equiv \left\langle \mu_w \int_{-\infty}^{+\infty} dx dy \left[\delta(\mathbf{X}_i^{(0)}(0) - \nu^{(0)}(x, y, \epsilon)) \delta(\mathbf{X}_i^{(1)}(0)) \prod_{m=1}^{n-1} \delta(\mathbf{Y}_i^{(m)}(0)) \right. \right. \\
&\quad \left. \left. + \delta(\mathbf{X}_i^{(0)}(0) - \nu^{(0)}(x, y, h_z - \epsilon)) \delta(\mathbf{X}_i^{(1)}(0)) \prod_{m=1}^{n-1} \delta(\mathbf{Y}_i^{(m)}(0)) \right] \right\rangle \quad (5.26)
\end{aligned}$$

$$= \frac{4\mu_w \pi^2 \epsilon^2}{h_z^3}. \quad (5.27)$$

⁸The continuous s representation of a macromolecule, is only acceptable for distances larger than ℓ_c . At distances smaller than $\ell_c \approx \ell$, the chain will appear stiff due to actual monomer bonds.

The fact that the wall links in a brush network only occur at $s = 0$, is portrayed in the above q -independent constant average, in contrast with the result for a “normal” surface-attached network (4.50).

The harmonic trial potential $\langle \mathbb{Q} \rangle$

The average of the harmonic trial potential for inhomogeneous localization is given by the following expression:

$$\begin{aligned} \langle \mathbb{Q} \rangle &= \left\langle \frac{\ell q_0^2}{6} \int_0^\tau ds (\mathbf{X}_i^{(1)})^2 + \sum_{m=1}^{n-1} |\mathbf{Y}_i^{(m)}|^2 + \frac{\ell q_1^2}{6} \int_\tau^L ds (\mathbf{X}_i^{(1)})^2 + \sum_{m=1}^{n-1} |\mathbf{Y}_i^{(m)}|^2 \right\rangle \quad (5.28) \\ &= \frac{n\ell}{8} \left(2[(L-\tau)q_1^2 + \tau q_0^2] \sinh \frac{\ell q_0}{3} \tau \cosh \frac{\ell q_1}{3} (L-\tau) \right. \\ &\quad \left. + Lq_0q_1 \left\{ \sinh \frac{\ell}{3} ([L-\tau]q_1 + \tau q_0) + \sinh \frac{\ell}{3} ([L-\tau]q_1 - \tau q_0) \right\} \right) \\ &\quad \times \left(q_0 \cosh \frac{\ell q_0}{3} \tau \cosh \frac{\ell q_1}{3} (L-\tau) + q_1 \cosh \frac{\ell q_1}{3} (L-\tau) \cosh \frac{\ell q_0}{3} \tau \right)^{-1}, \quad (5.29) \end{aligned}$$

When the hyperbolic functions in (5.29) are written as exponentials, the average simplifies to

$$\langle \mathbb{Q} \rangle \simeq \frac{n\ell}{4} [(q_0 - q_1)\tau + q_1 L], \quad (5.30)$$

which is valid when the conditions, $q_0 \geq \frac{3}{\ell\tau}$ and $q_1 \geq \frac{3}{\ell(L-\tau)}$, are satisfied.

In the limit of homogeneous localization, that is $q_0 \equiv q_1$, the average (5.28) reduces to the familiar result given in (4.53).

5.3 The variational Free energy

In order to obtain an approximate free energy of the original gel system (Figure 5.4), we first have to find values of q_0 , q_1 and τ that minimize the variational free energy F_{var} . At these stationary points, denoted by $\{q_0^*, q_1^*, \tau^*\}$, the variational free energy is expected to be a good upper bound for the real free energy of a *replicated* system. In the last step the replica limit, which amounts to $n \rightarrow 0$, should be taken. However, for polymer network theories it is generally accepted that the replica limit and the minimization procedure may be safely interchanged [2, 9]. We shall approach the problem in the manner of Deam and Edwards, by first taking the replica limit to obtain the variational free energy $\tilde{\mathcal{F}}$ of a single system, followed by minimizing the resultant free energy.

The variational free energy (5.20) in 3 ($n + 1$) replica space is obtained by assembling all the averages of Section 5.2.2:

$$\mathcal{Z}_{\text{var}}(n) = e^{-F_{\text{var}}(n, q_0, q_1, \tau)/k_{\text{B}}T} \quad (5.31)$$

$$= \prod_{i=1}^{N_{\text{w}}} e^{\langle \mu_{\text{c}} \mathbb{X}_{\text{c}} + \mu_{\text{w}} \mathbb{X}_{\text{w}} + \mathbb{Q} + \mathbb{A} - \mathbb{A}_0 \rangle_{\mathcal{G}}} \left(\int \mathcal{G} \right) \quad (5.32)$$

$$= \prod_{i=1}^{N_{\text{w}}} \oint \frac{N_{\text{c}}! d\mu_{\text{c}}}{\mu_{\text{c}}^{N_{\text{c}}+1}} e^{\mu_{\text{c}} \langle \mathbb{X}_{\text{c}} \rangle} \oint \frac{N_{\text{w}}! d\mu_{\text{w}}}{\mu_{\text{w}}^{N_{\text{w}}+1}} e^{\mu_{\text{w}} \langle \mathbb{X}_{\text{w}} \rangle} e^{\frac{n\ell}{4} [(q_0 - q_1)\tau + q_1 L]} \\ \times \left(\frac{4\epsilon}{h_z} e^{-\frac{\ell\pi^2 L}{6(1+n\lambda_z^2)h_z^2}} \left(\frac{4q_0}{q_0 + q_1} \right)^{\frac{3n}{2}} e^{-\frac{n\ell}{2} [(q_0 - q_1)\tau + q_1 L]} \right) \quad (5.33)$$

$$= \prod_{i=1}^{N_{\text{w}}} \langle \mathbb{X}_{\text{c}} \rangle^{N_{\text{c}}} \langle \mathbb{X}_{\text{w}} \rangle^{N_{\text{w}}} e^{-\frac{n\ell}{4} [(q_0 - q_1)\tau + q_1 L]} e^{-\frac{\ell\pi^2 L}{6(1+n\lambda_z^2)h_z^2}} \left(\frac{4q_0}{q_0 + q_1} \right)^{\frac{3n}{2}} \frac{4\epsilon}{h_z}. \quad (5.34)$$

In Section 5.2.2 some of the averages were simplified in the limit $\sqrt{N\ell} \gg h_z$. For a dense network in a relatively narrow confinement, it is expected that the localization near the walls should not be appreciably different from that further away in the “bulk” region. We portray this expectation⁹ by letting

$$q_0 \equiv (1 + \gamma) q_1, \quad \gamma \in \mathbb{R}. \quad (5.35)$$

With the above substitution, the variational partition function becomes

$$\mathcal{Z}_{\text{var}} = \prod_{i=1}^{N_{\text{w}}} \left(\frac{q_1}{2\pi} \right)^{\frac{3n}{2}} \langle \mathbb{X}_{\text{c}} \rangle^{N_{\text{c}}} \langle \mathbb{X}_{\text{w}} \rangle^{N_{\text{w}}} e^{-\frac{nq_1\ell}{4} [\gamma\tau + L]} e^{-\frac{\ell\pi^2 L}{6(1+n\lambda_z^2)h_z^2}} \left(\frac{4(1 + \gamma)}{2 + \gamma} \right)^{\frac{3n}{2}} \frac{4\epsilon}{h_z}. \quad (5.36)$$

5.3.1 The Replica limit

The variational free energy of the *original* three dimensional system, say $\tilde{\mathcal{F}}$, can be identified as the coefficient of n in (5.6), by employing the following procedure [9],

$$-\tilde{\mathcal{F}}/k_{\text{B}}T \equiv \frac{\partial \mathcal{Z}_{\text{var}}/\partial n|_{n=0}}{\mathcal{Z}_{\text{var}}(n=0)}, \quad (5.37)$$

⁹This substitution is also chosen to simplify the minimization task at hand.

which results in the following variational free energy for the brush network:

$$\begin{aligned}
\tilde{\mathcal{F}}(q_1, \gamma, \tau)/k_B T = & \\
& \frac{\ell N_w}{4} (L + \gamma \tau) q_1 - \frac{\ell L \lambda^2 N_w \pi^2}{6 h_z^2} - \frac{3}{2} N_w \ln \left(\frac{4(1 + \gamma)}{2 + \gamma} \right) - \frac{3}{2} N_c N_w \ln \left(\frac{q_1}{2\pi} \right) \\
& - N_c N_w \left[\frac{3}{2} \ln(1 + \gamma) \left\{ \frac{3}{\pi \ell h_z} \left(\ell_c - \sqrt{\ell_c^2 + \tau^2} + \frac{\tau}{2} \ln \left[\frac{\sqrt{\ell_c^2 + \tau^2} + \tau}{\sqrt{\ell_c^2 + \tau^2} - \tau} \right] \right) + \frac{2N_w \tau^2}{V} \right\} \right. \\
& + \frac{3}{2} \ln \left[\frac{2(1 + \gamma)}{2 + \gamma} \right] \left\{ \frac{4N_w (L - \tau) \tau}{V} - \frac{3}{\pi \ell h_z} \left(\ell_c + \sqrt{\ell_c^2 + L^2} - \sqrt{\ell_c^2 + (L - \tau)^2} - \sqrt{\ell_c^2 + \tau^2} \right. \right. \\
& \left. \left. - L \ln \left[\frac{\sqrt{\ell_c^2 + (L - \tau)^2} - L + \tau}{\sqrt{\ell_c^2 + L^2} - L} \right] - \tau \ln \left[\frac{\sqrt{\ell_c^2 + \tau^2} - \tau}{\sqrt{\ell_c^2 + (L - \tau)^2} - L + \tau} \right] \right\} \right] \\
& - \frac{N_w L^2}{V} \sum_{i=x,y,z} \lambda_i^2 - \frac{3\lambda_z^2}{2\pi \ell h_z} \left(\ell_c - \sqrt{\ell_c^2 + L^2} + \frac{L}{2} \ln \left[\frac{\sqrt{\ell_c^2 + L^2} + L}{\sqrt{\ell_c^2 + L^2} - L} \right] \right) \\
& \times \left(\frac{2N_w L^2}{V} + \frac{3}{\pi \ell h_z} \left(\ell_c - \sqrt{\ell_c^2 + L^2} + \frac{L}{2} \ln \left[\frac{\sqrt{\ell_c^2 + L^2} + L}{\sqrt{\ell_c^2 + L^2} - L} \right] \right) \right)^{-1}. \tag{5.38}
\end{aligned}$$

At this point, all that remains to be done, is to minimize the above expression with respect to the variational parameters $\{q_1, \gamma, \tau\}$.

5.3.2 The minimization problem

The formidable task of finding the stationary points $\{q_1^*, \gamma^*, \tau^*\}$, where $\tilde{\mathcal{F}}$ has a global minimum, is equivalent to solving the following equations simultaneously,

$$\frac{\partial \tilde{\mathcal{F}}(q_1^*, \gamma^*, \tau^*)}{\partial q_1} = 0 \tag{5.39}$$

$$\frac{\partial \tilde{\mathcal{F}}(q_1^*, \gamma^*, \tau^*)}{\partial \gamma} = 0 \tag{5.40}$$

$$\frac{\partial \tilde{\mathcal{F}}(q_1^*, \gamma^*, \tau^*)}{\partial \tau} = 0 \quad \text{on region } \tau \in (\ell_c, L - \ell_c), \tag{5.41}$$

together with the condition that the Hessian H [25] of $\tilde{\mathcal{F}}$,

$$H = \begin{vmatrix} \frac{\partial^2 \tilde{\mathcal{F}}}{\partial q_1^2} & \frac{\partial^2 \tilde{\mathcal{F}}}{\partial q_1 \partial \gamma} & \frac{\partial^2 \tilde{\mathcal{F}}}{\partial q_1 \partial \tau} \\ \frac{\partial^2 \tilde{\mathcal{F}}}{\partial \gamma \partial q_1} & \frac{\partial^2 \tilde{\mathcal{F}}}{\partial \gamma^2} & \frac{\partial^2 \tilde{\mathcal{F}}}{\partial \gamma \partial \tau} \\ \frac{\partial^2 \tilde{\mathcal{F}}}{\partial \tau \partial q_1} & \frac{\partial^2 \tilde{\mathcal{F}}}{\partial \tau \partial \gamma} & \frac{\partial^2 \tilde{\mathcal{F}}}{\partial \tau^2} \end{vmatrix}_{(q_1, \gamma, \tau) = (q_1^*, \gamma^*, \tau^*)} \tag{5.42}$$

and any second derivative, for example $\frac{\partial^2 \tilde{\mathcal{F}}}{\partial q_1^2} |_{(q_1^*, \gamma^*, \tau^*)}$, are both positive at the stationary point. Solving the problem analytically seems intractable due to the transcendental equation (5.41). However, it is possible to find solutions, q_1^* and γ^* , for (5.39) and (5.40). The localization parameters are found to be

$$q_1^* = \frac{6 N_c}{\ell (L + \gamma^*)} \quad \text{and} \quad q_0^* = \frac{6 N_c (1 + \gamma^*)}{\ell (L + \gamma^*)}, \tag{5.43}$$

where γ^* is still a function of τ . The extremum points of $\tilde{\mathcal{F}}$ are calculated numerically. Next, the value τ^* , which minimizes the free energy $\tilde{\mathcal{F}}$, is found by plotting the free energy as a function of τ , and identifying τ^* as the value, on region $(\ell_c, L - \ell_c)$, where $\tilde{\mathcal{F}}(\tau)$ has a global minimum.

5.4 Analysis and Results

In this section we probe the physics of the system, without beforehand obtaining closed form solutions for the variational parameters $\{q_1, \tau, \gamma\}$ that satisfy the minimization equations (5.39)–(5.41).

5.4.1 The homogeneous brush limit

In a homogeneous brush network the crosslinks impose a uniform localization on the system. This situation is obtained, by letting $\tau = 0$ or $\gamma = 0$ in (5.43) and (5.38) respectively. In this limit we obtain the usual Deam and Edwards [9] localization parameters

$$q_1^* = \frac{6 N_c}{\ell L} = q_0^*, \quad (5.44)$$

and the following free energy of deformation

$$\begin{aligned} \mathcal{F}_{\text{uniform}}/k_B T &\geq \frac{3N_c N_w}{2} \left(1 + \ln \left[\frac{3N_c}{\pi \ell L} \right] \right) - \frac{\pi^2 \ell L \lambda_z^2 N_w}{6 h_z^2} - \frac{3}{2} N_w \ln 2 \\ &\quad + \frac{1}{2} \frac{N_c N_w \left[\sum_{i=x,y,z} \lambda_i^2 + \frac{c}{\rho} \lambda_z^2 \right]}{(1 + c/\rho)} \end{aligned} \quad (5.45)$$

$$= \frac{\frac{1}{2} N_c N_w \left[\sum_{i=x,y,z} \lambda_i^2 + \frac{c}{\rho} \lambda_z^2 \right]}{(1 + c/\rho)} - \frac{\pi^2 \ell L \lambda_z^2 N_w}{6 h_z^2} + \lambda\text{-independent terms}, \quad (5.46)$$

$$\text{with } \rho = \frac{N_w L}{V} \text{ and } c \equiv \frac{3}{2\pi \ell h_z L} \left(\ell_c - \sqrt{\ell_c^2 + L^2} + \frac{L}{2} \ln \left[\frac{\sqrt{\ell_c^2 + L^2} + L}{\sqrt{\ell_c^2 + L^2} - L} \right] \right). \quad (5.47)$$

In the last step (5.46) we show only the important λ -dependent terms. In the limit of uniform localization, we obtain a deformation free energy closely resembling the result (4.64) of the previous chapter¹⁰. The free energy $\mathcal{F}_{\text{uniform}}$ has the typical Deam and Edwards deformation term $\frac{1}{2} N_c \sum \lambda_i^2$ and front factor $\sim (1 + c/\rho)^{-1}$ [see (4.66)], apart from a different c -value which now also depends on h_z . The second term in (5.46) represents the typical confinement of a macromolecule between planar surfaces, and is common to the gel described in Chapter 4, as well as the stitch network of Chapter 3.

¹⁰Here, the total number of crosslinks in the sample is given by $N_w N_c$.

5.4.2 The single chain limit

In Section 5.1 we mentioned that a polymer brush is (by definition) a very dense array of polymer chains, that is $N_w \gg 1$. However, if the crosslink density in the bulk is sufficiently high, we find a global minima for the free energy $\tilde{\mathcal{F}}$, even if we only have a brush network synthesized from one chain, as in Figure 5.6(a). When $N_w = 1$, we have a single chain network with one wall-link. The effect of the wall linkages relative to the bulk linkages, is then expected to be negligible, so that we are essentially dealing with a confined *bulk* network. A bulk network can be thought of as one giant chain, having no wall-links.

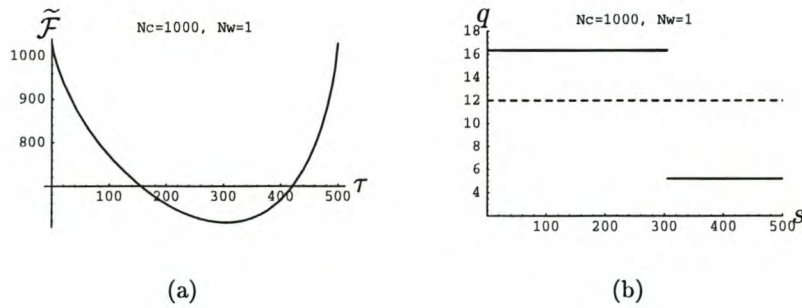


Figure 5.6: Illustrating the case of only one wall-link, $N_w \equiv 1$. (a) The plot of the variational free energy of the brush network $\tilde{\mathcal{F}}$ versus τ exhibits a global minimum at $\tau^* \simeq 305$. (b) Plot of the localization parameters, q_0 and q_1 (5.43), versus s for the brush network (solid line), in comparison with a uniformly localized bulk network (dashed line), (5.44). Constant plot parameters: $L = 500$, $h_z = 20$, $\ell = \ell_c = 1$, $\rho = \frac{N_w L}{V} = 0.4$, $\lambda = 1$.

From Figure 5.6(b) we can infer that the localization of a bulk network is expected to be the average of the inhomogeneous brush network localization contributions, q_0 and q_1 .

5.4.3 Localization of the polymer brush network

Next, we examine the graphs in Figure 5.7 to see how the linking density N_c influences the localization of the polymer. Each row in Figure 5.7 corresponds to a different value of N_c . The first observation that can be made, is that the chains in the “surface” region (q_0) are localized to a greater extent than the chains away from the walls (q_1). This follows from the fact that γ^* is positive in the middle column of Figure 5.7, and so we have that $q_1 < q_0$ from (5.43). The measure of the fluctuations of the crosslinks from their affine positions, given by the q -values, is greater for a chain that is lightly crosslinked ($N_c < N_w$) as shown in Figure 5.7, than for a network where $N_c \geq N_w$. Since $\gamma^* < 1$, the q -values (5.43) are primarily influenced by the number of crosslinks N_c .

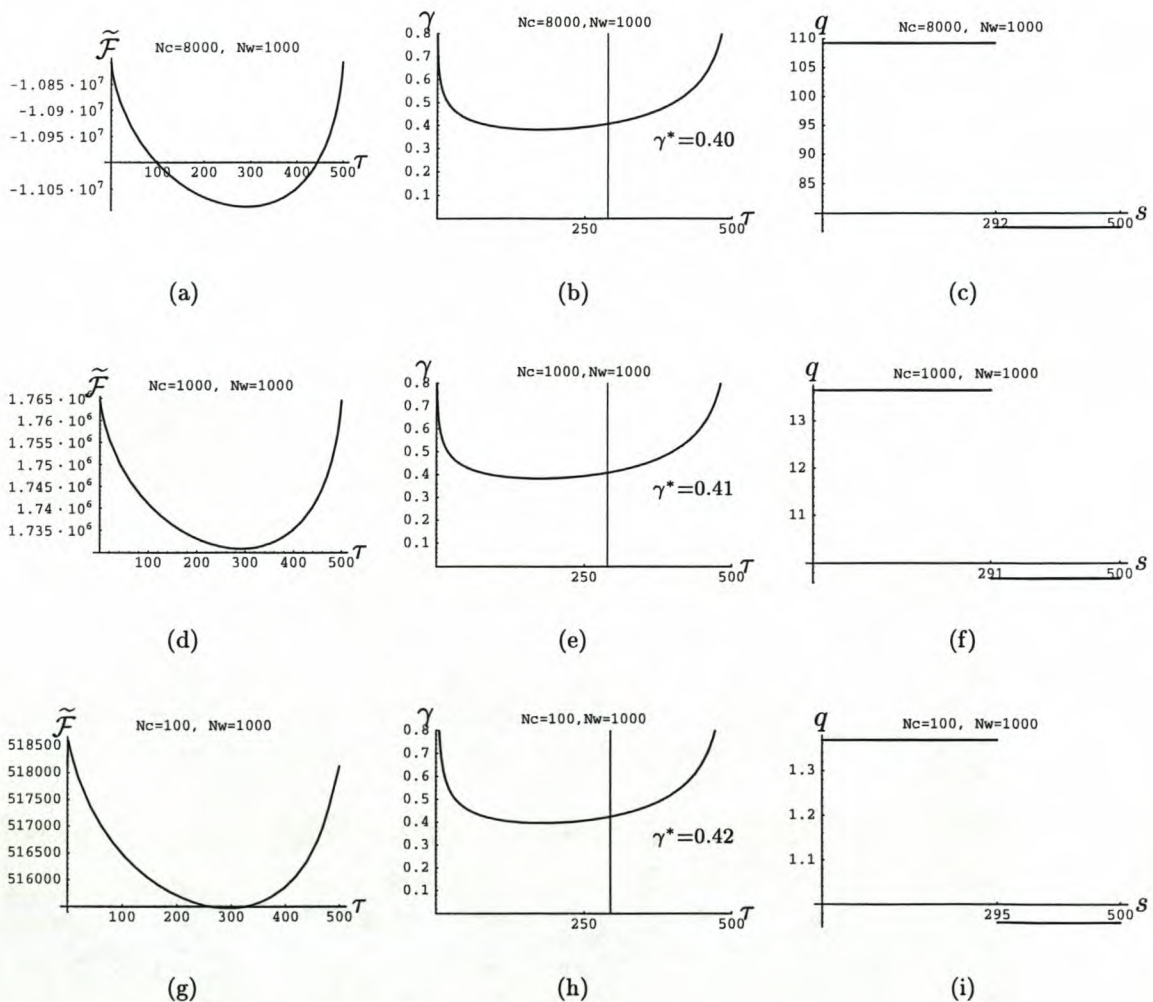


Figure 5.7: Investigating the influence of the crosslink density N_c on the localization of the polymer. The leftmost column of graphs depicts the variational free energy as a function of τ . Global minima were found at $\tau^* \simeq 291$ in (a), $\tau^* \simeq 292$ in (d) and $\tau^* \simeq 295$ in (g). These values are represented by vertical lines in the second column. The value γ^* is given by the intersection of the vertical line with the $\gamma(\tau)$ -curve. The rightmost column illustrates that $q_0 > q_1$. Also, the localization of the polymer decreases as the number of bulk-links decreases (5.43). Plots were rendered with the following kept constant: $L = 500$, $h_z = 20$, $\lambda = 1$, $\ell = \ell_c = 1$, $\rho = 0.4$.

5.4.4 Confinement and the free energy

When a macromolecule is placed in a geometric confinement, the total number of its possible chain conformations is reduced. This leads to a decrease in the entropy, or equivalently, to an increase of the free energy.

However, the case of a confined, surface-attached network is more involved, since the crosslink constraints also influence the network chain conformations. We find that the entropy of the brush network *increases* as the distance between the planar surfaces gets narrower, with the volume of the sample kept *constant*. This phenomenon is illustrated in Figure 5.8(a), where we plot the variational free energy $\tilde{\mathcal{F}}(\tau)$ for two values of the wall separation h_z .

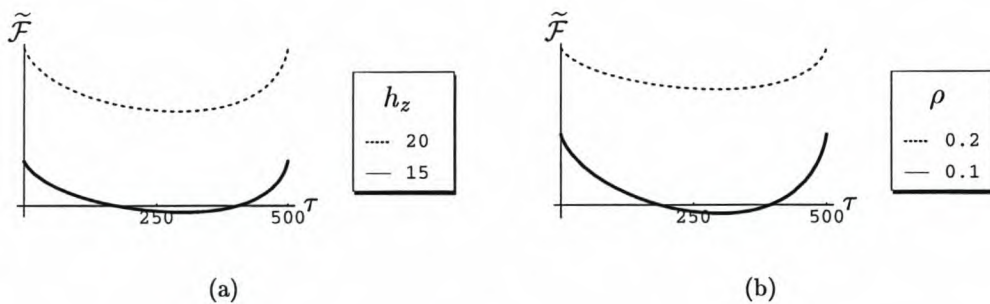


Figure 5.8: Illustrations of the variational free energy $\tilde{\mathcal{F}}$ as a function of τ , for (a) different values of h_z at constant volume V , and (b) different values of polymer chain density $\rho = \frac{N_w L}{V}$ for the the gel. Constant plot parameters were: $L = 500$, $N_c = N_w = 1000$, $l = l_c = 1$ and $\lambda = 1$.

At a sufficiently high cross link density and wall separation, the chains in a brush network may be thought of as highly stretched strings. When h_z decreases, the tension in the chains will decrease, thereby allowing more possible conformations to the network chains, and an associated increase in the entropy.

In this model the network is not confined in the xy -plane. This means that the average size of the chain is smaller than the x and y dimensions of the volume containing the gel sample. An increase in the box volume is equivalent to a decrease in the polymer chain density. As a result the free energy (entropy) of the network decreases (increases), when the polymer density decreases, as shown in Figure 5.8(b). The difference in the two graphs, lies in the fact that the chains are only confined and fixed in the z -dimension.

5.4.5 Elasticity

It is possible to calculate the stress-strain relationship for the polymer brush network, even though a closed-form of the free energy cannot be obtained. This is so, because the localization parameters q_0 and q_1 and the parameter τ do not depend on the affine deformation of the system, that is, they are λ -independent. By differentiating the variational free energy in (5.38) with respect to λ , one obtains the following stress-strain relationship:

$$f(\lambda) = \frac{k_B T}{V} \left[\frac{N_c N_w}{(1 + c/\rho)} \left\{ \lambda - 1/\lambda^2 + \frac{c}{\rho} \lambda \right\} - \frac{\pi^2 \ell L N_w}{3 h_z^2} \lambda \right], \quad (5.48)$$

where the polymer density ρ and the factor c are defined in (5.47).

The factor $\lambda - 1/\lambda^2$ gives the form of the characteristic stress-strain plot so typical of the classical theory of rubber elasticity [48]. However, the deformation factor is altered by the constant front factor $g \equiv (1 + c/\rho)^{-1}$, analogous to the result of the previous chapter (4.68), and the Deam and Edwards [9] result for an unconfined network. The above result is consistent with the stress-strain relation obtained in (4.68), for a surface-attached network where the wall-links and bulk-links are formed simultaneously. In the latter network, the wall-links have the freedom to form anywhere along the length of the polymer chains, in contrast with a brush network. This difference is portrayed in the $N_w \lambda$ term in (4.68), which is absent from the brush network stress-strain equation.

As an example, we list numerical estimates of the front factor constants for the Deam and Edwards model (unconfined network), and the confined network models of the previous and present chapter:

	Unconfined	Confined	
	Deam Edwards	Real Confined Network	Brush Network
c	0.17	0.31	0.14
ρ	0.4	0.4	0.4
front factor g	0.70	0.56	0.74

Table 5.1: The g -factors give a rough estimate of the percentage fraction of crosslinks that are elastically-active. The estimates in the example were computed for a network fabricated from $N_w = 1000$ chains of chain length $L = 500$, chain cut-off length $\ell_c = 1 = \ell$, and confinement $h_z = 20$, where lengths are in units of ℓ .

The front factor alters the classic [31] elastic constant of $N_w N_c k_B T$, since the number of elastically-able crosslinks are reduced from $N_w N_c$ to $g N_w N_c$. This phenomena can be attributed to the fact that there was no concise way of excluding network defects, like closed loops, from the start. Note that the λ term containing the front factor should not be translated into the elastic modulus of the system. In the new theories there are clearly other λ_z -dependent terms due to the confinement and wall-links, which will also play a role in the elasticity of the system.

The second, h_z -dependent term in (5.48) coincides with the stress of a single chain, of length $N_w L$, confined between walls of width h_z . Furthermore, the term $\frac{c}{\rho} \lambda$, seems to be a distinctive

feature of a surface attached network, with the constant c depending only on the method of network formation.

In this chapter we introduced *inhomogeneous* crosslinking in the simplest manner, by means of a confined surface-attached network fabricated from two polymer brushes. We saw that the polymer is localized to a greater degree in the “surface” region. The surface region is defined by $s < \tau^*$, which turned out to be larger than expected. However, this should be ascribed to the fact that the calculations are only valid for the case when we consider relatively large macromolecules, $\sqrt{L\ell} \gg h_z$. The stress-strain relationship (which contains the macroscopic information of the network) is not affected by the inhomogeneity that was introduced in the model.

Chapter 6

Concluding Remarks

In this thesis we described three different confined, surface-attached network models: the stitch network, the real confined network and lastly the brush network.

The stitch network in Chapter 3 captured the essence of confinement, and laid the groundwork (together with Chapter 2) — in terms of the relevant Green's function approach — for the more sophisticated models in subsequent chapters. Above all, the stitch network served as a preliminary exercise in treating *disorder*. The origin of the quenched disorder was the random, albeit permanent, crosslinking in the system. It was shown in Chapter 3 that one can handle the random crosslinking mathematically by applying the *replica* method. The controversial problems sometimes associated with spin glass systems, are not applicable to our simple polymer networks, and it was sufficient to employ only the replica-symmetric approximation. The stitch network, can be described as a *sum* of smaller star-polymers (or two stitches), with four arms emanating from fixed positions on the parallel walls. Each bulk-link favoured the arrangement corresponding to minimum tension of the chains, namely at half of the chain contour lengths. It is therefore not surprising that the stitch network lacked the essential (classical) features of a typical network free energy.

In Chapter 4, we implemented the ideas of confinement and disorder of the first two chapters, to develop a more acceptable model of network formation. This was done by adapting an existing model of network formation of Deam and Edwards [9], to incorporate two parallel, confining surfaces (walls) and random wall-linking. The network was formed from pre-existing, confined macromolecules, that were crosslinked simultaneously to each other (polymer-polymer links) and to the confining surface (polymer-wall links). Calculations were performed under the following assumptions:

1. The network was fabricated from a sufficiently dense melt, such that excluded volume effects were ignored. Consequently, in the *phantom* network, the chains could intersect each other and the possibility of entanglements was neglected.
2. The crosslink density was sufficiently high, such that the gel was solid and not near the sol-gel transition point.
3. The distance between the confining walls, h_z was smaller than $\sqrt{\mathcal{L}\ell}$, the effective size of the macroscopic network chain.

4. The infinite square potential, which represents the hard wall potential, was *softened* in the framework of a variational calculation.

Since we employed an harmonic potential identical to that of Deam and Edwards, with isotropic, homogeneous localization, we found the localization parameters to be equal, $q_x = q_z$, and analogous to that of an unconfined network model. They were namely strain independent, and proportional to the mean square radius of gyration of a chain piece between two junction points. In terms of localization, the wall-links were treated as bulk-links, $q = \frac{6(N_c + N_w)}{\ell \mathcal{L}}$, where \mathcal{L} is the effective contourlength of the giant network polymer, ℓ the Kuhn steplength, and N_c and N_w is the total number of bulk-links and wall-links, respectively. The quantity $q^{-1/2}$ gives a measure of the fluctuation of the network chains from the mean affine deformation path. In other words, it defines the relative diameter of a tube in which each chain is confined due to the surrounding crosslink constraints.

In Chapter 5 we investigated a surface-attached network, fabricated via an instantaneous crosslinking of two pre-existing polymer brushes. This architecture was specifically chosen to facilitate an *inhomogeneous* localization scheme. This scheme modeled the effect of the crosslink and wall constraints by two constant localization parameters, which were arclength-dependent. It was found that each chain is localized to a greater degree near the surface at which it is attached, than far away from its grafting surface. The great advantage of this scheme, is in the fact that the wall-links were not treated as bulk-links, but played a role in the arc length distance over which each constant localization takes effect.

Common to both the brush network and the real confined network, was the general form (apart from constants) of the stress-strain relationship $f(\lambda)$. Under the influence of an uniaxial, isovolumetric deformation, we obtain the following expression:

$$f(\lambda) = \frac{k_B T}{V} \left[\frac{N_c}{(1 + c/\rho)} \left\{ \lambda - \frac{1}{\lambda^2} + \frac{c}{\rho} \lambda \right\} - \frac{\ell \pi^2 \mathcal{L}}{3 h_z^2} \lambda \right],$$

with c a constant dependent on the chain length and confinement, and ρ the polymer density. The underlined part gives the characteristic curve of classic rubber elasticity models: a type of Hooke's law for small λ 's and a sharp rise in slope for larger strains. However, this slope is characterized by a *different* elastic modulus than encountered in the usual unconfined models. There are two new additions to the result of Deam and Edwards for an unconfined phantom model. The first is the c/ρ term, due to wall-links and the second, h_z -dependent term, due to the confinement. The denominator $(1 + c/\rho)$ gives a measure of the elastically active crosslinks in the system, and was also encountered in the Deam and Edwards model.

In all of the calculations, we assumed a phantom model. Thus, an obvious improvement of the model would be to include trapped entanglements and excluded volume effects. This extension could for example be based on a non-Gaussian tube model or slip-link model [18] with non-affine deformation.

The variational calculation is extremely difficult when the localization potential depends on the relevant spatial position, say $Z(s)$, between the parallel plates. For this reason, we chose a simple arclength-dependence. However, it might still be possible to find a potential that is

tractable, and more representative of the problem.

Another future consideration is the study of the effect of *fillers* in the network. These volume-giving components can influence the network's response to deformation, by reducing the internal stress. It is known that a filler, like carbon black, leads to the reinforcement of network structure [29], meaning increased stiffness, elastic modulus, tensile strength and abrasion resistance. The study of these improved properties, in the context of confinement and surface-attachments, may have a range of possible applications, and would be a worthwhile research endeavour.

Appendix A

Coordinate transformation

The coordinates $X_j^{(\beta)}(s) = T_j^{\beta\alpha} R_j^{(\alpha)}(s)$ define an orthogonal transformation with Jacobian equal to one¹. In matrix form the transformation T may look as follows:

$$T_j = \begin{pmatrix} (1+n\lambda_j^2)^{-\frac{1}{2}} & \lambda_j(1+n\lambda_j^2)^{-\frac{1}{2}} & \lambda_j(1+n\lambda_j^2)^{-\frac{1}{2}} & \dots \\ \sqrt{n}\lambda_j(1+n\lambda_j^2)^{-\frac{1}{2}} & -\frac{1}{\sqrt{n}}(1+n\lambda_j^2)^{-\frac{1}{2}} & -\frac{1}{\sqrt{n}}(1+n\lambda_j^2)^{-\frac{1}{2}} & \dots \\ 0 & \frac{1}{\sqrt{n}}e^{(2\pi im\alpha)/n} & \frac{1}{\sqrt{n}}e^{(2\pi im\alpha)/n} & \dots \\ \vdots & \vdots & \vdots & \ddots \end{pmatrix}. \quad (\text{A.1})$$

This is the most symmetric transformation method [9], but there also exist other transformations, notably in [3], where all entries are chosen to be real. The factor $(1+n\lambda_j^2)^{1/2}$ ensures the orthonormality of the transformation.

The wall-crosslink position vectors $\eta^{(\alpha)}$ are transformed in the same way as the polymer chain coordinates $\mathbf{R}^{(\alpha)}$ by the transformation T (A.1) as follows:

$$\nu_j^{(0)} = \frac{\eta_j^{(0)} + \sum_{\alpha=1}^n \lambda_j \eta_j^{(\alpha)}}{(1+n\lambda_j^2)^{\frac{1}{2}}} \quad (\text{A.2})$$

$$\nu_j^{(1)} = \frac{\sqrt{n}\lambda_j \eta_j^{(0)} - \frac{1}{\sqrt{n}} \sum_{\alpha=1}^n \eta_j^{(\alpha)}}{(1+n\lambda_j^2)^{\frac{1}{2}}} \quad (\text{A.3})$$

$$\omega_j^{(m)} = \frac{1}{\sqrt{n}} \sum_{\alpha=1}^n e^{(2\pi im\alpha)/n} \eta_j^{(\alpha)}, \quad m = 1, 2, \dots, (n-1). \quad (\text{A.4})$$

The above calculation can be done explicitly for each Cartesian coordinate. For example:

$$\nu_x^{(0)} = \frac{x + \sum_{\alpha=1}^n \lambda_x^2 x}{(1+n\lambda_x^2)^{\frac{1}{2}}} = \sqrt{1+n\lambda_x^2} x \quad (\text{A.5})$$

$$\nu_x^{(1)} = \frac{\sqrt{n}\lambda_x x - \frac{1}{\sqrt{n}} \sum_{\alpha=1}^n \lambda_x x}{(1+n\lambda_x^2)^{\frac{1}{2}}} = 0 \quad (\text{A.6})$$

$$\omega_x^{(m)} = \frac{\lambda_x x}{\sqrt{n}} e^{(2\pi im)/n} \left(\frac{1 - e^{2\pi im}}{1 - e^{(2\pi im)/n}} \right) = 0, \quad m = 1, 2, \dots, (n-1). \quad (\text{A.7})$$

¹Cartesian coordinates x, y, z are represented by j . The index m runs from 1 to $n-1$; $\therefore m=1 \Leftrightarrow \beta=2$.

All except the *zeroth* replica variables vanish during the T transformation.

After substitution of the coordinate transformation (A.1), the pseudo-Hamiltonian of the generalised partition function can be written as follows:

$$\begin{aligned}
-\frac{\mathcal{H}_z}{k_B T} &= -\frac{3}{2\ell} \int_0^{\mathcal{L}} \dot{X}_z^{(0)2} ds - \frac{3}{2\ell} \int_0^{\mathcal{L}} \dot{X}_z^{(1)2} ds - \frac{3}{2\ell} \sum_{m=1}^{n-1} \int_0^{\mathcal{L}} \dot{Y}_z^{(m)2} ds \\
&+ \int_0^{\mathcal{L}} A \left[T_z^{0\alpha} X_{zs}^{(0)} + T_z^{1\alpha} X_{zs}^{(1)} \right] ds \\
&+ \sum_{\alpha=1}^n \int_0^{\mathcal{L}} A' \left[T_z^{0\alpha} X_{zs}^{(0)} + T_z^{1\alpha} X_{zs}^{(1)} + \sum_{m=1}^{n-1} T_z^{(m+1)\alpha} Y_{zs}^{(m)} \right] ds \\
&+ \mu_c \int_0^{\mathcal{L}} ds \int_0^{\mathcal{L}} ds' \prod_{\alpha=0}^n \delta \left[T_z^{0\alpha} \left(X_{zs}^{(0)} - X_{zs'}^{(0)} \right) + T_z^{1\alpha} \left(X_{zs}^{(1)} - X_{zs'}^{(1)} \right) \right. \\
&\quad \left. + \sum_{m=1}^{n-1} T_z^{(m+1)\alpha} \left(Y_{zs}^{(m)} - Y_{zs'}^{(m)} \right) \right] \\
&+ \mu_w \int_0^{\mathcal{L}} ds \int dx dy \left\{ \prod_{\alpha=0}^n \delta \left[T_z^{0\alpha} \left(X_z^{(0)}(s) - \nu_z^{(0)}(x, y, \epsilon) \right) + T_z^{1\alpha} \left(X_z^{(1)}(s) - \nu_z^{(1)}(x, y, \epsilon) \right) \right. \right. \\
&\quad \left. \left. + \sum_{m=1}^{n-1} T_z^{(m+1)\alpha} \left(Y_z^{(m)}(s) - \omega_z^{(m)}(x, y, \epsilon) \right) \right] + \prod_{\alpha=0}^n \delta \left[T_z^{0\alpha} \left(X_z^{(0)}(s) - \nu_z^{(0)}(x, y, h_z - \epsilon) \right) \right. \right. \\
&\quad \left. \left. + T_z^{1\alpha} \left(X_z^{(1)}(s) - \nu_z^{(1)}(x, y, h_z - \epsilon) \right) \right. \right. \\
&\quad \left. \left. + \sum_{m=1}^{n-1} T_z^{(m+1)\alpha} \left(Y_z^{(m)}(s) - \omega_z^{(m)}(x, y, h_z - \epsilon) \right) \right] \right\} \tag{A.8} \\
&= -\frac{3}{2\ell} \int_0^{\mathcal{L}} \dot{X}_z^{(0)2} ds - \frac{3}{2\ell} \int_0^{\mathcal{L}} \dot{X}_z^{(1)2} ds - \frac{3}{2\ell} \sum_{m=1}^{n-1} \int_0^{\mathcal{L}} \dot{Y}_z^{(m)2} ds \\
&+ \int_0^{\mathcal{L}} A \left[T_z^{0\alpha} X_{zs}^{(0)} + T_z^{1\alpha} X_{zs}^{(1)} \right] ds \\
&+ \sum_{\alpha=1}^n \int_0^{\mathcal{L}} A' \left[T_z^{0\alpha} X_{zs}^{(0)} + T_z^{1\alpha} X_{zs}^{(1)} + \sum_{m=1}^{n-1} T_z^{(m+1)\alpha} Y_{zs}^{(m)} \right] ds \\
&+ \mu_c \int_0^{\mathcal{L}} ds \int_0^{\mathcal{L}} ds' \delta \left[X_{zs}^{(0)} - X_{zs'}^{(0)} \right] \delta \left[X_{zs}^{(1)} - X_{zs'}^{(1)} \right] \prod_{m=1}^{n-1} \delta \left[Y_{zs}^{(m)} - Y_{zs'}^{(m)} \right] \\
&+ \mu_w \int_0^{\mathcal{L}} ds \int dx dy \left\{ \delta \left[X_z^{(0)}(s) - \nu_z^{(0)}(x, y, \epsilon) \right] \delta \left[X_z^{(1)}(s) \right] \prod_{m=1}^{n-1} \delta \left[Y_z^{(m)}(s) \right] \right. \\
&\quad \left. + \delta \left[X_z^{(0)}(s) - \nu_z^{(0)}(x, y, h_z - \epsilon) \right] \delta \left[X_z^{(1)}(s) \right] \prod_{m=1}^{n-1} \delta \left[Y_z^{(m)}(s) \right] \right\}. \tag{A.9}
\end{aligned}$$

Only the \hat{z} -dimension was shown, since this is the part of the free energy, which embodies all the constraints at this stage. In (A.9) we applied the fact that $\nu^{(\beta)} = 0$ for $\beta \neq 0$, as was seen in (A.8).

Appendix B

The average $\langle \mathbb{A} - \mathbb{A}_0 \rangle$ in the variational principle

We have to calculate the following:¹

$$e^{\mathbb{A}} = \Theta(T_z^{\beta 0} X_z^{(\beta)}) \Theta(h_z - T_z^{\beta 0} X_z^{(\beta)}) \prod_{\alpha=1}^n \Theta(T_z^{\beta \alpha} X_z^{(\alpha)}) \Theta(\lambda_z h_z - T_z^{\beta \alpha} X_z^{(\beta)}) \quad (\text{B.1})$$

$$\text{and } e^{\mathbb{A}_0} = \Theta(T_z^{00} X_z^{(0)}) \Theta(h_z - T_z^{00} X_z^{(0)}) = \Theta(X_z^{(0)}) \Theta(a h_z - X_z^{(0)}). \quad (\text{B.2})$$

Now, \mathbb{A} is a very hard potential that we choose to *soften*, by writing

$$\Theta(Z) \Theta(h - Z) \simeq e^{-\phi^2 (1 - \Theta(Z)) \Theta(h - Z)}, \quad (\text{B.3})$$

where ϕ is a big enough scalar, and Z stands for the transformed variables such that

$$e^{\langle \mathbb{A} \rangle} \longrightarrow e^{-\phi^2 \left(n+1 - \langle \Theta(T_z^{\beta 0} X_z^{(\beta)}) \Theta(h_z - T_z^{\beta 0} X_z^{(\beta)}) \rangle - \sum_{\alpha=1}^n \langle \Theta(T_z^{\beta \alpha} X_z^{(\alpha)}) \Theta(\lambda_z h_z - T_z^{\beta \alpha} X_z^{(\beta)}) \rangle \right)} \quad (\text{B.4})$$

$$e^{-\langle \mathbb{A}_0 \rangle} \longrightarrow e^{+\phi^2 \left(1 - \langle \Theta(T_z^{00} X_z^{(0)}) \Theta(h_z - T_z^{00} X_z^{(0)}) \rangle \right)}, \quad (\text{B.5})$$

where $\langle \dots \rangle$ denotes averaging with respect to the Green's functions listed in Section 4.5.1.

Next, we employ the fact that the integration limits, for the "centre-of-mass" coordinate of all the replicas $X_z^{(0)}$, keep the argument of the theta-function positive and in the allowed region:

$$\langle \Theta \left(\underbrace{X_z^{(0)} + n^{\frac{1}{2}} \lambda X_z^{(1)}}_{\sqrt{1+n\lambda_z^2} R_z^{(0)}} \right) \Theta \left(\underbrace{\sqrt{1+n\lambda_z^2} h_z - X_z^{(0)} - n^{\frac{1}{2}} \lambda X_z^{(1)}}_{(1+n\lambda_z^2) h_z - R_z^{(0)}} \right) \rangle = 1 \quad (\text{for } \mathbb{A}\text{-term}) \quad (\text{B.6})$$

$$\text{and } \langle \Theta(X_z^{(0)}) \Theta(\sqrt{1+n\lambda_z^2} h_z - X_z^{(0)}) \rangle = 1 \quad (\text{for } \mathbb{A}_0\text{-term}). \quad (\text{B.7})$$

Substituting the above results for the $\beta = 0$ and $\alpha = 0$ terms in (B.4) and (B.5), we obtain

$$e^{\langle \mathbb{A} \rangle} \simeq e^{-\phi^2 \left(n - \sum_{\alpha=1}^n \langle \Theta(T_z^{\beta \alpha} X_z^{(\alpha)}) \Theta(\lambda_z h_z - T_z^{\beta \alpha} X_z^{(\beta)}) \rangle \right)} \quad (\text{B.8})$$

$$e^{-\langle \mathbb{A}_0 \rangle} \simeq 1. \quad (\text{B.9})$$

¹Note that there is a summation convention implied with respect to the β 's, and $a \equiv (T_z^{00})^{-1} = \sqrt{1+n\lambda_z^2}$. Also, since the transformation T is orthogonal, we immediately wrote $(T_z^{-1})^{\alpha\beta}$ as its transponent $T_z^{\beta\alpha}$.

The n remaining terms in the sum in (B.8) can be written in terms of inverse Fourier integrals, where the Fourier transform of a stepfunction is

$$\mathfrak{F}[\Theta(Z)] = \frac{1}{\sqrt{2\pi}} \left(\frac{i}{\omega} + \pi\delta(\omega) \right). \quad (\text{B.10})$$

Since the coordinates $X_z^{(\beta)}$, for $\beta > 0$, are simply fluctuations relative to the “centre-of-mass-of-all-the-replicas” coordinate $X_z^{(0)}$, we may expand the Fourier expressions in powers of $X_z^{(\beta)}$:

$$\langle \Theta(T^{\beta\alpha} X^{(\beta)}) \Theta(\lambda_z h_z - T^{\beta\alpha} X^{(\beta)}) \rangle \quad (\text{B.11})$$

$$= \left(1 + \frac{1}{2\pi} \int \frac{i d\omega}{\omega} \langle e^{-i\omega T_z^{\beta\alpha} X_z^{(\beta)}(s)} \rangle \right) \left(1 + \frac{1}{2\pi} \int \frac{i d\omega'}{\omega'} \langle e^{-i\omega'(\lambda_z h_z - T_z^{\beta\alpha} X_z^{(\beta)}(s))} \rangle \right) \quad (\text{B.12})$$

$$= 1 + \frac{1}{q} \left[\int d\omega \text{ terms} \right] + \mathcal{O} \left(\frac{1}{q_z^{2m-1}} \right) \left[\int d\omega \text{ terms} \right], \quad m = 1, 2, \dots \quad (\text{B.13})$$

In the above average only the *even* terms $[X_z^{(\beta)}(s)]^{2m}$ survive the averaging over the Gaussian Green’s functions [see Section 4.5.1], and each of these terms contribute a $q^{-(2m-1)}$ factor, where m is a positive integer.

We thus have the following result:

$$\langle \mathbb{A} - \mathbb{A}_0 \rangle \simeq \phi^2 \frac{n}{q_z} (q\text{-independent terms}) + \phi^2 \mathcal{O} \left(n, \frac{1}{q_z^{2m-1}} \right) - \text{terms} \quad (\text{B.14})$$

In this thesis, we assume a high crosslink density. This implies that the localization parameter q is large, so that terms of the order q^{-1} are negligible relative to other terms, $\sim q$ and $\sim \ln q$, which play the dominant roles in minimizing the free energy in (4.60). On the other hand, the scalar ϕ is also large in order to decently approximate the hard potential \mathbb{A} , and will tend to make the $1/q$ terms important. However, since these path integrals are not tractable, we approximate \mathbb{A} by a *soft* enough potential so as to make the ϕ -influence insignificant. This assumption is thus inherent in the Ansatz of (4.36). The centre-of-mass coordinate $X_z^{(0)}$ is the *only* transformed coordinate that represents physical position of the polymer chains; the other coordinates are simply relative to it. In the variational calculation, the $\beta > 0$ (or ϕ -terms) are therefore only expected to play a relatively insignificant role in localizing the network.

Appendix C

The First Variational Calculation

We set out here to evaluate the average $\langle \mathbb{Q} + \mu_c \mathbb{X}_c + \mu_w \mathbb{X}_w \rangle$ of Section 4.5.2 by using the Green's functions listed in Section 4.5.1.

C.1 The Bulk Cross-links $\langle \mu_c \mathbb{X}_c \rangle$

The $\beta = 0$ term for the constrained \hat{z} -dimension is given by:

$$\langle \delta(X_z^{(0)}(s) - X_z^{(0)}(s')) \rangle_{\mathcal{G}_0} \quad (\text{C.1})$$

$$= \frac{\int dX_{z0}^{(0)} dX_{zs'}^{(0)} dX_{zs}^{(0)} dX_{z\mathcal{L}}^{(0)} \mathcal{G}_0(X_{zs'}, X_{z0}^{(0)}, s') \mathcal{G}_0(X_{zs}, X_{zs'}, |s-s'|) \delta(X_{zs}^{(0)} - X_{zs'}^{(0)}) \mathcal{G}_0(X_{z\mathcal{L}}^{(0)}, X_{zs}^{(0)}, |\mathcal{L}-s|)}{\int dX_{z0}^{(0)} dX_{z\mathcal{L}}^{(0)} \mathcal{G}_0(X_z^{(0)}(\mathcal{L}), X_z^{(0)}(0), \mathcal{L})}$$

$$= \left(\frac{8\sqrt{1+n\lambda^2}h_z}{\pi^2} \sum_{p=1,3,\dots}^{\infty} \frac{1}{p^2} \exp \left\{ -\frac{\ell\pi^2 p^2 \mathcal{L}}{6(1+n\lambda^2)h_z^2} \right\} \right)^{-1}$$

$$\times \left(\frac{2}{\sqrt{1+n\lambda^2}h_z} \right)^3 \sum_{r=1}^{\infty} \sum_{p,\rho=1,3,\dots}^{\infty} \frac{4(1+n\lambda^2)h_z^2}{\pi^2 p \rho} e^{-\frac{\ell\pi^2 p^2}{6(1+n\lambda^2)h_z^2}|s'|} e^{-\frac{\ell\pi^2 r^2}{6(1+n\lambda^2)h_z^2}|s-s'|} e^{-\frac{\ell\pi^2 \rho^2}{6(1+n\lambda^2)h_z^2}|\mathcal{L}-s|}$$

$$\times \int_0^{\sqrt{1+n\lambda^2}h_z} dX_z^{(0)}(s') \sin \left[\frac{\pi p X_z^{(0)}(s')}{\sqrt{1+n\lambda^2}h_z} \right] \sin^2 \left[\frac{\pi r X_z^{(0)}(s')}{\sqrt{1+n\lambda^2}h_z} \right] \sin \left[\frac{\pi \rho X_z^{(0)}(s')}{\sqrt{1+n\lambda^2}h_z} \right] \quad (\text{C.2})$$

$$\simeq \frac{3}{2\sqrt{1+n\lambda^2}h_z}, \quad \text{when } p = r = \rho. \quad (\text{C.3})$$

The solution to the integral in (C.2) follows from the following result:

$$\int dX \sin aX \sin^2 bX \sin cX = \frac{\sin(a-c)X}{4(a-c)} - \frac{\sin(a-2b-c)X}{8(a-2b-c)}$$

$$- \frac{\sin(a+2b-c)X}{8(a+2b-c)} + \frac{\sin(a-2b+c)X}{8(a-2b+c)} - \frac{\sin(a+c)X}{4(a+c)} + \frac{\sin(a+2b+c)X}{8(a+2b+c)}, \quad (\text{C.4})$$

where $a \equiv \frac{\pi p}{\sqrt{1+n\lambda^2}h_z}$, $b \equiv \frac{\pi r}{\sqrt{1+n\lambda^2}h_z}$, $c \equiv \frac{\pi \rho}{\sqrt{1+n\lambda^2}h_z}$ and $X \equiv X_z^{(0)}$. Each of the above terms can only contribute to an integration of $X = 0$ to $X = \sqrt{1+n\lambda^2}h_z$ if the quantities in round brackets go to zero. This immediately rules out the last two terms given in (C.4) since $p, r, \rho \geq 1$. The most straightforward combination to choose, is when $a = b = c$ for each term, which implies that $p = q = \rho$, so that the three exponential functions reduce to one, with exponent $\frac{\ell\pi^2 p^2}{6a^2 h_z^2} L$. Also, in the limit $\sqrt{\ell} \gg h_z$, the exponential function (C.2) is dominated by the first term in the sum, that is, $p = q = \rho = 1$. Consequently, for $\epsilon \ll h_z$, $\sin\left(\frac{\pi p \epsilon}{h_z}\right) \cos\left(\frac{\pi \rho \epsilon}{h_z}\right) \simeq \frac{\pi \epsilon}{h_z}$, which leads

to the result in (C.2).

The $\beta = 0$ terms for the \hat{x} and \hat{y} coordinates are given by:

$$\langle \delta(X_i^{(0)}(s) - X_i^{(0)}(s')) \rangle_{\mathcal{G}_0} \quad (\text{C.5})$$

$$= \frac{\int dX_0 dX_{s'} dX_s dX_{\mathcal{L}} \mathcal{G}_0(X_{s'}, X_0, s') \mathcal{G}_0(X_s, X_{s'}, |s - s'|) \delta(X_s - X_{s'}) \mathcal{G}_0(X_{\mathcal{L}}, X_s, |\mathcal{L} - s|)}{\int dX_0 dX_{\mathcal{L}} \mathcal{G}_0(X_i(\mathcal{L}), X_i(0), \mathcal{L})}$$

$$= \frac{1}{V_i (1 + n\lambda_i^2)^{\frac{1}{2}}} + \left(\frac{3}{2\pi\ell|s - s'|} \right)^{\frac{1}{2}}, \quad (\text{C.6})$$

where for example X_s in the above is shortcut notation that stands for $X_i^{(0)}(s)$.

The $\beta \in \{1, 2, \dots, n\}$ terms are identical, apart from different q -values. In particular, for $X_i^{(1)}$ the average is given by:

$$\langle \delta(X_i^{(1)}(s) - X_i^{(1)}(s')) \rangle_{\mathcal{G}_1} \quad (\text{C.7})$$

$$= \frac{\int dX_0 dX_{s'} dX_s dX_{\mathcal{L}} \mathcal{G}_1(X_{s'}, X_0, s') \mathcal{G}_1(X_s, X_{s'}, |s - s'|) \delta(X_s - X_{s'}) \mathcal{G}_1(X_{\mathcal{L}}, X_s, |\mathcal{L} - s|)}{\int dX_0 dX_{\mathcal{L}} \mathcal{G}_1(X_i(\mathcal{L}), X_i(0), \mathcal{L})}$$

$$= \sqrt{\frac{q e^{-\frac{\ell q}{6}|2\mathcal{L}-s+s'|} \left(e^{\frac{2\ell\mathcal{L}q}{3}} - 1 \right)}{2\pi \left(e^{\frac{\ell q}{3}|s-s'|} - 1 \right) \left(\sinh \frac{\ell q}{6}|2\mathcal{L}-s-3s'| - \sinh \frac{\ell q}{6}|2\mathcal{L}-3s-s'| + 2 \sinh \frac{\ell q}{6}|2\mathcal{L}-s+s'| \right)}} \quad (\text{C.8})$$

Each Green's function in (C.7) can be written as a sum of exponential functions multiplied by a product of eigenfunctions [19], as follows:

$$\mathcal{G}_1(X_s, X_{s'}, |s - s'|) = \sum_{k=0}^{\infty} e^{-\frac{q}{3}(k+\frac{1}{2})|s-s'|} \phi_k[X_s] \phi_k[X_{s'}] \quad (\text{C.9})$$

$$\simeq \left(\frac{q_z}{\pi} \right)^{\frac{1}{2}} e^{-\frac{q_z}{2} \left[X_z^{(1)2}(s) + X_z^{(1)2}(s') + \frac{\ell}{3}|s-s'| \right]} \equiv \tilde{\mathcal{G}}_1. \quad (\text{C.10})$$

where the last step follows from the assumption that the lowest eigenfunction,

$$\phi_0(X_s) = \left(\frac{q}{\pi} \right)^{\frac{1}{4}} e^{-\frac{q_z}{2} X_i^{(1)2}(s)}, \quad (\text{C.11})$$

dominates the sum in (C.9). This is the case when $\ell q_i |s - s'|$ in (4.43) is large, so that $\cosh \frac{1}{3} \ell q_i |s - s'| \rightarrow \frac{1}{2} \exp \left\{ \frac{\ell q_i}{3} |s - s'| \right\}$. In this limit, the integration in (C.7) can be repeated with the approximate Green's function $\tilde{\mathcal{G}}_1$ in (C.10), such that the average becomes

$$\langle \delta(X_i^{(1)}(s) - X_i^{(1)}(s')) \rangle_{\mathcal{G}_1} \simeq \left(\frac{q_i}{2\pi} \right)^{\frac{1}{2}}, \quad q_i \in \{q_x, q_z\}. \quad (\text{C.12})$$

Since the Green's functions $\mathcal{G}_1(X_{i_s}^{(1)}, X_{i_{s'}}^{(1)}, |s - s'|)$ of (4.43) and $\mathcal{G}_m(Y_{i_s}^{(m)}, Y_{i_{s'}}^{(m)}, |s - s'|)$ of (4.44) for $i \in \{x, y, z\}$, all have the same form, the remaining averages are:

$$\langle \delta(Y_z^{(m)}(s) - Y_z^{(m)}(s')) \rangle_{\mathcal{G}_m} \simeq \left(\frac{q_z}{2\pi} \right)^{\frac{1}{2}} \quad (\text{C.13})$$

$$\langle \delta(Y_i^{(m)}(s) - Y_i^{(m)}(s')) \rangle_{\mathcal{G}_m} \simeq \left(\frac{q_x}{2\pi} \right)^{\frac{1}{2}}. \quad (\text{C.14})$$

Putting all the averages together, the bulk crosslink contribution (4.22) becomes

$$\therefore \langle \mu_c \mathbb{X}_c \rangle = \mu_c \langle \mathbb{X}_{cx} \mathbb{X}_{cy} \mathbb{X}_{cz} \rangle \quad (\text{C.15})$$

$$= \left\langle \mu_c \int_0^{\mathcal{L}} ds \int_0^{\mathcal{L}} ds' \prod_{i=x,y,z} \delta(X_i^{(0)}(s) - X_i^{(0)}(s')) \delta(X_i^{(1)}(s) - X_i^{(1)}(s')) \right. \\ \left. \times \prod_{m=1}^{n-1} \delta(Y_i^{(m)}(s) - Y_i^{(m)}(s')) \right\rangle \quad (\text{C.16})$$

$$= \frac{3\mu_c}{2\sqrt{1+n\lambda^2} h_z} \left(\frac{q_z q_x^2}{8\pi^3} \right)^{\frac{n}{2}} \int ds ds' \left[\frac{1}{V_x V_y (1+n/\lambda)} + \left(\frac{3}{2\pi\ell |s-s'|} \right) \right] \quad (\text{C.17})$$

$$= \frac{3\mu_c}{2\sqrt{1+n\lambda^2} h_z} \left(\frac{q_z}{2\pi} \right)^{n/2} \left(\frac{q_i}{2\pi} \right)^n \left[\frac{\mathcal{L}^2}{V_x V_y (1+n/\lambda)} + \frac{3\mathcal{L}}{2\pi\ell} \int_{\ell_c}^{\mathcal{L}} \frac{du}{u} \right] \quad (\text{C.18})$$

$$= \frac{3\mu_c}{2\sqrt{1+n\lambda^2} h_z} \left(\frac{q_z q_i^2}{8\pi^3} \right)^{n/2} \left[\frac{\mathcal{L}^2}{V_x V_y (1+n/\lambda)} + \frac{3\mathcal{L}}{2\pi\ell} \ln \left(\frac{\mathcal{L}}{\ell_c} \right) \right]. \quad (\text{C.19})$$

C.2 The Wall Crosslinks $\langle \mu_w \mathbb{X}_w \rangle$

The wall cross-links are completely specified by the vectors $\nu^{(0)}(x, y, \epsilon)$ and $\nu^{(0)}(x, y, h_z - \epsilon)$, for cross-links situated an infinitesimal distance ϵ from the wall surface. Letting $a \equiv \sqrt{1+n\lambda^2}$, the centre-of-mass average is given by:

$$\langle \delta(X_z^{(0)}(s) - \nu^{(0)}(x, y, \epsilon)) \rangle_{\mathcal{G}_0} \\ = \frac{\int dX_{z0}^{(0)} dX_{zs}^{(0)} dX_{z\mathcal{L}}^{(0)} \mathcal{G}_0(X_{zs}^{(0)}, X_{z0}^{(0)}, s) \delta(X_{zs}^{(0)} - \eta(x, y, \epsilon)) \mathcal{G}_0(X_{z\mathcal{L}}^{(0)}, X_{zs}^{(0)}, |\mathcal{L} - s|)}{\int dX_{z0}^{(0)} dX_{z\mathcal{L}}^{(0)} \mathcal{G}_0(X_z^{(0)}(\mathcal{L}), X_z^{(0)}(0), \mathcal{L})} \quad (\text{C.20})$$

$$= \frac{\left(\frac{2}{ah_z} \right)^2 \sum_{p,r=1,3,\dots}^{\infty} \left(\frac{ah_z}{\pi p} \right) \sin \frac{2\pi p \epsilon}{h_z} e^{-\frac{\ell^2 \pi^2 p^2 s}{6(a h_z)^2}} \left(\frac{ah_z}{\pi r} \right) \sin \frac{2\pi r \epsilon}{h_z} e^{-\frac{\ell^2 \pi^2 r^2 |\mathcal{L}-s|}{6a^2 h_z^2}}}{\frac{8ah_z}{\pi^2} \sum_{p=1,3,\dots}^{\infty} \frac{1}{p^2} \cos^2 \left(\frac{\pi p \epsilon}{h_z} \right) \exp \left\{ -\frac{\ell \pi^2 p^2 \mathcal{L}}{6 a^2 h_z^2} \right\}} \quad (\text{C.21})$$

$$\simeq \frac{\left(\frac{2}{ah_z} \right) \left(\frac{\pi \epsilon}{ah_z} \right)^2 \sum_{p,r=1,3,\dots}^{\infty} e^{-\frac{\ell^2 \pi^2 p^2 s}{6 h_z^2}} e^{-\frac{\ell^2 \pi^2 r^2 |\mathcal{L}-s|}{6 h_z^2}}}{\sum_{p=1,3,\dots}^{\infty} \frac{1}{p^2} \exp \left\{ -\frac{\ell \pi^2 p^2 \mathcal{L}}{6 h_z^2} \right\}} \underbrace{\text{if } \left(\frac{\pi p \epsilon}{h_z} < 1 \right) \text{ and } \left(\frac{\pi r \epsilon}{h_z} < 1 \right)}_{\therefore p=1=r} \quad (\text{C.22})$$

$$= \frac{2\pi^2 \epsilon^2}{\sqrt{1+n\lambda^2} h_z^3}. \quad (\text{C.23})$$

The $\beta = 0$ terms for the \hat{x} and \hat{y} coordinates are given by:

$$\langle \delta(X_i^{(0)}(s) - \nu^{(0)}(x, y, \epsilon)) \rangle_{\mathcal{G}_0} = \frac{2}{V_i (1+n\lambda_i^2)^{\frac{1}{2}}}, \quad i = x, y, \lambda_i = \frac{1}{\sqrt{\lambda}}.$$

Originally, in terms of the $\mathbf{R}^{(\alpha)}$ coordinates, there was a clear cut distinction between the undeformed ($\alpha = 0$) and deformed ($\alpha = 1, 2, \dots, n$) replica s , and these were different by the deformation tensor Λ (2.26). The wall constraint vectors were given by $\eta(x, y, h_z - \epsilon)$ for the

$\alpha = 0$ replica, and $\eta(\frac{x}{\sqrt{\lambda}}, \frac{y}{\sqrt{\lambda}}, \lambda h_z - \epsilon)$ for the $\alpha > 0$ deformed replica systems. Note that after the coordinate transformation \mathbb{T} , the only vectors that do not vanish are $\eta^{(0)}$ (A.2) for the top and bottom walls. When the network system undergoes an isovolumetric, affine deformation the averages are given by

$$\langle \delta(X_z^{(1)}(s)) \rangle_{\mathcal{G}_1} = \left[\frac{q_z \sinh \frac{1}{3} \ell q_z \mathcal{L}}{2\pi \cosh \frac{1}{3} \ell q_z |s| \cosh \frac{1}{3} \ell q_z |\mathcal{L} - s|} \right]^{\frac{1}{2}} \quad (\text{C.24})$$

$$\langle \delta(X_i^{(1)}(s)) \rangle_{\mathcal{G}_1} = \left[\frac{q_x \sinh \frac{1}{3} \ell q_x \mathcal{L}}{2\pi \cosh \frac{1}{3} \ell q_x |s| \cosh \frac{1}{3} \ell q_x |\mathcal{L} - s|} \right]^{\frac{1}{2}} \quad (\text{C.25})$$

$$\langle \delta(Y_z^{(m)}(s)) \rangle_{\mathcal{G}_m} = \left[\frac{q_z \sinh \frac{1}{3} \ell q_z \mathcal{L}}{2\pi \cosh \frac{1}{3} \ell q_z |s| \cosh \frac{1}{3} \ell q_z |\mathcal{L} - s|} \right]^{\frac{1}{2}} \quad (\text{C.26})$$

$$\langle \delta(Y_i^{(m)}(s)) \rangle_{\mathcal{G}_m} = \left[\frac{q_x \sinh \frac{1}{3} \ell q_x \mathcal{L}}{2\pi \cosh \frac{1}{3} \ell q_x |s| \cosh \frac{1}{3} \ell q_x |\mathcal{L} - s|} \right]^{\frac{1}{2}}. \quad (\text{C.27})$$

Putting all the contributions together as dictated by (4.49), results in the following:

$$\therefore \langle \mu_w \mathbb{X}_w \rangle = \mu_w \langle \mathbb{X}_{wx} \mathbb{X}_{wy} \mathbb{X}_{wz} \rangle \quad (\text{C.28})$$

$$= \left\langle 2\mu_w \int_0^{\mathcal{L}} ds \int_{-\infty}^{+\infty} dx dy \delta(X_x^{(0)}(s) - \nu_x^{(0)}) \delta(X_y^{(0)}(s) - \nu_y^{(0)}) \delta(X_z^{(0)}(s) - \nu_z^{(0)}) \right. \\ \left. \times \delta(X_x^{(1)}) \delta(X_y^{(1)}) \delta(X_z^{(1)}) \prod_{m=1}^{n-1} \delta(Y_x^{(m)}) \delta(Y_y^{(m)}) \delta(Y_z^{(m)}) \right\rangle \quad (\text{C.29})$$

$$= 2\mu_w \frac{2\pi^2 \epsilon^2}{h_z^3 (1+n\lambda^2)^{1/2} V_x V_y (1+n/\lambda)} \\ \times \int_0^{\mathcal{L}} ds \int_{-\infty}^{+\infty} dx \int_{-\infty}^{+\infty} dy \left(\frac{q \sinh \frac{1}{3} \ell q \mathcal{L}}{2\pi \cosh \frac{1}{3} \ell q s \cosh \frac{1}{3} \ell q |\mathcal{L} - s|} \right)^n \\ \times \left(\frac{q_z \sinh \frac{1}{3} \ell q_z \mathcal{L}}{2\pi \cosh \frac{1}{3} \ell q_z s \cosh \frac{1}{3} \ell q_z |\mathcal{L} - s|} \right)^{\frac{n}{2}} \quad (\text{C.30})$$

$$= 8\mu_w \frac{2\pi^2 \epsilon^2}{h_z^3 (1+n\lambda^2)^{1/2}} \int_0^{\mathcal{L}} ds \left(\frac{q \sinh \frac{1}{3} \ell q \mathcal{L}}{2\pi \cosh \frac{1}{3} \ell q s \cosh \frac{1}{3} \ell q |\mathcal{L} - s|} \right)^n \\ \times \left(\frac{q_z \sinh \frac{1}{3} \ell q_z \mathcal{L}}{2\pi \cosh \frac{1}{3} \ell q_z s \cosh \frac{1}{3} \ell q_z |\mathcal{L} - s|} \right)^{\frac{n}{2}} \quad (\text{C.31})$$

$$\simeq \frac{16\mu_w \pi^2 \epsilon^2 \mathcal{L}}{h_z^3 (1+n\lambda^2)^{1/2}} \left(\frac{q_z}{\pi} \right)^{n/2} \left(\frac{q}{\pi} \right)^n \quad \text{for } \frac{\ell q}{3} \geq 1. \quad (\text{C.32})$$

The integral in (C.31) cannot be evaluated analytically. However, in the limit of $\mathcal{L} \geq \frac{3}{\ell q}$, the integrand is constant, except at the boundaries near $s = 0$ and $s = \mathcal{L}$, as illustrated in Figure C.1. This limit contains the localization factor q , which is found from (4.62) to be $q_i = \frac{6(N_w + N_c)}{\ell \mathcal{L}}$ for $i = \{x, y, z\}$. The magnitude of the non-constant contribution \mathcal{I}_{err} (near $s = 0$ and $s = \mathcal{L}$) is then of the order of $\mathcal{I}_{\text{err}} \sim \frac{\mathcal{L}}{2(N_c + N_w)}$. This means that the assumption of a densely linked network ($\mathcal{I}_{\text{err}} < 1$) ensures that the integrand in (C.33) can be safely approximated by a constant. The

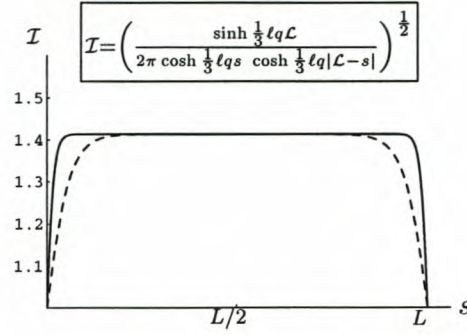


Figure C.1: Plot illustrating the constant behaviour of the integrand in (C.31) and (C.33). The solid line corresponds to $\frac{1}{3}lq \geq 1$ (high crosslink density) and the dashed line to when the linking density decreases to $\frac{1}{3}lq \ll 1$.

approximate solution to the integral

$$\int I^n ds = \left(\frac{\sinh \frac{1}{3}lq\mathcal{L}}{2\pi \cosh \frac{1}{3}lqs \cosh \frac{1}{3}lq|\mathcal{L}-s|} \right)^{\frac{n}{2}} \approx 2^{\frac{n}{2}} \mathcal{L} \quad (\text{C.33})$$

then leads to the result in (C.32). It can also be obtained by rewriting the hyperbolic functions as exponentials and investigating the limit of large exponents.

C.3 The harmonic trial potential $\langle \mathbb{Q} \rangle$

Implementing only Green's functions \mathcal{G}_1 and \mathcal{G}_m which have the same form for all the coordinates, results in n identical terms. These solutions differ only in terms of the parameters q_x and q_z :

$$\langle X_z^{(1)2}(s) \rangle_{\mathcal{G}_1} = \frac{\cosh \frac{1}{3}lq_z|\mathcal{L}-s| \cosh \frac{1}{3}lq_z|s|}{q_z \sinh \frac{1}{3}lq_z\mathcal{L}} = \langle |Y_z^{(m)}(s)|^2 \rangle_{\mathcal{G}_m} \quad (\text{C.34})$$

$$\langle X_i^{(1)2}(s) \rangle_{\mathcal{G}_1} = \frac{\cosh \frac{1}{3}lq_x|\mathcal{L}-s| \cosh \frac{1}{3}lq_x|s|}{q_x \sinh \frac{1}{3}lq_x\mathcal{L}} = \langle |Y_i^{(m)}(s)|^2 \rangle_{\mathcal{G}_m}, \quad (\text{C.35})$$

where i collectively denotes x and y coordinates.

The complete average (4.24) is found by integrating over the sum of the above terms:

$$\therefore \langle \mathbb{Q} \rangle = \left\langle \sum_{i=x,y,z} \frac{q_i^2 \ell}{6} \int_0^{\mathcal{L}} ds \left[X_i^{(1)2} + \sum_{m=1}^{n-1} |Y_i^{(m)}|^2 \right] \right\rangle \quad (\text{C.36})$$

$$= \frac{n\ell}{6} \int_0^{\mathcal{L}} ds \left[\frac{2q_i \cosh \frac{1}{3}lq_i|\mathcal{L}-s| \cosh \frac{1}{3}lq_i|s|}{\sinh \frac{1}{3}lq_i\mathcal{L}} + \frac{q_z \cosh \frac{1}{3}lq_z|\mathcal{L}-s| \cosh \frac{1}{3}lq_z|s|}{\sinh \frac{1}{3}lq_z\mathcal{L}} \right] \quad (\text{C.37})$$

$$= \frac{n}{4} \left(3 + \frac{\ell}{3}q_z\mathcal{L} \coth \frac{\ell}{3}q_z\mathcal{L} + \frac{2\ell}{3}q_i\mathcal{L} \coth \frac{\ell}{3}q_i\mathcal{L} \right) \quad (\text{C.38})$$

$$\approx \frac{n}{4} \left(3 + \frac{\ell\mathcal{L}}{3}(q_z + 2q_x) \right) \quad \text{for } \frac{q\ell\mathcal{L}}{3} > 1. \quad (\text{C.39})$$

Appendix D

The Second Variational Calculation

We set out here to evaluate the average $\langle \mathbb{Q} + \mu_c \mathbb{X}_c + \mu_w \mathbb{X}_w \rangle$ of Section 5.2.2 by using the Green's functions listed in Section 4.5.1.

D.1 The Bulk Cross-links $\langle \mu_c \mathbb{X}_c \rangle$

The $\beta = 0$ term for the \hat{z} -dimension corresponds with the average in the previous chapter (C.3), and is given by

$$\langle \delta(X_z^{(0)}(s) - X_z^{(0)}(s')) \rangle_{\mathcal{G}_0} \simeq \frac{3}{2\sqrt{1+n\lambda^2} h_z}, \quad \text{when } p = r = \rho. \quad (\text{D.1})$$

The solution to the integral in (D.1) follows from the result (C.4) and assumptions, previously presented in C.1.

The $\alpha = 0$ terms for the \hat{x} and \hat{y} coordinates are given by (where i and j are chain indices):

$$\begin{aligned} & \langle \delta(X_{xi}^{(0)}(s) - X_{xi}^{(0)}(s')) \rangle_{\mathcal{G}_0} \quad (\text{D.2}) \\ &= \frac{\int dX_0 dX_{is'} dX_{is} dX_{iL} \mathcal{G}_0(X_{is'}, X_{i0}, s') \mathcal{G}_0(X_{is}, X_{is'}, |s - s'|) \delta(X_{is} - X_{is'}) \mathcal{G}_0(X_{iL}, X_{is}, |L - s|)}{\int dX_{i0} dX_{iL} \mathcal{G}_0(X_{iL}, X_{i0}, L)} \\ &= \frac{2}{V_x (1 + n\lambda_i^2)^{\frac{1}{2}}} + \left(\frac{3}{2\pi\ell |s - s'|} \right)^{\frac{1}{2}}, \quad (\text{D.3}) \end{aligned}$$

where V_x denotes the length in the x -dimension of the original box volume, $V = V_x V_y h_z$, containing the sample. The above result is for the special case when the polymer links with itself ($i = j$) to form a loop of length $|s - s'|$. When $i \neq j$, two *different* chains are crosslinked, and the average is s -independent:

$$\begin{aligned} & \langle \delta(X_{xi}^{(0)}(s) - X_{xj}^{(0)}(s')) \rangle_{\mathcal{G}_0} \quad (\text{D.4}) \\ &= \frac{\int dX_{i0} dX_{j0} dX_{j's'} dX_{iL} dX_{jL} \mathcal{G}_0(X_{j's'}, X_{i0}, s) \mathcal{G}_0(X_{iL}, X_{j's'}, |L - s|) \mathcal{G}_0(X_{j's'}, X_{j0}, s') \mathcal{G}_0(X_{jL}, X_{j's'}, |L - s'|)}{\int dX_{i0} dX_{j0} dX_{iL} dX_{jL} \mathcal{G}_0(X_{iL}, X_{i0}, L) \mathcal{G}_0(X_{jL}, X_{j0}, L)} \\ &= \frac{2}{V_x (1 + n\lambda_i^2)^{\frac{1}{2}}}. \quad (\text{D.5}) \end{aligned}$$

The above result occurs $N_w - 1$ times.

The rest of the bulk cross-link averages are performed in terms of Green's functions which are either q_0 or q_1 dependent, and therefore we have to employ the scheme in (5.22). For large $\ell q |s - s'|$, we approximate the Green's function by $\tilde{\mathcal{G}}_1$ given in (C.10). There are $3n$ remaining averages, given by

(D.6) – (D.9), where $X^{(\alpha)}$ stands for any cartesian component of $\{\mathbf{X}_i^{(1)}, \mathbf{Y}_i^{(m)} | m=1 \dots n-1\}$:

$$\langle \delta(X_s^{(\alpha)} - X_{s'}^{(\alpha)}) \rangle_{s < \tau, s' < \tau} = \sqrt{\frac{q_0}{2\pi}} \quad (\text{D.6})$$

$$\langle \delta(X_s^{(\alpha)} - X_{s'}^{(\alpha)}) \rangle_{s < \tau, s' > \tau} = \sqrt{\frac{q_0 q_1}{\pi (q_0 + q_1)}} \quad (\text{D.7})$$

$$\langle \delta(X_s^{(\alpha)} - X_{s'}^{(\alpha)}) \rangle_{s > \tau, s' < \tau} = \sqrt{\frac{q_0 q_1}{\pi (q_0 + q_1)}} \quad (\text{D.8})$$

$$\langle \delta(X_s^{(\alpha)} - X_{s'}^{(\alpha)}) \rangle_{s > \tau, s' > \tau} = \sqrt{\frac{q_1}{2\pi}} \quad (\text{D.9})$$

Putting all the averages together, the complete bulk crosslink contribution (5.23) becomes

$$\therefore \langle \mu_c \mathbb{X}_c \rangle = \mu_c \langle \mathbb{X}_{cx} \mathbb{X}_{cy} \mathbb{X}_{cz} \rangle \quad (\text{D.10})$$

$$\begin{aligned} &= \frac{3\mu_c}{2h_z \sqrt{1+n\lambda^2}} \int_0^\tau ds \int_0^\tau ds' \left(\frac{2N_w h_z}{V(1+n/\lambda)} + \frac{3}{2\pi\ell|s-s'|} \right) \left(\frac{q_0}{2\pi} \right)^{\frac{3n}{2}} \\ &+ 2 \int_0^\tau ds \int_\tau^L ds' \left(\frac{2N_w h_z}{V(1+n/\lambda)} + \frac{3}{2\pi\ell|s-s'|} \right) \left(\frac{q_0 q_1}{\pi(q_0 + q_1)} \right)^{\frac{3n}{2}} \\ &+ \int_\tau^L ds \int_\tau^L ds' \left(\frac{2N_w h_z}{V(1+n/\lambda)} + \frac{3}{2\pi\ell|s-s'|} \right) \left(\frac{q_1}{2\pi} \right)^{\frac{3n}{2}} \end{aligned} \quad (\text{D.11})$$

The above integrals should be evaluated carefully, since some of the terms diverge when $s = 0$. However, the Gaussian chain model and continuous chain coordinates s , are only valid when we look at length scales larger than a certain length, say ℓ_c . When $s < \ell_c$, the molecule is no longer a flexible, continuous chain: it consists of monomers with rigid bonds. We therefore make the substitution: $|s - s'|^{-1} \rightarrow \lim_{\ell_c \rightarrow 0} [(s - s')^2 + \ell_c^2]^{-1/2}$. The integrals are now straightforward to calculate and lead to the result shown in (4.46).

D.2 The Wall Crosslinks $\langle \mu_w \mathbb{X}_w \rangle$

The wall cross-links are completely specified by the vectors $\nu^{(0)}(x, y, \epsilon)$ in (5.24) and $\nu^{(0)}(x, y, h_z - \epsilon)$ in (5.25), for cross-links situated an infinitesimal distance ϵ from the wall surface. The wall crosslinks and endpoints ($s = 0$) of each chain will deform affinely together with the walls. Letting $a \equiv \sqrt{1+n\lambda^2}$, the centre-of-mass average is given by:

$$\begin{aligned} &\langle \delta(X_z^{(0)}(0) - \nu^{(0)}(x, y, \epsilon)) \rangle_{\mathcal{G}_0} \\ &= \frac{\int dX_z^{(0)}(0) dX_z^{(0)}(L) \mathcal{G}_0(X_z^{(0)}(0), a\epsilon; 0) \delta(X_z^{(0)}(0) - a\epsilon) \mathcal{G}_0(X_z^{(0)}(L), X_z^{(0)}(0); L)}{\int dX_z^{(0)}(L) \mathcal{G}_0(X_z^{(0)}(L), a\epsilon; L)} \\ &= \frac{2\pi^2 \epsilon^2}{\sqrt{1+n\lambda^2} h_z^3}, \end{aligned} \quad (\text{D.12})$$

since $X_z^{(0)}(s=0) = a\epsilon = \sqrt{1+n\lambda^2}$.

The \hat{x} and \hat{y} average for the ‘‘centre-of-mass-of-replicas’’ term, is

$$\langle \delta(X_i^{(0)}(s) - \nu^{(0)}(x, y, \epsilon)) \rangle_{\mathcal{G}_0} = \frac{h_z}{V \sqrt{1+n\lambda_i^2}}, \quad i = x, y, \lambda_i = \frac{1}{\sqrt{\lambda}}, \quad (\text{D.13})$$

where V is the volume of the original undeformed system.

The remaining averages are the identity because

$$\langle \delta(\mathbf{X}^{(1)}(0)) \rangle = \left\langle \prod_{m=1}^{n-1} \delta(\mathbf{Y}^{(m)}(0)) \right\rangle = \mathbf{1}, \quad (\text{D.14})$$

$$\text{because } \mathbf{X}^{(\alpha)}(s=0) = \mathbf{Y}^{(m)}(s=0) = \nu^{(\alpha)}(x, y, h_z - \epsilon) = \nu^{(\alpha)}(x, y, \epsilon) = 0, \quad \text{for } \alpha > 0$$

as shown in Appendix A.

D.3 The harmonic trial potential $\langle \mathbb{Q} \rangle$

Implementing only Green's functions \mathcal{G}_1 and \mathcal{G}_m which have the same form for all the coordinates, results in n identical terms for each of the s domains, for example for the $X^{(1)}$ coordinate:

$$\begin{aligned} \langle X_z^{(1)2}(s) \rangle_{s < \tau} & \quad (\text{D.15}) \\ &= \frac{3q_0 \cosh \frac{\ell q_0}{3} s \left(q_0 \cosh \frac{\ell q_0}{3} (\tau - s) \cosh \frac{1}{3} \ell q_1 (L - \tau) + q_1 \sinh \frac{\ell q_0}{3} (\tau - s) \sinh \frac{\ell q_1}{3} (L - \tau) \right)}{q_0 \sinh \frac{\ell q_0}{3} \tau \cosh \frac{\ell q_1}{3} (L - \tau) + q_1 \sinh \frac{\ell q_1}{3} (L - \tau) \cosh \frac{\ell q_0}{3} \tau} \end{aligned}$$

$$\begin{aligned} \langle X_z^{(1)2}(s) \rangle_{s > \tau} & \quad (\text{D.16}) \\ &= \frac{3q_0 \cosh \frac{\ell q_1}{3} (L - s) \left(q_0 \sinh \frac{\ell q_0}{3} \tau \sinh \frac{1}{3} \ell q_1 (s - \tau) + q_1 \cosh \frac{\ell q_1}{3} (s - \tau) \cosh \frac{\ell q_0}{3} \tau \right)}{q_0 \sinh \frac{\ell q_0}{3} \tau \cosh \frac{\ell q_1}{3} (L - \tau) + q_1 \sinh \frac{\ell q_1}{3} (L - \tau) \cosh \frac{\ell q_0}{3} \tau} \end{aligned}$$

The complete average (5.16) is found by integrating over the sum of the above terms, which is shown in the main text (5.28).

Bibliography

- [1] ALLEGRA, G. and RAOS, G., "Confined polymer networks: The harmonic approach." *J. Chem. Phys.*, 2002, Vol. 116, pp. 3109–3118.
- [2] BALL, R. C. and EDWARDS, S. F., "Elasticity and Stability of a Dense Gel." *Macromolecules*, 1980, Vol. 13, pp. 748–761.
- [3] BALL, R. C., EDWARDS, S. F., DOI, M., and WARNER, M., "Elasticity of entangled networks." *Polymer*, 1981, Vol. 22, pp. 1010–1018.
- [4] BINDER, K. and YOUNG, A. P., "Spin glasses: Experimental facts, theoretical concepts, and open questions." *Rev. Mod. Phys.*, 1986, Vol. 58, pp. 801–976.
- [5] CARSLAW, H. S. and JAEGER, J. C., *Conduction of Heat in Solids*. Second edition. Clarendon Press, 1959.
- [6] CAVAGNA, A., GIARDINA, I., PARISI, G., and MÉZARD, M., "On the formal equivalence of the TAP and thermodynamic methods in the SK model." *Preprint cond-mat /0210665*, 2002.
- [7] DE GENNES, P. G., "Conformations of Polymers Attached to an Interface." *Macromolecules*, 1980, Vol. 13, pp. 1069–1075.
- [8] DE GENNES, P. G., *Scaling Concepts in Polymer Physics*. Ithaca: Cornell University Press, 1985.
- [9] DEAM, R. T. and EDWARDS, S. F., "The Theory of Rubber Elasticity." *Phil. Trans. R. Soc. London A. Math. Phys. Sciences*, 1976, Vol. 280, pp. 317–353.
- [10] DERRIDA, B., "Random-Energy Model: Limit of a Family of Disordered Models." *Physical Review Letters*, 1980, Vol. 45, pp. 79–82.
- [11] DERRIDA, B., "Random-Energy model: An exactly solvable model of disordered systems." *Physical Review B*, 1981, Vol. 24, pp. 2613–2623.
- [12] DES CLOIZEAUX, J. and JANNINK, G., *Polymers in Solution: their modelling and structure*. Oxford: Oxford University Press, 1989.
- [13] DOI, M., *Introduction to Polymer Physics*. Oxford: Clarendon Press, 1996.
- [14] EDWARDS, S. F., "The statistical mechanics of rubbers." in *Polymer Networks* (CHOMPFF, A. J. E. A. (Ed.)), New York: Plenum Press, 1972.
- [15] EDWARDS, S. F. and ANDERSON, P. W., "Theory of Spin Glasses." *J. Phys.*, 1975, pp. 965–974.
- [16] EDWARDS, S. F. and DOI, M., *The Theory of Polymer Dynamics*. Oxford: Clarendon Press, 1986.
- [17] EDWARDS, S. F. and MUTHUKUMAR, M., "The size of a polymer in random media." *J. Chem. Phys.*, November 1988, Vol. 89, pp. 2435–2441.

- [18] EDWARDS, S. F. and VILGIS, T. A., "The tube model theory of rubber elasticity." *Rep. Prog. Phys.*, 1988, Vol. 51, pp. 243–297.
- [19] FEYNMAN, R. P. and HIBBS, A. R., *Quantum mechanics and Path Integrals*. New York: McGraw-Hill, 1965.
- [20] FISCHER, K. H. and HERTZ, J. A., *Spin Glass Theory*. Cambridge: Cambridge University Press, 1991.
- [21] FLORY, P. J., *Statistical mechanics of chain molecules*. New York: Interscience, 1969.
- [22] FREED, K. F. and EDWARDS, S. F., "The entropy of a confined polymer chain." *J. Phys. A (Gen. Phys.)*, November 1969, Vol. 2, pp. 145–150.
- [23] GOLDBART, P. and GOLDENFELD, N., "Microscopic theory for cross-linked macromolecules. I. Broken symmetry, rigidity, and topology." *Phys. Rev. A*, 1989, Vol. 39, pp. 1402–1411.
- [24] GOLDBART, P. and GOLDENFELD, N., "Microscopic theory for cross-linked macromolecules. II. Replica theory of the transition to the solid state." *Phys. Rev. A*, 1989, Vol. 39, pp. 1412–1419.
- [25] GRADSHTEYN, I. S. and RYZHIK, I., *Table of Integrals, Series, and Products*. Fifth edition. London: Academic Press, Inc., 1994.
- [26] GROSBERG, A. Y. and KHOKLOV, A. R., *Statistical Physics of Macromolecules*. New York: American Institute of Physics, 1994.
- [27] GROSS, D. J. and MÉZARD, M., "The Simplest Spin Glass." *Nucl. Phys.*, 1984, pp. 431–452.
- [28] HASSANI, S., *Foundations of Mathematical Physics*. Boston, Mass.: Allyn and Bacon, 1991.
- [29] HEINRICH, G., KLÜPPEL, M., and VILGIS, T. A., "Reinforcement of Elastomers." *Current Opinion in Solid State and Materials Science*, 2002, Vol. 6, pp. 195–203.
- [30] IMTEK, U. O. F., "Chemistry and Physics of Interfaces: Research Projects." <http://www.imtek.de/cpi/projects-list.htm> 2001.
- [31] JAMES, H. M. and GUTH, E., "Theory of the Elastic Properties of Rubber." *J. Chem. Phys.*, 1943, Vol. 11, pp. 455–480.
- [32] KHOLODENKO, A. L. and VILGIS, T. A., "Some geometrical and topological problems in polymer physics." *Physics Reports*, 1998, Vol. 298, pp. 251–370.
- [33] KUHN, W. *Kolloid Z.*, 1934, Vol. 68, p. 2.
- [34] MÉZARD, P. G., M. and VIRASARO, M. V., *Spinglass Theory And Beyond*. First edition. Singapore: World Scientific, 1987.
- [35] MORSE, P. M. and FESHBACH, H., *Methods of Theoretical Physics*. New York: McGraw-Hill, 1953.
- [36] MÜLLER-NEDEBOCK, K. K. and EDWARDS, S. F., "Entanglements in polymers: II. Networks." *J. Phys. A: Math. Gen.*, 1999, Vol. 32, pp. 3301–3320.
- [37] MÜLLER-NEDEBOCK, K. K., EDWARDS, S. F., and McLEISH, T. C. B., "Scattering from deformed polymer networks." *J. Chem. Phys.*, 1999, Vol. 111, pp. 8196–8208.
- [38] PANYUKOV, S. V., "Inhomogeneities as consequences of a stretching of polymer networks." *JETP Lett.*, 1993, Vol. 58, p. 118.

- [39] PAUL, S., *Surface Coatings: Science and Technology*. Second edition. J. Wiley and Sons, 1986.
- [40] PRUCKER, O., MÜLLER, K., and RÜHE, J., "Surface-attached Polymer Networks." in *Interfaces, Adhesion and Processing in Polymer Systems* (S.H. ANASTASIADIS, G. F., A. KARIM (Ed.)), vol. 629, Materials Research Society, April 2000.
- [41] RATNER, B. D., "Biomedical Applications of Synthetic Polymers." in *The Synthesis, Characterization, Reactions and Applications of Polymers*, vol. 7, New York: Pergamon Press, 1989.
- [42] READ, D. J. and MCLEISH, T. C. B., "'Lozenge' Contour Plots in Scattering from Polymer Networks." *Phys. Rev. Lett.*, 1997, Vol. 79, pp. 87–90.
- [43] READ, D. J. and MCLEISH, T. C. B., "Microscopic Theory for the 'Lozenge' Contour Plots in Scattering from Stretched Polymer Networks." *Macromolecules*, 1997, Vol. 30, pp. 6376–6385.
- [44] SHERRINGTON, D. and KIRKPATRICK, S., "Solvable Model of a Spin-Glass." *Phys. Rev. Lett.*, 1975, Vol. 35, pp. 1792–1796.
- [45] SOLF, M. P. and VILGIS, T. A., "Statistical mechanics of macromolecular networks without replicas." *J. Phys. A*, 1995, Vol. 28, p. 6655.
- [46] TRELOAR, GEE, and STERN *Trans. Faraday Soc.*, 1950, Vol. 46, p. 1101.
- [47] TRELOAR, L. R. G., *Introduction to Polymer Science*. London: Wykeham Publications, 1974.
- [48] TRELOAR, L. R. G., *The Physics of Rubber Elasticity*. Oxford: Clarendon Press, 1975.
- [49] URAYAMA, K. E. A., "Experimental Tests of Molecular Entanglement Models of Rubber Elasticity." *Macromolecules*, 2001, Vol. 34, pp. 8261–8269.
- [50] VAN HEMMEN, J. L. and PALMER, R. G., "The replica method and a solvable spin glass." *J. Phys.*, 1979, Vol. A 12, pp. 563–580.
- [51] VILGIS, T. A., "Rubber Elasticity and Network Defects: Inhomogeneities in Crosslink Density and Entanglements." in *Elastomeric Polymer Networks* (MARK, J. E. and ERMAN, B. (Eds)), New Jersey: Prentice-Hall, Inc., 1992.
- [52] WARNER, M. and EDWARDS, S. F., "Neutron scattering from strained polymer networks." *J. Phys. A*, 1978, Vol. 11, pp. 1649–1655.
- [53] WIEGEL, F. W., *Introduction to Path Integral Methods in Physics and Polymer Science*. First edition. Philadelphia: World Scientific, 1986.
- [54] YOUNG, R. J. and LOVELL, P. A., *Introduction to Polymers*. Second edition. Cheltenham, Great Britain: Stanley Thornes, 1991.

List of Figures

1.1	Schematic description of instantaneous crosslinking and surface attachment.	5
2.1	(a) An ideal, long flexible phantom chain, and (b) its Gaussian model counterpart.	7
2.2	A single polymer chain stitch.	9
2.3	Illustrating the relationship between the size of the polymer and the confinement dimensions.	10
2.4	Polymer stitch in the unstrained state, and after a uniaxial compression	12
2.5	Stress-strain plot for a polymer stitch confined between two parallel planar surfaces.	13
2.6	Polymer stitch in a box in the unstrained state, and after a uniaxial compression.	14
2.7	Plot of stress versus strain for a long polymer confined in a box.	15
2.8	Introducing a junction point in a two-stitch polymer system.	15
2.9	Maximum entropy and the single bulk-link.	17
2.10	Stress-strain plot for the confined, single bulk-link plate system.	17
3.1	A confined polymer network of stitches.	19
3.2	Isolating two stitches with a common linkage.	20
4.1	A very dense melt of phantom chains, confined between two walls.	29
4.2	A gel network formed at and between two, parallel planar surfaces.	31
4.3	Linking mechanism: (a) A slip link (b) Permanent link	32
4.4	Examples of three network imperfections.	34
5.1	Simplified illustration of a polymer brush attached to a solid surface.	47
5.2	Schematic illustration of polymers grafting from a solid surface.	48
5.3	Spatial profiles of the potential associated with adsorption, and confinement between two plates.	49
5.4	A brush network confined between two parallel planar surfaces.	50
5.5	Depicting the domains of the variational parameters in (5.10).	53
5.6	Illustrating the case of only one wall-link, $N_w \equiv 1$	61
5.7	Investigating the influence of the crosslink density on the localization of the polymer.	66
5.8	Investigating the influence of (a) the wall confinement h_z and (b) the polymer density ρ	67
C.1	Illustrating the behaviour of the integrand in (C.31).	79